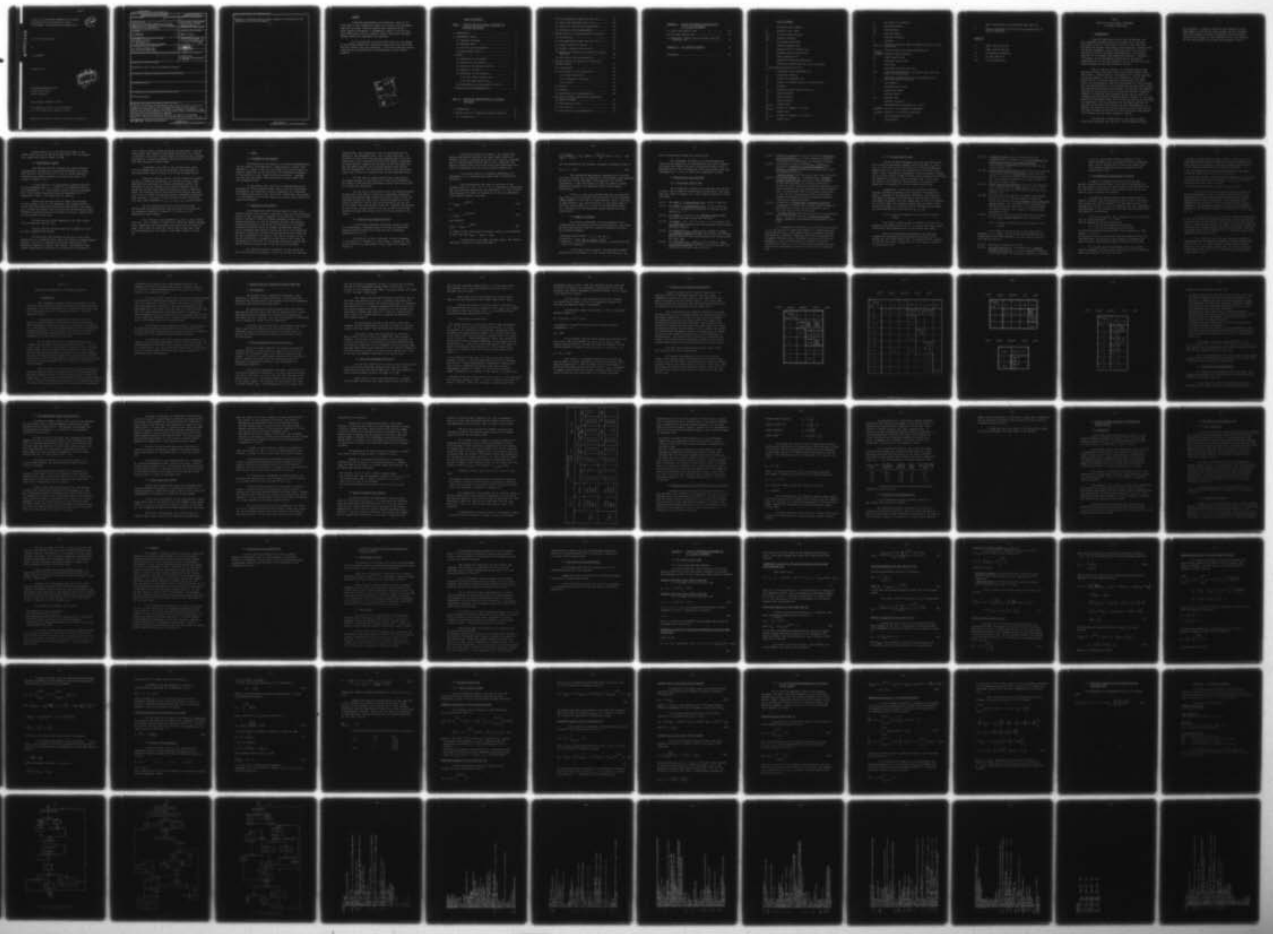
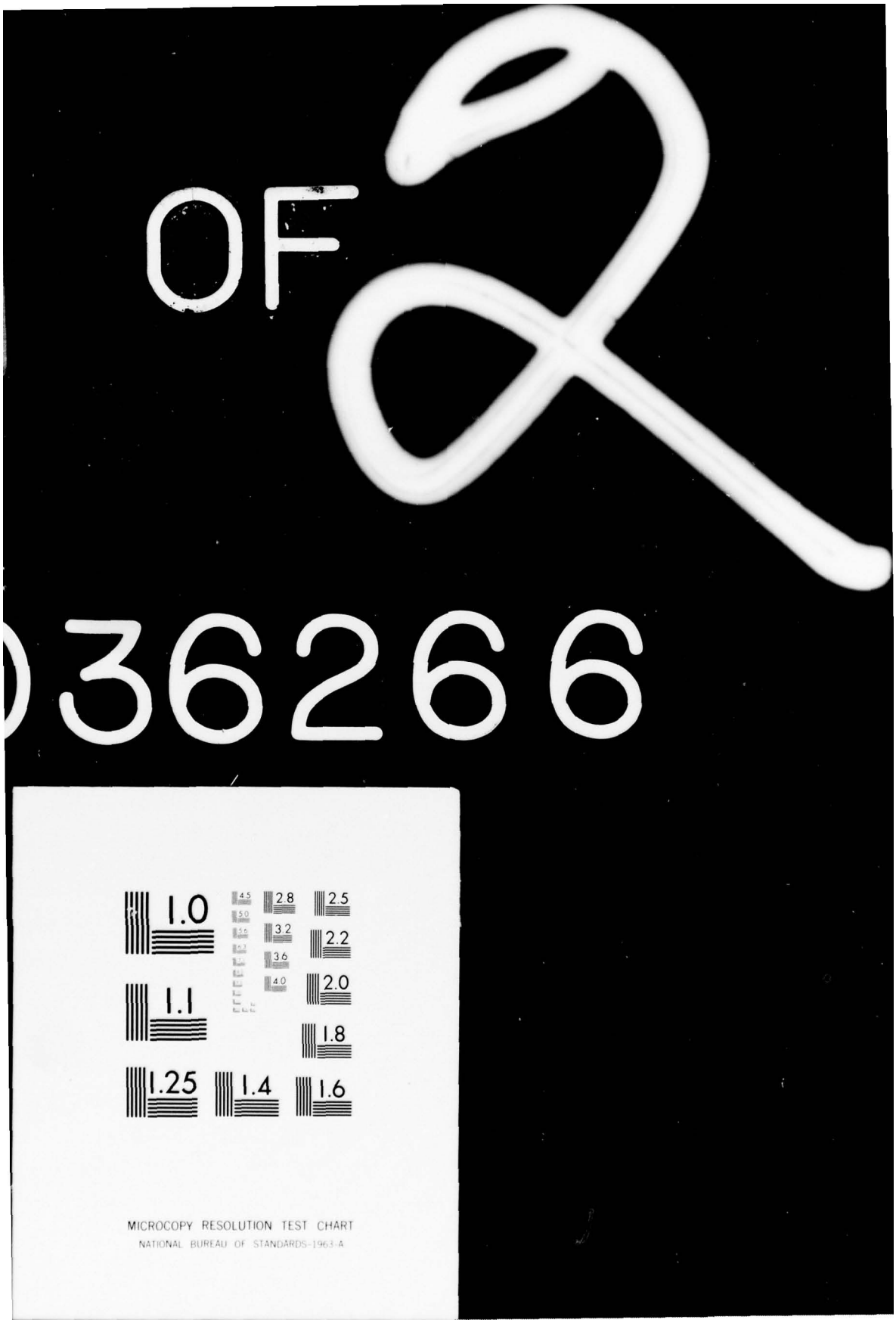
AD-A036 266 VON KARMAN INST FOR FLUID DYNAMICS RHODE-SAINT-GENESE--ETC F/G 9/5
STUDY OF THE SWITCHING MECHANISM IN BISTABLE AMPLIFIERS WITH AP--ETC(U)
NOV 76 M CARBONARO
DA-ERO-75-G-073
UNCLASSIFIED
NL

1 OF 2
AD
A036266




OF
036266
1.0
1.1
1.25
1.4
1.6
1.8
2.0
2.2
2.5
2.8
3.2
3.6
4.0
4.5
5.0
5.6
MICROCOPY RESOLUTION TEST CHART
NATIONAL BUREAU OF STANDARDS-1963-A

AD

STUDY OF THE SWITCHING MECHANISM IN BISTABLE AMPLIFIERS WITH APPLICATION TO THEIR DEVELOPMENT, OPTIMIZATION AND CONSTRUCTION

(12)

AD A036266

Final Technical Report

by

M. CARBONARO

November 1976



EUROPEAN RESEARCH OFFICE
United States Army
London, England

Grant Number DA-ERO 75-G-073

von Karman Institute for Fluid Dynamics
B - 1640 Rhode Saint Genèse, Belgium

Approved for public release; distribution unlimited

UNCLASSIFIED

SECURITY CLASSIFICATION OF THIS PAGE *(When Data Entered)*

REPORT DOCUMENTATION PAGE

READ INSTRUCTIONS BEFORE COMPLETING FORM

1. REPORT NUMBER	2. GOVT ACCESSION NO.
3. RECIPIENT'S CATALOG NUMBER	
4. TITLE *(and Subtitle)*: STUDY OF THE SWITCHING MECHANISM IN BISTABLE AMPLIFIERS WITH APPLICATION TO THEIR DEVELOPMENT, OPTIMIZATION AND CONSTRUCTION.	5. TYPE OF REPORT & PERIOD COVERED: Final Technical Report Nov 75 - Nov 76
	6. PERFORMING ORG. REPORT NUMBER
7. AUTHOR(s): M. CARBONARO	8. CONTRACT OR GRANT NUMBER(s): DAERO-75-G-073
9. PERFORMING ORGANIZATION NAME AND ADDRESS: von Karman Institute, Ch. de Waterloo 72, B - 1640 Rhode Saint Genese, Belgium	10. PROGRAM ELEMENT, PROJECT, TASK AREA & WORK UNIT NUMBERS: 6.11.02A-1T161102B35E-00-294
11. CONTROLLING OFFICE NAME AND ADDRESS: U.S. ARMY R&S GROUP (EUR), BOX 65, FPO NEW YORK 09510	12. REPORT DATE: November 1976
	13. NUMBER OF PAGES: 172
14. MONITORING AGENCY NAME & ADDRESS *(if different from Controlling Office)*	15. SECURITY CLASS. *(of this report)*: Unclassified
	15a. DECLASSIFICATION/DOWNGRADING SCHEDULE

16. DISTRIBUTION STATEMENT *(of this Report)*

Approved for public release, distribution unlimited.

17. DISTRIBUTION STATEMENT *(of the abstract entered in Block 20, if different from Report)*

18. SUPPLEMENTARY NOTES

19. KEY WORDS *(Continue on reverse side if necessary and identify by block number)*

Bistable amplifiers

20. ABSTRACT *(Continue on reverse side if necessary and identify by block number)*

A detailed experimental and theoretical study of the flow field in the interaction region of a fluidic wall-attachment amplifier was made. Velocity profiles were measured using a laser doppler velocimeter. A mathematical model of the flow was also established, using an integral method. Reasonable agreement between theory and experiments was obtained.
As a continuation of previous work ~~(Ref.11)~~, the design of two bistable amplifiers, operating respectively with turbulent and with laminar flow, was

DD FORM 1 JAN 73 1473 EDITION OF 1 NOV 65 IS OBSOLETE

UNCLASSIFIED

SECURITY CLASSIFICATION OF THIS PAGE *(When Data Entered)*

367 475

optimized. A simplified chemical etching technique was established for the manufacture of such fluidic elements.

SUMMARY

A detailed experimental and theoretical study of the flow field in the interaction region of a fluidic wall-attachment amplifier was made. Velocity profiles were measured using a Laser Doppler Velocimeter. A mathematical model of the flow was also established, using an integral method. Reasonable agreement between theory and experiments was obtained.

As a continuation of previous work (Ref.11), the design of two bistable amplifiers, operating respectively with turbulent and with laminar flow, was optimized. A simplified chemical etching technique was established for the manufacture of such fluidic elements.

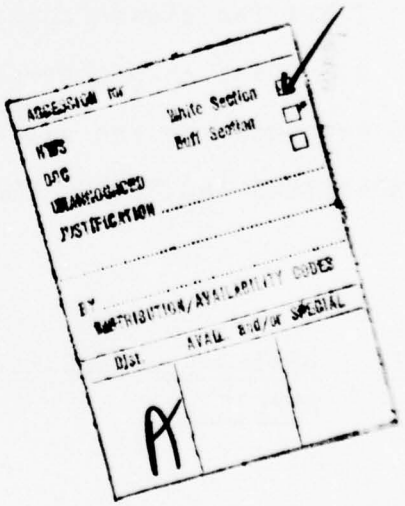


TABLE OF CONTENTS

PART I : STUDY OF THE JET-TO-WALL ATTACHMENT IN BISTABLE AMPLIFIERS

1. INTRODUCTION 1
2. EXPERIMENTAL STUDY 3
   2.1 Research programme 3
   2.2 Bistable model 3
   2.3 Test set up and procedure 4
   2.4 Experimental results 5
3. THEORY 7
   3.1 Statement of the problem 7
   3.2 Approach to the problem 7
   3.3 Choice of the velocity profile 8
   3.4 Summary of unknowns 10
   3.5 Definition of the equations 11
      3.5.1 The closed control case 11
      3.5.2 The open control case 13
   3.6 Presentation and discussion of results 15
4. CONCLUSIONS AND RECOMMENDATIONS 18

PART II : DESIGN AND CONSTRUCTION OF A BISTABLE AMPLIFIER

1. INTRODUCTION 19
2. DESIGN STUDY OF A TURBULENT BISTABLE AMPLIFIER .. 21
   2.1 Introduction 21

2.2 The experimental model and test set up 21

2.3 Tests with attachment walls only 22

2.4 Effects of splitter and output ducts 25

2.5 Conclusions and recommendations 30

3. DESIGN STUDY OF A LAMINAR BISTABLE AMPLIFIER ... 32

3.1 Introduction 32

3.2 The experimental model and test set up 33

3.3 Steady state test results 34

3.4 Dynamic switching test results 36

3.5 Design and scaling of the laminar bistable amplifier 39

3.6 Conclusions and recommendations 41

4. CHEMICAL ETCHING TECHNIQUE FOR FABRICATING FLUIDIC DEVICES 43

4.1 Introduction 43

4.2 Description of the process used 44

4.2.1 Mask preparation 44

4.2.2 Photoresist treatment 44

4.2.3 Etching 45

4.3 Results 45

4.4 Products 48

4.5 Conclusions and recommendations 49

5. TESTING OF BISTABLE AMPLIFIERS CONSTRUCTED BY CHEMICAL ETCHING 50

5.1 Description of tests 50

5.2 Test results 50

5.3 Conclusions and recommendations 52

APPENDIX A : SYSTEM OF EQUATIONS DESCRIBING THE JET TO WALL ATTACHMENT

A-1 The closed control case 53

A-2 The open control case 65

A-3 Additional relation for the length along the attachment wall 71

APPENDIX B : THE COMPUTER PROGRAMS 72

REFERENCES 96

LIST OF SYMBOLS

a	attachment wall setback
b_c	potential core width
$b_{e,i}$	jet half width (Fig.19)
D_{sp}	splitter distance
E	jet spread coefficient
J_c	control momentum flux
J_f	momentum flux of forward flow
J_r	momentum flux of return flow
J_s	supply momentum flux
K_1	momentum diffusivity coefficient
K_2	diffusivity coefficient due to jet curvature
$\ell_{e,i}(XL1,2)$	width defined in Fig.19
L	coordinate along attachment wall
L_a	attachment distance
L_w	length of attachment wall
ℓ_s	length of straight portion of supply nozzle
p	pressure
$p_{e,i}$	pressure on both sides of the jet
p_o	output pressure
p_t	total pressure
p_s	supply pressure
$Q_{c,e,i}$	control flow
$Q_{ent,e,i}$	defined in appendix A (p.66)
Q_s	supply flow
$Q_{s,e,i}$	defined in appendix A (p.54-55)
Q_o	output flow

R	jet radius of curvature
R_p	pressure recovery
R_q	flow recovery
Re	Reynolds number
T	bistable thickness
u	velocity
$U_{max,e,i}$	maximum velocity at edge of potential core or on jet centerline
$U_{rm,e,i}$	maximum reverse velocity outside the jet
$U_o = \sqrt{2P_s/\rho}$	reference supply velocity
w_s	supply nozzle width
w'	secondary throat width
w_v	vent width
x	coordinate along the jet axis
y,y'	coordinate perpendicular to the jet axis, with the origin on the jet axis
y''	coordinate perpendicular to the attachment wall, with the origin on the wall
y	vent setback
α	attachment wall angle
β	output wall angle
γ	splitter angle
Δp	pressure loss
ε	apparent viscosity
η	non-dimensional coordinate $(y - b_c)/b$
η_a (XHBD)	value of η on attachment streamline
η_b (XHID)	value of η on dividing streamline
ν	fluid kinematic viscosity
ρ	fluid density

τ	shear stress (part I) or switching time (part II)
ϕ	angular coordinate of a flow section perpendicular to the jet centerline

Suffixes

e	outer side of the jet
i	inner side of the jet
sw	at switching conditions
N	at flow section N
N-1	at flow section N-1

PART I

STUDY OF THE JET-TO-WALL ATTACHMENT IN BISTABLE AMPLIFIERS

1. INTRODUCTION

Since the beginning of the fluidic technology, the wall attachment bistable amplifier has been one of the units most widely used in fluidic logic circuits. It has also been the object of numerous experimental and theoretical investigations. The recent references 1 and 2 review the state of the art in relating the static and dynamic performances of the bistable amplifier to its geometry and operating conditions. Reference 2 indicates that a satisfactory prediction of the overall performances of the bistable amplifier can be achieved using the theory proposed by Goto and Drzewiecki (Ref.3).

What is lacking, however, is a detailed and accurate description of the flow field inside the fluidic element. Such flow field is characterized by the presence of a curved turbulent jet moving towards a side wall and attaching to it by Coanda effect (Fig.1). Existing theoretical descriptions are based (Ref.1) on the assumption that the jet develops as a free straight jet, and therefore that its non-dimensional velocity profile, spread and centerline velocity decay are known. Overall mass and momentum balances are then written, and the resulting system of algebraic equation is solved for the attachment point, the jet radius of curvature and the separation bubble pressure. However, in all these theoretical treatments, some of the following simplifying hypotheses are introduced : the jet curvature and the bubble pressure are constant in the entire flow field, only the attachment wall is present; the velocity and relative pressure in the region outside the convex boundary of the jet are zero; physically unacceptable flow patterns are thus often assumed or implied.

The need for a theory which is not based on those simplifying hypotheses was thus felt, and originated the work

here reported. In addition, detailed Laser-Doppler velocity measurements in the entire region between the two attachment walls were needed to provide a comparison with such theory. Pressure distributions on the attachment walls, also required for the same purpose, had already been measured in Ref.4.

2. EXPERIMENTAL STUDY

2.1 Research programme

The object of the study was to determine the steady-state flow field in the interaction region (Fig.1) of a bistable amplifier model. This was done by measuring, along several sections, perpendicular to the attachment wall, the velocity component parallel to the same wall. In order not to perturbate the flow, a non-obtrusive instrumentation, the Laser Doppler Velocimeter, had to be used for such measurements. As a first approach, the investigation was conducted on bistable configurations without vents and splitter, operated with no control flow injection. Two modes of operation were used with control channels either closed (Fig.1a) or open (Fig.1b) to atmosphere.

2.2 Bistable model

One of the models used in Ref.4 was again employed for the present research. It is schematically shown in Fig.2. In order to get experimental data comparable with the prediction of the theory (§ I-3) which assumes two-dimensional flow and very long attachment walls, it was decided that the model should have a high aspect ratio T/W_s to decrease the importance of three-dimensional secondary flows, and an attachment wall length L_w/W_s significantly larger than the expected jet attachment distance (L_a/W_s about 5 to 10). A model having $T/W_s = 8$ and $L_w/W_s = 17$ was therefore selected. All the other relevant dimensions are given in Fig.2.

The model was constructed by sandwiching aluminum blocks between two side plates. The latter were made out of plexiglass, except in the zone where LDV measurements had to be made and where thin (2mm) glass plates had to be used. The aluminum blocks forming the attachment walls were interchangeable, so that the wall angle α and set back A could be varied.

2.3 Test set up and procedure

For conducting the tests, a Laser Doppler Velocimeter developed at the VKI was employed. This LDV uses a 15 mW Spectra Physics Helium Neon Laser, a beam splitting and focussing optical unit, a light collecting optical unit incorporating a photo-detector, and an electronic data processing unit. This last item was completely designed and constructed at VKI. It differs substantially from commercially available units and is described in references 5 and 6. Also the two optical units were assembled at VKI (Ref.5).

For the present research, the VKI Laser Doppler Velocimeter was operated in the dual-beam, forward scattering mode. The two beams were .40 mm in diameter, and were crossing each other at an angle of 2,73°. The probe volume was thus of .40 mm × .40 mm × 8.47mm, the last dimension being measured in the direction of the bisectrix of the smaller angle formed by the axes of the two laser beams. Within the probe volume, the interference fringe spacing was of 6,67 μm. The bistable model was mounted so that the largest axis of the probe volume was perpendicular to the glass side plates, and was located at mid distance between them. The fringe planes were perpendicular to the attachment wall.

The air injected in the supply nozzle of the model had to be seeded with small particles. These were obtained using a standard smoke generator, producing a mist of condensed oil droplets.

The tests were conducted by displacing the LDV probe volume perpendicularly to the attachment wall of the bistable, and by continuously recording on an X-Y plotter velocity profile. Such measurement was repeated at various distances L measured along the attachment wall, as shown in Fig.2.

Gauge pressure p_s in the settling chamber of the supply nozzle was set at 100 mm WG (981 N/m^2). This corresponds to a supply jet Reynolds number of 6660.

2.4 Experimental results

The velocity profiles, measured for seven different configurations, obtained by varying the attachment wall angle (10° and 15°), the set back (0.1; 1 and 2) and the opening or closing of the control channels are given by the solid line curves in figures 3 to 9.

In such figures, u is the velocity component parallel to the attachment wall, $u_o = \sqrt{2\ p_s/\rho}$ is a reference velocity, the coordinate $\bar{y} = y"$ is the normal distance from the attachment wall. The distance L measured along the attachment wall, is expressed in terms of the supply nozzle width W_s.

Because the LDV used does not detect the direction of the velocity, but only its magnitude, the recorded profiles do not show the reverse flow existing on both sides of the supply jet. In those two regions, the true trend of the velocity has been obtained by manually drawing the dotted line curves, symmetrically to the recorded (solid) ones.

The dash and dot curves appearing in the same figures will be described later (§ 1.3).

Various velocity profiles have been assembled in Fig.10 to give a complete flow picture.

The data shows the existence in the jet, close to the nozzle exit, of a potential core, where the velocity is approximately constant. This core is bounded by two shear layers which are themselves adjacent to reverse flow regions. The potential core extends downstream of the nozzle exit section for a distance of

3 or 4 nozzle widths. Further downstream of this point , the two shear layers join together along thejet centerline. This latter is defined as the locus of points where the velocity has a maximum amplitude or, inside the potential core as the line dividing the core into two parts of equal width.

Furthermore, the width of the reversed flow region existing between the jet and the attachment wall decreases to zero when moving from the nozzle exit to the attachment point.

From each velocity profile, the jet centerline velocity and the jet width can be derived. If similarity exists, these quantities are sufficient to define the velocity profile. The jet width is usually defined as the distance between the jet centerline and the point where the velocity reaches a specified value, for instance, that of the reverse flow (outside the jet), plus 0.5 or 0.1 times the maximum velocity difference (centerline minus outside). This can of course be done on each side of the jet; thus, four parameters $b_{i.5}$, $b_{i.1}$, $b_{e.5}$, $b_{e.1}$ can be defined.

The jet centerline velocity and widths were thus derived from the measured data; they are given as a function of the downstream distance in figures 11 to 12 and 13 to 18 respectively (open symbols).

For a free jet, the parameters $b_{.5}$ and $b_{.1}$ vary linearly with X/W_s. This is shown in figures 13 to 18 by the dotted straight lines. Comparison with the present data shows that all along the outer side as well as along the initial part of the inner side of the attaching jet, the spread is the same as that of a free jet.

3. THEORY

3.1 Statement of the problem

The objective of the theory is to describe mathematically the two kinds of two-dimensional, incompressible, viscous flows depicted in figures 1a and 1b. Such flows are of the jet type, or boundary layer type in the sense that the longitudinal component of the velocity is much larger than the transversal component and that the transversal velocity gradient is much larger than the longitudinal one.

In the present case, the flow is characterized by the existence of curved turbulent shear layers, with non negligeable longitudinal and transversal pressure gradients; of a separated flow bubble with reverse flow; and of two irrotational flow regions, i.e. the potential core of the supply jet and the region beyond the convex jet boundary.

3.2 Approach to the problem

The mathematical model here described is based on an integral method, which assumes a realistic shape for the transversal profile of the longitudinal component of the velocity. This velocity profile, defined in terms of unknown parameters (widths and maximum velocities) is used to integrate the mass and momentum conservation equations. The latter are written by using Prandtl constant diffusivity theory to compute the Reynolds stresses, and by neglecting the variation across the jet of the streamlines curvature. Additional inviscid flow relationships are written for the two irrotational flow regions. The rate of increase of the two jet half-widths is assumed to be the same as for a free jet. Two geometrical relations for the widths of the two reverse flow regions existing on each side of the jet are also written.

The resulting system of equations is then solved for the velocity profile parameters, as well as for the wall pressure

distributions, the trajectory of the jet centerline and its curvature, the attachment point. This is done numerically, by dividing the flow field into sections perpendicular to the jet centerline, and by successively solving the system of equations for each section, assuming the curvature of the jet centerline and the bubble pressure to be constant between each section and its neighbouring. The calculation starts at the nozzle exit plane, and finishes in a section close to the attachment point.

For the case of closed control ports, the value of the bubble pressure at the nozzle exit plane, not predicted by the theory is derived from experimental results (Ref.4) and used to initiate the calculation.

For the case of open control ports, the bubble pressure at the nozzle exit plane is given by an additional expression relating the pressure drop through the control ports to the flow entrained through the same ports. Continuity equation is also used to relate this flow to the flow entrained by the jet and to the return flow existing out of the jet. Therefore the pressure at nozzle exit, on both sides of the jet, as well as the flows entrained through both control ports are also predicted by the theory.

3.3 Choice of the velocity profile

A curvilinear orthogonal coordinate system is used. The X-coordinate is measured along the curved jet centerline starting from the nozzle exit plane and the Y-coordinate perpendicularly to it.

The profile, in the Y-direction, of the X-component of the velocity is assumed to be that shown in figure 19. This is justified by the experimental results shown for instance in figure 10.

The profile is made of five layers : two reverse flow regions with uniform velocity, two shear layers, where the velocity profile is supposed to be similar to that of a straight jet in a counterflowing stream (Ref.7), and a potential core region, existing only close to the nozzle exit plane where the flow is irrotational and the velocity profile almost flat.

The velocity profile is therefore determined by 9 parameters, i.e. 5 characteristic widths and 4 characteristic velocities.

The law describing the velocity variation in the potential core, i.e. for $- b_c < Y < b_c$, is obtained by integrating the inviscid Euler equation in the Y-direction, i.e. $\partial p/\partial y = \rho U^2/R$. Then, assuming the radius of curvature R of the jet streamlines to be constant along y, one gets :

$$u = U_{max,e} \cdot e^{(b-y)/R} \tag{1a}$$

or

$$u = U_{max.i} \cdot e^{-(b_c+y)/R} \tag{1b}$$

and therefore

$$U_{max.i} = U_{max.e} \cdot e^{2b_c/R} \tag{2}$$

Of course in the established flow region, where b_c has decreased to zero, one gets $U_{max.i} = U_{max.e} = U_{max}$.

In the inner (i) or outer (e) shear layer, the velocity variation, suitably non-dimensionalized as

$$\frac{u - U_{r.m.k}}{U_{max.k} - U_{r.m.k}} = f(\eta), \text{ where } \eta = \frac{[y] - b_c}{b_k} \text{ and } (k = i,e) \qquad (3a)$$

will be expressed by the relation, proposed by Abramovich (Ref.7)

$$f(\eta) = (1 - \eta^{1.5})^2 \qquad (3b)$$

This expression approximates reasonably well (Fig.20), the exact solution, due to Goertler, to the boundary layer equations written for a free, turbulent, two-dimensional jet (Ref.8). Furthermore, it does not involve, as does the Goetler solution hyperbolic functions, and therefore leads to much simpler calculations.

Finally, it has to be stressed that the two velocities U_{rme} and U_{rmi} of the reversed flow outside the jet are obviously always negative in the case of closed controls, while in the case of open controls, U_{rmi} can be positive, in the region close to the inner control part. This is due to the fact that ambient air is entrained into the separation bubble through this inner control part.

3.4 Summary of unknowns

As previously explained, the flow equations can be integrated once the velocity profile has been defined. This leads for the closed control case to a system of equations relating the following unknowns :

5 velocity profile widths : ℓ_i, b_i, b_c, b_e, ℓ_e
4 velocities : U_{rmi}, $U_{max.i}$, $U_{max.e}$, $U_{r.me}$
2 pressures : p_i (in the separation bubble), p_e (outside the jet)
1 radius of curvature R.

In the case of open controls, two additional unknown quantities are introduced i.e., the volume flow rates Q_{ci}, Q_{ce}

which are entrained through the control ports.

The independent variable is the abscissa measured along the jet centerline, or alternatively, the angle Φ between the nozzle exit plane (x=0) and a flow section plane, which is perpendicular to the jet centerline. Also the distance along the attachment wall L, will be used as an independent variable.

3.5 Definition of the equations

3.5.1 The closed control case

The 12 equations relating the 12 unknowns were derived in Ref.9. One of them has already been written (Eq.2). The other ones are listed in appendix A-1. Their physical meaning is given here below :

Eq.(4) : the width b_e is proportional to X, as for a free jet

Eq.(5) : the width b_i is proportional to X, as for a free jet, if $\ell_i > 0$; otherwise this equation is replaced by the identity $\ell_i = 0$

Eq.(6) : the width ℓ_e is given by the available space between the outer jet edge and the wall (Fig.21)

Eq.(7) : the width ℓ_i (if > 0) or b_i (if $\ell_i = 0$) is given by the available space between the inner jet edge and the attachment wall (Fig.21)

Eq.(8) : the velocities $U_{max.e}$ and U_{rme} are related by a mass conservation condition equating the reverse flow existing outside the jet to the flow entrained into the jet along its outer edge

Eq.(9) : the velocities $U_{max.i}$ and U_{rme} are related by a mass conservation condition similar to the previous one, and written for the inner side of the jet.

Eq.(10) : Bernoulli's equation is used to relate the pressure p_e and the velocity U_{rme}, in the irrotational reversed flow region existing outside the convex jet boundary

Eq.(11) : An additional relation between $U_{max.e}$ and U_{rme} is obtained by combining the previous equation with Bernoulli's equation written at the outer edge of the jet potential core, and a momentum balance across the outer shear layer of the jet

Eq.(12) : The bubble pressure p_i is obtained from a momentum balance across the jet, from the dividing streamline to the outer jet edge. The dividing streamline is defined by a mass conservation condition equating, in the region bounded by the jet centerline and the attachment wall, the jet forward flow to the nozzle supply flow. In this case of closed control ports, the dividing streamline coincides with the attachment streamline, bounding the separation bubble

Eq.(13) : A condition of conservation of momentum along the X-direction is written for a control volume defined by the nozzle exit plane, the jet boundaries, and an arbitrary cross section of the flow

Eq.(14) : A momentum balance along the direction of the attachment wall is written for the flow in the recirculating bubble, bounded by two adjacent cross sections of the flow.

It is important to note that, for the first flow section X = 0, the system of 12 equations reduces to 7 identities, each specifying the value of one unknown and to 4 equations relating the remaining 5 unknowns. Indeed Eq.(14) loses its meaning and disappears from the system. Therefore, the value of one of the unknowns, p_i, has to be arbitrarily specified to start the calculation at section X = 0, and the results obtained are then used for the calculation at the next section and the following ones.

3.5.2 The open control case

The main difference between this case and the previous one is that two additional unknowns have to be added, Q_{ce} and Q_{ci}, i.e. the rate at which the fluid is entrained through each control port. As a result, the problem has to be solved in two steps : first a system of 14 equations in the 14 unknowns, written for an initial control volume is solved, thus yielding in particular, the values of Q_{ce} and Q_{ci}. Then the second step is involving the solution, at successive flow sections, of a system of 12 equations in 12 unknowns, as in the closed control case.

Furthermore, in this case the dividing streamline and the attachment streamline do not coincide. The separation bubble is bounded by the attachment streamline. The pressure in the bubble is assumed to be the same as the pressure along the attachment streamline. The flow scheme shown in Fig.22 is adopted. As it may be seen, the separation bubble does not begin at the control port edge, as in reality, but at the flow section where the calculated value of the velocity U_{rmi} is zero.

3.5.2.1 System of equations for the initial control volume

The initial control volume is defined in Fig.22. It is bounded by the nozzle exit plane (X = 0) and by that flow section intersecting the attachment wall at the control port edge.

Nine of the fourteen flow equations are identical respectively to equations (2)(4)(5)(6)(7)(10)(11)(12')(13), written for the closed control case. The remaining five, derived in Ref.(9), are listed in Appendix A-2. Their physical meaning is given here below :

Eq.(15) : A momentum balance along the direction of the attachment wall is written for the flow bounded by the dividing streamline and the attachment wall. This equation corresponds to Eq.(14) written for the closed controls case

Eq.(16) : A mass conservation condition equates the flow entrained into the jet along its outer edge to the sum of the control flow and the reverse flow existing outside the jet. This equation corresponds to Eq.(8) written for the closed controls case

Eq.(17) : A mass conservation condition similar to the previous one, is written for the inner side of the jet. This equation corresponds to Eq.(9) written for the closed controls case

Eq.(18) : The static pressure outside the curved outer boundary of the jet, p_e, is given by Bernoulli's equation, taking into account the total pressure loss in the outer control channel. This pressure loss is a function of the rate Q_{ce} at which the fluid is entrained through the control channel. Such function is obtained from experimental data

Eq.(19) : An expression similar to the previous one is written for the inner control channel to give pressure p_i

3.5.2.2 System of equations for each successive flow section

This problem is quite similar to that described in paragraph 3.5.1. Indeed, ten out of the twelve equations have already been established (equations 2,4,5,6,7,10,11,13,16,17). The remaining two are :

Eq.(21) : Same physical meaning as Eq.(15)

Eq.(20) : The bubble pressure p_i is obtained from a momentum balance across the jet, from the attachment streamline to the outer edge. The attachment streamline is defined

by a mass conservation condition equating, in the region bounded by the jet centerline and the attachment wall, the jet forward flow to the nozzle supply flow; this equation corresponds to Eq.12 written for the closed control case

3.6 Presentation and discussion of results

A numerical procedure was used to solve the two systems of equations established in the previous paragraph for the two cases of closed or open control parts. This was done first for the initial flow section or the initial control volume, and then for each successive flow section.

Two computer programs were written, using Fortran IV computer language. They are described in Ref.9. Their flow charts and listings are given in Appendix B of the present report. The programs were run on a CII Mitra 15 computer, for the 7 geometrical configurations of the bistable amplifier that had previously been experimentally investigated.

For the calculations, four constants had to be specified :
the jet spread coefficient $E = 0.274$
the jet momentum diffusivity coefficient
$K_1 = 9,77$ (in the potential core region)
$K_1 = 7,67$ (in the established flow region)
the coefficient expressing the effect of jet curvature on shear stress $K_2 = 10$
The values of E and K_1 are derived from well-known data for free turbulent jets. The value of K_2 was obtained by averaging the data of several investigations made on curved turbulent jets.

As a result of the calculations, the nine velocity profile parameters and the relative pressures on the two bistable walls were obtained. This data was used :

- to draw the dimensional velocity profiles (Figs 3 to 9). The calculated velocity component parallel to the jet centerline is given versus the distance y' from the attachment wall measured in the direction perpendicular to the jet centerline.

- to plot the decay with increasing distance from the nozzle of the jet center line velocity (Figs 11 and 12).

- to plot the increase, with increasing distance from the nozzle, of two typical shear layer thicknesses ($b_{.5}$ and $b_{.1}$), for the two sides of the jet (Figs 13 to 18).

- to plot wall pressure distributions (Figs 23 to 27).

On Figs 3 to 18, were already plotted the results of the LDV measurements, taken at sections perpendicular to the attachment wall, while the calculations were made at sections perpendicular to the jet centerline. Thus experimental and theoretical data are given in two different reference systems. Comparison is nevertheless meaningful, because the difference between the two reference systems is a rotation of a small angle $(\alpha - \Phi)$.

On Figs 23 to 27 are also plotted results of measurements of the wall pressure distribution previously carried out (Ref.4). As may be seen from the figures, the overall trend of the velocity field is correctly predicted by the theory. The computed centerline velocities are slightly greater than the measured ones. Also the calculated length of the potential core is about one nozzle width greater than the measured one.

Figs 13 and 14, show very good agreement between the experimental and the theoretical spread of the jet on the outer side of the jet. This result could of course be anticipated, because Eq.(4) specifically assumes that the curved jet spread is the same as for a free jet, as verified by the experimental investigation (§ 2.4).

Figs 15 and 16 show that good agreement is obtained for the inner region of the jet only far before the attachment. This could also be expected. Indeed the width $b_{i.1}$, first increases with X at the same rate as a free jet, but then decreases when approaching the attachment point. Again this is implied by the physical meaning of Eq.(5b) and (7).

Figs 17 and 18 do not show for the inner side of the jet good agreement between the predicted and measured values of the half-velocity shear layer thickness $b_{i.5}$, when approaching the attachment point. Even the trends are opposite. This disagreement when compared with the good agreement observed between the full widths indicate that, when approaching the attachment point, the true shape of the velocity profiles differs from that assumed (Eq.3) in the theory.

Figs 23 and 24, related to the closed control case, show reasonable agreement between theory and experiment except for the value of the pressure peak associated with attachment. The abscissa of this peak, i.e. the attachment point location is correctly predicted. Figs 25 to 27 show that in the open control case a better agreement is obtained.

In the case of open controls, the theory also reasonably predicts the value of the flow entrained through the control channels, as shown by the following table :

α	a/W_s	Q_{ci}/Q_s theory	Exper.
10°	1	0.152	0.131
10°	2	0.174	0.161
15°	1	0.162	0.144

4. CONCLUSIONS AND RECOMMENDATIONS

Detailed data on the flow field inside the interaction region of a bistable amplifier was obtained by LDV measurements.

This flow field was reasonably modelled by an integral method.

Improvement to the theory and continuation of this work should be carried out, so that

- Eq.(3) describing the velocity profile, should be written

$$f(n) = (1 - n^n)^2$$

so that the value n = 1.5 adapted for the present theory could be relaxed. Thus the shape of the profile could change when approaching reattachment.

- The effect of forced control flow injection could be taken in account by adding an extra pressure term in Eq.(19). Using one of the three usual switching criteria, the switching point could thus be predicted.

PART II

DESIGN AND CONSTRUCTION OF A BISTABLE AMPLIFIER

1. INTRODUCTION

Wall attachment bistable amplifiers operating in the turbulent flow regime are commercially available since more than ten years. They are characterised by a pressure recovery of about 35%, a pressure gain which is generally below 5, a fan out generally below 4.

An experimental investigation carried out at VKI (Ref.11), on the mechanisms of bistable switching showed that these performances could be improved. The research was conducted, in a first phase, on bistable configurations without splitter and without output ducts. Its purpose was to optimize the geometry of the two straight attachment walls. This was done in the turbulent and in the laminar flow regimes.

In the turbulent regime, the optimal geometry was obtained for the usual value of the aspect ratio $t/w_s = 2$, with a wall angle α of 10°, a wall length L_w equal to 6 to 8 times the nozzle width, and a wall setback a of 1/10 of the nozzle width. For this optimum configuration, the ratio of the supply momentum flux to the minimum control momentum flux required for switching the device was of 48. Furthermore, the average jet dynamic pressure at the end of the attachment wall was about 45% of the supply total pressure.

From this data, it is possible to estimate approximately the performance of the best bistable which would incorporate the optimized attachment walls with the addition of the splitter and output ducts. Thus maximum achievable pressure recovery would also be of 45%. For this estimation the output ducts are supposed to collect all the jet flow, and the losses in the vent region are neglected.

Furthermore the pressure gain, approximately equal to the momentum ratio times the estimated pressure recovery, would be of about 20. These performances compare favourably with those relative to a commercial device.

The tests in the laminar flow regime (Ref.11) demonstrated the possibility, theoretically predicted by Goto and Drzewiecki (Ref.3) of designing a fluidic bistable amplifier based on the wall attachment of a laminar jet. The optimal geometry of the attachment walls was found to be the same as in the turbulent flow case. For such configuration the maximum ratio of supply to control momentum fluxes at switching was lying between 300 and 500. It was therefore concluded that a laminar bistable amplifier could have a much greater gain than a turbulent one.

On the basis of such promising results, it was decided to continue the research described in Ref.11 by designing two bistable amplifiers with splitter and with output ducts, operating respectively in the laminar and the turbulent regimes.

The objective was first to optimize experimentally the geometry of the bistable amplifiers using a large scale model with interchangeable and moveable walls, splitter and output ducts. In a second phase, real scale amplifiers would then be constructed using a chemical etching technique, and would be tested for evaluating their performances.

2. DESIGN STUDY OF A TURBULENT BISTABLE AMPLIFIER

2.1 Introduction

The purpose of this study was to determine a good design for a turbulent bistable amplifier. The assumption was made that the optimization of the attachment walls was independent of that of the splitter and output ducts.

The optimization of the attachment walls had already been carried out (Ref.11) in the case of straight walls. It was therefore decided to complete this research by investigating the effects of wall curvature. Thus the best geometry of attachment walls, straight or curved, would be determined.

A splitter and two additional walls bounding the output ducts, would then be added to this best configuration. The divergence angle of the splitter and of the output ducts, as well as the width and offset of vents would be varied to get the best design.

2.2 The experimental model and test set up

Out of the models used for the previous experimental research (Ref.11), the one having an aspect ratio $t/w_s=2$ was selected for the present study. This choice was made for two reasons : first it is a good bistable configuration according to Ref.11; second this aspect ratio is sufficiently small to guarantee a reasonable simplicity in the manufacture of a miniaturized amplifier.

Fig.28 shows schematically the model, and defines its significant geometrical parameters. The supply settling chamber and nozzle, not shown in Fig.28, have the same planform as the model shown in Fig.2. The control channels have the same width as the supply channel. The splitter and the output walls have a rounded leading edge. The attachment walls, the output walls

and the splitter are moveable, so that a, y and w_v can be varied. The use of interchangeable pieces allows to vary also α, β, γ as well as the attachment wall shape. Five wall shapes, also shown in Fig. 28, were investigated.

Wall type A has the optimal shape according to Ref.11. The others are derived from it by : enlarging and shaping the vent duct (type B); rounding the leading edge (type E); replacing the straight wall by a constant curvature with the leading and the trailing edges at the same location as on the straight wall, and having a leading edge angle of 5° (type C); rotating wall type C around its leading edge by 5° towards the centerline of the bistable (type D).

The main nozzle and one of the control ports were connected to two independently regulated air supplies. The main (supply) and the control flows were measured by two rotameters.

The output volume flow was measured by using the device shown in Fig.28, made of a 200mm long, 20mm internal diameter, cylindrical duct incorporating a total head tube and a static pressure hole. The resulting pressure differential was calibrated by comparison with a rotameter. Static pressures were measured under steady state conditions in the settling chamber of the supply nozzle, as well as in the control channel and in one of the settling chambers connected to the output ducts.

2.3 Tests with attachment walls only

For the five types of walls shown in Fig.28, the control flow required to switch the supply jet was measured. Supply pressure was varied from 400 to 4000 N/m^2. This corresponds to a supply Reynolds number varying from 4,200 to 13,340.

Walls type A, B and E were positioned at a setback (Fig.28) equal to 1/10 of the supply nozzle width. For wall E,

this led to a secondary throat width w' (Fig.28) larger than for wall type A or B. For this reason also a test with w' = w was made, for wall type E.

Walls type C and D were mounted with their leading edge at the same position as the leading edge of wall type A.

Results are given in Fig.29 in terms of the ratio of the required control flow to a reference flow $Q_{sth} = tw_c \sqrt{2p_s/\rho}$. The latter is the ideal supply flow, i.e. calculated assuming a nozzle discharge coefficient of unity.

The results indicate that :

- the change from wall A, having the optimal shape according to Ref. 11, to wall B, having a shaped vent duct has, as could be expected, no influence on the switching. Furthermore, when increasing the supply Reynolds number, the switching flow ratio first varies, then rapidly reaches a constant value. The latter is of 0.12 for Re > 7000 approximately. Taking into account the actual value of the discharge coefficient of the supply nozzle (measured as $C_d = 0.86$) and an estimated value of the output to supply flow recovery ratio (around 1.5), the previous figure leads to an estimated flow gain of the bistable amplifier of about 11.

- with curved walls like type C or type D, the same trend is observed. However a constant switching flow ratio is obtained only for Re > 10,000 approximately. Furthermore, adopting such kind of walls instead of the previous ones does not seem advantageous, because it causes, in the region of Reynolds number independence, an increase in the control flow requirement.

- straight walls with rounded leading edge (type E), when positioned with the same setback as walls A, yield a switching flow ratio of about 0.2 for Re > 8000. This indicates a larger control flow

requirement than in case A. When the secondary throat width, and therefore the setback, are decreased, the required contral flow decreases, but remains dependent on Reynolds number. This of course is an undesirable feature.

One conclusion from these tests can be the adoption of straight walls (type A or B), as a compromise between high flow gain and Reynolds number independence.

An additional remark can be made : in Ref.2, a modified Reynolds number Re'.

$$Re' = R_e/(\ell_s/W_s + 1)(1 + w_s/t)^2$$

is proposed for assessing the condition of Reynolds number independence, i.e.

$$R_e' > 1000$$

In the present case the supply nozzle and contraction are quite long. They were designed in such a way to yield a very regular velocity profile. But when the previous criterion for the minimum Reynolds is applied, one gets ($\ell_s/w_s = 12$ and $t/w_s = 2$)

$$R_e > 29.3 \times 1000$$

This figure is in apparent conflict with some of the results shown in Fig.29, specially for the use of straight walls, where the condition Re > 7000 was found. On the other hand, it justifies the result relative to wall E with $w' = w_s$. Furthermore, it suggests that nozzles much shorter than that shown in Fig.2 should be used for the final design of a bistable amplifier.

2.4 Effects of splitter and output ducts

Using the straight walls (type A) discussed in the previous section, 46 different bistable amplifiers were assembled by varying the vent width w_v, the output walls set-back y and angle α and the splitter angle β. The leading edge of the splitter was located at the same downstream distance from the nozzle as the leading edges of the output walls.

Each configuration was tested to determine its output characteristic curve. The latter relates the output pressure and the output volume flow. All points on such curve are obtained by progressively closing the active outlet. Thus output flow decreases and output pressure increases. Under certain circumstances the maximum output pressure with zero output flow cannot be obtained, because the jet switches to the unrestricted outlet. This undesirable phenomenon, known as load-switching, was found to occur for 22 bistable configurations. For the remaining 24 configurations, the pressure (R_p) and flow (R_q) recoveries, defined as the maximum ratio of an output quantity to the corresponding supply quantity, were derived from the measured curves.

The tests were conducted with control ports either both closed or both open to atmosphere.

The results are summarized in the five following tables. They indicate which configurations are switching under load (LS) and for the others, give the pressure recovery (figures on upper line) and the flow recovery (figure on lower line). When two figures are given for the pressure recovery, the first one replies to the closed control case, the second one to the open control case.

$\alpha=10°$ $L/w_s=8$ $a/w_s=0.1$ $\beta=10°$ $\gamma=10°$

y/w_s ↓ \ w_v/w_s →	2	3	4
0	.49/.44 .99	poor per-form.	poor per-form.
1	L.S.	.36/.38 1.34	.34/.33 1.45
2		.33/.35 1.52	poor per-form.
3		L.S.	L.S.
4		L.S.	

$\alpha=10°$ $L/w_s=8$ $a/w_s=0.1$ $\beta=7.5°$ $\gamma=10°$

y/w_s \ w_e/w_s	1	1.5	1.6	1.82	1.9	2.0	4.0
0	L.S.	L.S.	L.S.	.49/.41 1.33	.47/.41 1.40	.42/.41 1.38	
0.2				L.S.			
0.4				L.S.			
0.5					×.48/.44 1.52		
0.6				L.S.			
0.8						×.48/.44 1.57	
1.0		L.S.		L.S.		× .47 1.5	
1.1						L.S.	
1.2						L.S.	
2.0						L.S.	low R_p

$\alpha=10°$ $L/w_s=8$ $a/w_s=0.1$ $\beta=5°$ $\gamma=10°$

y/w_s \ w_v/w_s	1.5	1.6	1.82	2.0
0	L.S.	L.S.	L.S.	poor perform.
1				.45/.42 1.6
2				L.S.

$\alpha=10°$ $L/w_s=8$ $a/w_s=0.1$ $\beta=10°$ $\gamma=15°$

y/w_s	w_v/w_s = 1.9
0	.42/.35 1.45
0.5	.49/.43 1.57

$\alpha=10°$ $L/w_s=6$ $\bar{a}/w_s=0.1$ $\beta=7.5°$ $\gamma=10°$

y/w_s \ w_e/w_s	1.92	2.42
0	.56/.51 1.20	poor per-form.
0.8	.53/.51 1.40	
1.0	.55/.53 1.38	.45 1.54
1.1	.53/.52 1.38	
1.2	L.S.	
1.5	L.S.	
2.0	L.S.	

Inspection of these tables reveals that :

- switching under load occurs when the vent width is too small, as could be expected, or when the output wall setback y is too large. In other terms, the vent width required to avoid load switching increases with increasing output wall setback. The dotted line on the tables separates the cases in which load switching does occur from the others.
- increasing the vent width causes as could be expected a decrease in pressure recovery, due to turbulent mixing losses, and an increase in flow recovery, due to the increased entrainment of air through the vents.
- increasing the wall offset seems to cause an increase both in flow and pressure recoveries.
- it appears that several designs give good performances. They are indicated by an asterisk in the tables, and are characterized by a pressure recovery above .45 and by a flow recovery above 1.50.

Among these, the design characterized by $\alpha = 10°$, $L/w_s = 8$, $a/w_s = 0.1$, $\beta = 5.5°$, $\gamma = 10°$, $w_e/w_s = 2$ and $y/w_s = 1.0$ was selected for the construction of a fluidic bistable amplifier with smaller dimensions than the model used.

For this configuration, Fig.30 gives the measured output characteristic, in the two cases of controls open or closed, and in the two cases of straight or shaped vents.

2.5 Conclusions and recommendations

As a result of the parametric study undertaken, some geometrical parameters of a bistable amplifier operating in the turbulent regime were optimized.

It was found that straight attachment walls were performing better than curved ones. Straight attachment walls

with rounded leading edge might yield even better performances, though dependent on Reynolds number, thus on supply pressure. Ways of reducing this dependence, eventually by modifying the shape of the supply nozzle should be investigated.

It was found that optimum width of vents and optimum setback of output ducts were respectively of about 2 and 0.5 to 1 times the supply nozzle width. Optimum divergence of output ducts was about 2.5° to 5°.

Furthermore shaping the vent channel (wall type B) has no effect on the input characteristic and improves the output characteristic.

As a conclusion of this study, the silhouette of a turbulent flow bistable amplifier, to be constructed by a chemical etching technique (Section II-4) was designed and is represented in Fig.31. It should have a maximum pressure and flow recoveries respectively of 0.47 and 1.50, together with a maximum flow gain of 11.

3. DESIGN STUDY OF A LAMINAR BISTABLE AMPLIFIER

3.1 Introduction

It is well-known that laminar flow fluidic devices have several advantages over turbulent ones : absence of random fluctuations in the flow, and therefore high signal to noise ratio and accurately defined switching conditions, low power consumption, possibility of miniaturization.

The only existing type of bistable amplifier operating with laminar flow is that designed by Drzewiecki (Ref.12). Its operation is not based on the phenomenon of jet-to-wall attachment, but rather on the instability of the power jet of a laminar proportional amplifier (Ref.13, 14). The device has a pressure gain of 15, a fan out of 8, a power consumption of 3.5 mW, the supply nozzle having a width of 1 mm and a thickness of 0.5mm.

The purpose of the present work was to design another type of laminar flow bistable amplifier, based on jet to wall attachment, a phenomenon which occurs not only in the turbulent flow regime, but also in the laminar one (Ref.11).

In Ref.11, laminar jet to wall attachment was investigated only in the case of bistable configurations without splitter and without output ducts. The aspect ratio t/w_s was of 8 and of 2, and the control ports were closed. To make the design practical, the case of open control ports, with a splitter and two additional walls, bounding the output ducts had to be considered. An aspect ratio of 2 was selected for this further study, because of the resulting simplicity in manufacturing the final device.

3.2 The experimental model and test set up

The model of aspect ratio 2 used in Ref.11 was employed for the present study, with the addition of three extra pieces (splitter and two output walls). The geometry of the model was varied during the research; it is defined by the parameters previously used (Fig.28).

As done in Ref.11, the tests were conducted with water. Indeed with air at low Reynolds numbers, the velocities are too small for accurate measurements. With water, the velocities are 15 times lower than with air, for the same Reynolds number, but flow visualizations are much easier. Furthermore the use of water leads to a more accurate measurement of switching times because they are 15 times greater than in air.

The model was placed in the VKI water table, 1 cm below the free surface. The output settling chamber shown in Fig.28 was removed.

The main nozzle was connected via a rotameter to a regulated water supply. A dye was injected into the settling chamber of the supply nozzle to visualize the flow. Steady state observations of the flow were thus made with the control and output ports independently open or closed.

Dynamic tests were also conducted. For this purpose, a second water supply was connected via a rotameter, to a two-way electrovalve, normally discharging the flow through one of its outputs in the water table. The second output of the electro-valve, normally closed, was connected via a short line of small impedance, to one of the control ports of the bistable model, the other control port being closed. Actuating the electro-valve resulted in an abrupt injection of water into one of the control ports, and this caused the bistable to switch.

This mode of operation is termed here "with controls initially closed". A second mode was achieved by injecting into the control port connected to the electro-valve an additional flow, equal to the flow that would normally be sucked into the control port if it were open. A separate water supply was used for this purpose. Actuating the electro-valve resulted in an abrupt increase, above an initial non-zero value, of the flow rate injected into one of the control ports. The other control port was kept open during all this process, and this mode of operation is termed here " with controls initially open".

The flow in the fluidic device was visualized by injecting a dye in the settling chamber of the supply nozzle and by using water of a different colour to feed the control port.

The switching of the coloured water jet was detected by a lamp-and-photodiode system, located across the initially inactive output channel. The switching time was measured, using an electronic counter, as the time elapsing from the activation of the electro-valve to the detection of the passage of the coloured water in front of the photo-diode.

3.3 Steady state test results

Steady state laminar flow tests were conducted first, with the purpose of determining a configuration exhibiting a bistable behaviour either with controls open or closed, and this independently of the loading or unloading of the outputs.

Fig.32 shows the geometry of the configuration investigated first. With a wall angle of 15°, the setback a was varied from 0.1 w_s to 1 w_s, and the wall length L_w from 6 to 14 times w_s. The triangular splitter was located downstream of the vents.

While such configurations were bistable when the controls were closed, they were not operating satisfactorily

when the controls were open. Indeed, two cases were observed :

- the laminar jet was attaching to one wall, but further downstream, was separating from it and impinging on the splitter leading edge. Thus part of the jet was diverted towards the wrong output. This situation, depicted in Fig.33, was occurring for the longer attachment walls.
- the laminar jet did not attach to the walls, but proceeded straight on and equally divided upon impingement of the splitter. This symmetrical situation, arising with the shorter walls, is depicted in Fig.34.

In order to facilitate the laminar jet attachment, a lower wall angle (α = 10°), as well as another shape for the splitter, as shown in Fig.35, were used, but without success.

It proved necessary to decrease the wall angle to 7° to get a configuration exhibiting bistable behaviour in both cases of closed or open control ports. This configuration, however, was not yet satisfactory, because it was load sensitive : when blocking the active output, switching occurred.

To eliminate this phenomenon of load-switching, two modifications were devised : the increase of the vent dimension w_v, and the decrease of the splitter distance D_{sp}.

The first action proved to be effective, as shown in Fig.36. A stable position with the active output blocked is obtained, no flow being spilled through the other output. However, the required vent dimension to achieve load insensitivity is too great ($w_v = 32\ w_s$), and probably implies a low pressure recovery, or a large sensitivity to external perturbations.

The second action proved to be uneffective, as shown in Fig.37. Indeed blocking the active output causes part of the jet to be deviated towards the other output, by the effect of the sharp splitter. On the other hand operation with outputs

unblocked was satisfactory.

Because of this observed bad effect of the sharp splitter, a blunt one was tried. This gave good results, as shown in Fig.38. Indeed the blunt leading edge of the splitter causes a vortex to form on the separated side of the laminar jet. Such vortex helps in keeping the jet attached to the wall, when the active output is blocked. This phenomenon, occurring here in laminar flow is similar to the well-known one (Ref.15) occurring in conventional turbulent flow bistables having blunt or cusped splitters.

The geometry of the final laminar flow device, bistable with control ports closed or open, is shown in Fig.39.

Because of the expected difficulties in accurately manufacturing the splitter in a miniaturized device, a further study was made on the effect of splitter shape and position. The following conclusions were drawn :

- the splitter has to be blunt, without rounded edges,
- the splitter width may be increased, except in the vicinity of its leading edge, where a nominal length of 1 w_s, with a width of 0.8 w_s has to be provided.
- the splitter distance may be varied from 12.6 to 16.4 times w_s.

3.4 Dynamic switching test results

For the two bistable configurations similar to that shown in Fig.39 and having D_{sp}/w_s = 12.6 and 16.4, the switching times were measured as explained in section 3.2. They are given in Figs 40 to 47, versus the amplitude of the step in the control momentum flux. Such curves are called "dynamic switching characteristics". The four cases of operation with controls and outputs open or blocked were considered. In the case of operation with

controls "initially open" (Section 3.2), also the momentum flux J_{ci} of the flow entrained into the control port prior to the application of the control step, is given in the figures.

The tests were carried out for four values varying from 350 to 1500 of the Reynolds number based on the average supply velocity and the nozzle width.

The minimum ratio of control to supply momentum flux required for switching can be derived from figures 40 to 47. The reciprocal of this quantity is proportional to the maximum, or steady state, gain. Also the switching time for an arbitrary ratio of supply to control momentum flux, for instance 1/20, can be derived from the figures. The effect on these two parameters, of a variation in splitter position D, in supply Reynolds number, and in the operating condition (controls and outputs open or closed) is shown in the following table. In the latter the first figure is 1000 $(J_c/J_s)_{min}$, the second is $\tau_{(J_s=20J_c)}$(sec).

Inspection of this table, and of Figs 40 to 47 shows that :

- the dynamic switching characteristics are Reynolds dependent. An increase in Reynolds number causes a decrease in switching time and in increase in the minimum control to supply momentum ratio, and therefore a decrease in maximum gain.

The dependence of the maximum gain on Reynolds number is equally strong in all the 32 cases investigated : by increasing the Reynolds number by less than one order of magnitude, the gain decreases of more than one order of magnitude. Only the case where D/w_s = 16.4, Re = 650 to 900, with controls open, is an exception.

The dependence of switching time on the Reynolds number is stronger when the splitter is located closer to the nozzle.

LAMINAR FLOW BISTABLE

$t/w_s = 2$ $\alpha = 7°$ $L_w/W_s = 12$ $a/w_s = 0.3$

	Controls	Outputs	$1000(J_c/J_s)_{min}$ and $\tau_{(J_s=20J_c)}$ (sec)							
			Re = 350		Re = 700		Re = 1060		Re = 1420	
D/w_s = = 12.6	closed	open	1.78	5.1	5.55	1.6	32.5	2.3	46.0	2.1
	closed	closed	1.79	4.2	9.68	3.0	13.0	2.8	19.8	2.5
	open	open	1.07	3.1	9.35	3.6	33.3	0.9	45.9	-
	open	closed	0.54	-	12.9	4.0	47.2	8.0	79.2	-
			Re = 650		Re = 900		Re = 1200		Re = 1500	
D/w_s = = 16.4	closed	open	1.04	1.8	6.63	2.0	53.4	-	36.7	-
	closed	closed	1.61	3.0	5.22	3.0	53.3	-	50.5	-
	open	open	3.52	2.5	2.61	2.4	21.4	2.2	79.2	-
	open	closed	5.71	2.8	2.16	2.5	29.6	3.0	90.2	-

Operating the device with the controls initially open or closed (i.e. respectively with or without vents in the control channels) does not modify this Reynolds number dependence. On the other hand, blocking the outputs causes a decrease in this dependence in the case of the shorter splitter distance D, and a small increase in the other case.

- the dynamic switching characteristics at a given Reynolds number are more dependent on the output condition (open or closed) in the case of the shorter splitter distance than in the other case.
- the best configuration appears to be that with $D/w_s = 16.4$, operated at moderately low Reynolds numbers (around 900, a decrease down to 650 being acceptable but not an increase up to 1200), and with control channels open (or vented). A value of about 1/400 for the minimum ratio of control to supply momentum flux is obtained. For a value of 1/20 of this ratio, a switching time of 2.5 seconds is obtained. For a practical device, about 10 times smaller than the model and operated with air rather than water, this switching time, proportional to w_s^2/ν, scales down to 1.7 ms. This data also indicates that, assuming a reasonable pressure recovery of 40%, a maximum momentum gain of 160 could be reached.

3.5 Design and scaling of the laminar bistable amplifier

A practical device will have much smaller dimensions than the model used here and will be operated with air. As in the turbulent flow case, geometric similarity will be used to scale down the device. Dynamic similarity will be imposed by operating the real device at the same Reynolds number as the model. Thus decreasing the bistable dimensions will lead to increasing supply velocities and pressures, as well as power consumption as indicated by the following relations :

average supply velocity	$U_o = Re \frac{\gamma}{w_s}$
supply volume flow	$Q = Re \frac{t}{w_s} \nu w_s$
supply pressure	$p_s = \frac{\rho}{2} Re^2 \frac{\nu^2}{w_s}$
supply power	$P = \frac{\rho}{2} \frac{t}{w} Re^3 \nu^3 \frac{1}{w_s}$

Two limits will be met in this miniaturization process : technological difficulties in manufacturing small nozzles, of about 0.1 mm width, and the occurrence of compressible flow phenomena in the supply nozzle. This indeed changes the nature of the flow field in the interaction region of the bistable. It leads to the limit

$$w_s > Re \frac{\nu}{C.M}$$

where C is the sonic velocity, and M the maximum acceptable Mach number. Assuming M=0.6, and for air at normal conditions

$$w_s > 7.3 \ 10^{-8} Re$$

For a Reynolds number of 900, this leads to the limit

$$w_s > 0{,}066 \text{ mm}$$

This indicates that at a Reynolds number of 900, compressible flow would occur for a nozzle width smaller than the smallest width (0.1 mm) that it is possible to manufacture. For this latter width, compressible flow would occur when the Reynolds number exceeds 1370.

This also indicates that selecting a laminar flow bistable instead of a turbulent one is a necessary step towards miniaturization.

The performance of a scaled down bistable amplifier, operated at the same Reynolds number as the original model, is described by non-dimensional parameters. One of them is the ratio of a control quantity (flow rate, momentum flux, or pressure) to the corresponding supply quantity. Another one is the non-dimensional switching time, which can be defined as $\tau\nu/w^2$. The use of this parameter instead of the more usual $\tau U_0/w_s$ is preferred here, because it directly relates, for a given fluid, switching time to geometrical scale.

As an example the following table gives the characteristics of a scaled down laminar bistable amplifier. These have been evaluated from the results of the tests conducted with water on the bistable model yielding the best performances, having w_s = 2.5 mm and operated at a Reynolds number of 900.

Nozzle width (mm)	Air flow consumption (lt/h)	Supply pressure (kN/m^2)	Supply power (mW)	Switching time for J_c/J_s=1/20 (ms)
0.5	48.5	0.45	6	6.7
0.3	29.1	1.24	10	2.4
0.2	19.4	2.79	15	1.1
0.1	9.7	11.16	30	.27

A silhouette of the laminar bistable amplifier here proposed is given in Fig.48.

3.6 Conclusions and recommendations

A wall attachment bistable amplifier operating in the laminar flow regime was designed.

Its performances compare favourably with those of a turbulent flow bistable amplifier. They are in the same range as those of the laminar bistable designed by Drzeviecki at HDL (Ref.12). The VKI design, however, is operated at a larger supply Reynolds

number than the HDL design. It has then a larger power consumption, for the same cross section of supply nozzle (0.5 mm^2), but also a greater steady state gain.

Extreme care has to be taken in the fabrication process to correctly reproduce the blunt shape of the splitter.

4. CHEMICAL ETCHING TECHNIQUE FOR FABRICATING FLUIDIC DEVICES

4.1 Introduction

A well-known method for fabricating devices is the chemical etching of several thin metal foils, which are then piled up together (Ref.16). A bistable amplifier constructed at the VKI using this technique is shown in Fig.49.

This process consists of covering the metal foil with a "photoresist" film which has the property of polymerizing under the action of UV light. Then the foil is exposed to UV light through a mask, reproducing the pattern to be etched. An organic solvent is used to eliminate the non polymerized areas of the photoresist film, and the metal below these is etched off by attack of a chemical agent (acid or alkali).

This process is reasonably well-known (Ref.17). Good photoresists are commercially available. Specialized films carry out excellent etchings (Ref.18), at the expense of moderately large investments.

The purpose of this study was to assess the possibility of carrying out in-house etchings of reasonably good quality, with minimal investment. For this purpose, several simplifications and modifications to the processes described in Ref.17, and in particular to the mask preparation, to the photoresist treatment and to the final etching, had to be made.

Etching tests were then made, with the purpose of determining the conditions for getting good quality products (i.e. with minimal and constant overetch) in the minimal time, and therefore with high etch rates.

4.2 Description of the process used

4.2.1 Mask preparation

As usual, the mask was obtained by photographic reduction of a larger scale drawing made on Mylar film or on any other drafting film dimensionally stable. A coordinatograph should normally be used for preparing the large scale drawing. Because this is an expensive piece of equipment, a normal drawing of the mask contour was made with pencil on a matte drafting film. Black adhesive tape of calibrated width was then used to manually fill in the light absorbing areas of the mask. This tape is normally available from the manufacturers of materials for electronic printed circuits.

The large scale artwork was then photographically reduced from 8:1 to 32:1, in several steps. The VKI photographic lab was already equipped for this kind of work. The final mask was made of two identical negative films, exactly superposed and fixed one to the other along, one of their edges, using adhesive tape. Reference crosses were made on the original drawing to allow a correct assembly to the two films under microscope observation.

As an example, a mask used for the fabrication of turbulent bistable amplifiers is reproduced in real dimensions in Fig. 50.

4.2.2 Photoresist treatment

Copper is the easiest material to be chemically etched, and was thus selected for the present application. As a consequence, the Kodak liquid photoresist KPR was also selected. It was deposited on a 0.1 mm thick copper plate, using the "dip-coating" technique. The plate had to be thoroughly cleaned before applying this coating. Cleaning was made with a usual house-hold product

for brass and copper. Scratches had to be absolutely avoided. A 10 seconds dip in a 10 % HCl solution was used to complete the cleaning.

Prebaking the dryed photoresist film, exposing to UV light, developping the photoresist image, and post-baking it were carried out as suggested in Ref.17. Eight high pressure mercury vapour lamps of 125 watts were used to expose the copper plate, placed in between the two negatives of the mask.

4.2.3 Etching

A ferric chloride solution is usually employed to etch copper. This is done in special machines where air-less sprays of the etching solution are directed against the metal plate. Movement of the spray nozzles to uniformly cover the plate is provided, as well as continuous filtration and heating at constant temperature of the etchant. Because the latter is very corrosive, all parts in contact with it must be made of ceramic, plastic, glass, or titanium. These machines, well adapted to moderately large production rates, are rather expensive.

Another approach requiring minimal investment, was adopted at the VKI. The copper plates were etched by simple immersion in a ferric chloride solution at ambient temperature. Still etching baths were first used. Agitating the bath by using a low speed rotating mixer or by tilting periodically the etchant container was also tried.

4.3 Results

Straight channels were etched in to 0.1 mm thick copper plates, immerged in still or agitated baths of ferric chloride solution.

The rate of copper removal, expressed in μ/min, and the overetch, expressed in μ and defined by comparison of the etched plate with the original mask, were measured.

These are given in Fig.51 for a still bath, as function of the depth below the liquid free surface. Inspection of this figure shows that :

- an increase in Fe Cl_3 concentration causes a decrease in over-etch. Also a decrease in etch rate is obtained for concentration greater than 40°B.
- Overetch and etch rate do not vary with the depth of the copper plate below the free surface level, except in the first 3 cm below free surface level, where etching is more intense and in the 3 to 4 cm above the bottom of the Fe Cl_3 container, where etching is slow. This is probably due to accumulation of the by products of the chemical reaction.
- The over-etch depends on the width of the etched channel.
- A fresh etchant yields higher etch rates than a used one. Etching rates are halved when approximately 2 mm^3 of copper per cm^3 of Fe Cl_3 solution have been etched.
- An etch rate of 1μ/min is unacceptably low : it means that it would take 1 h 40' to etch a 0.1 mm thick plate.
- An overetch varying from about 80 to 140 μ is obtained. This figure, of the same order as the plate thickness, is unacceptably large.

Still etching is therefore unsatisfactory, and tests were thus carried out by agitating the etching bath with a mixer. Two kinds of mixer were used : a simple one, L shaped, made from a bent glass rod of 5 mm diameter, and a second one, made of a rectangular 40 mm x 100 mm plate glued on a straight glass rod. These two mixers were rotated around a vertical axis at a speed of 670 RPM and 540 RPM respectively. The etching solution was placed in a cylindrical container, having its axis coinciding with that of the mixer. The plates to be etched were placed either parallel or perpendicular to the motion of the etching fluid.

Results are given in Fig.52. It may be seen that the motion of the etching fluid has a very strong influence on the chemical reaction. Furthermore, it is essential to have almost constant etch rates in all the bath, otherwise non-uniform and excessive overetches will be obtained (curve A). The trend of curve A can be explained considering that the L shaped mixer mainly agitates the lower part of the bath.

Curve C represents the best etching procedure. It means that the fluid must impinge perpendicularly onto the plate. Again the increase in overetch towards the bottom is due to the L shaped mixer.

Curves B and D demonstrate that with a mixer which should induce near the plate fluid velocities approximately constant, reasonably constant etch rates are also obtained. They are however much lower than in the previous cases A and C. This is parlty due to the lower rotational speed of the mixer, and partly to the higher $Fe\ Cl_3$ Beaumé density. The latter alone causes (Fig.51) a decrease of 33% in etching rate.

The following conclusions can be drawn :

- the etching bath must be agitated,
- this agitation must be uniform,
- positioning the plate parallel or perpendicular to the motion of the fluid has no effect on the minimum overetch,
- positioning the plate perpendicular to the motion of the fluid yields higher etch rates.

As a result of this study, the etching apparatus shown in Fig.53 was constructed. The periodic tilting of the etching bath provides uniform agitation, with velocities parallel to the place to be etched. This does not minimize etching time, but is the simplestand more economical apparatus. Tilting frequency is about 0.5 Hz.

4.4. Products

The bistable silhouette shown in Fig.31 was chemically etched on 0.1 mm thick copper plates, by using the process previously described. Several etchings were made with nominal nozzle widths of 1.0 mm, 0.5 mm and 0.25 mm. A photographic enlargement of this last etching obtained using the mask shown in Fig.50 is reproduced in Fig.54. The width of the rectangular plate is 8.90 mm in reality, and therefore magnification of Fig.52 is 9.89. Thus real width of supply and control nozzles can be measured. They are of 0.27 mm and 0.30 mm respectively, instead of 0.25 mm nominal. The difference between the width of the supply and control channels is probably due to the fact that the velocity in the etching bath is directed parallel to the supply nozzle and perpendicular to the control ones. Over-etch is therefore of 10 μ for the supply channel and 25 μ for the control channels. Etching time was 50 minutes, and therefore the etch rate was about 2 μ/min. These figures compare favourably with the results of the preliminary etching tests described in the previous section.

Fig.54 represents a sample out of a batch of 80 units. 14 units in this batch had to be rejected because they showed visible defects. The latter were mainly incomplete etching of channels. On the other hand when this study was undertaken, the defects were mainly localized over etch, or pin holes caused by bad photoresist adherence to the plate resulting from poor plate cleaning prior to photoresist application. Results presently obtained show therefore that the steps taken to improve plate cleaning were essential and effective.

4.5 Conclusions and recommendations

In house etching of copper plates with a minimal amount of investment proved to yield products of reasonable quality. An improvement to the process could be made by providing a continuous change in the direction of the velocities in the agitated etching bath.

5. TESTING OF BISTABLE AMPLIFIERS CONSTRUCTED BY CHEMICAL ETCHING

5.1 Description of tests

The purpose of this study was to check the performance of the turbulent bistable amplifier previously designed (Fig.31) and constructed using a chemical etching technique.

Tests were conducted on a bistable having a nominal width of the supply nozzle of 1 mm. The supply, output and input characteristics were determined in steady state operation.

Static pressures were measured in the 4 mm internal diameter plastic tubing connected to the supply, control and output ports of the bistable amplifier. Supply and control flow rates were measured using two rotameters. Output flow rates were obtained from the measurement of total and static pressures in a portion of rigid 4 mm internal diameter tubing connected to the output ports. For this purpose, a miniature pitot probe was mounted in the centerline of the output tubing.

5.2 Test results

Fig. 55 shows the measured supply characteristics, relating supply flow rate to supply pressure. The curve is dependent on the configuration of control channels (open or closed). Furthermore the discharge coefficient is rather low, about 0.77 and 0.86 with controls respectively open or closed.

Fig.56 shows the two characteristics measured at the two outputs. Again they depend on control configuration (open or closed). Furthermore the curves for the two outputs do not coincide. This indicates that the bistable is not exactly symmetrical, and therefore that appropriate steps have to be taken to improve the symmetry of the etched plates.

The maximum pressure recoveries (0.41 with controls open, 0.37 with controls closed) are smaller than expected (0.47). Scaling effects or inaccuracies in the etching process account for these differences.

The maximum flow recoveries are also smaller than expected. This is due to a restriction to the flow cross sectional area, existing between the output duct (8 mm^2) and the outlet tubing (3.14 mm^2).

Fig. 57 indicates a weak variation of the maximum pressure but not of the maximum flow recovery with the supply pressure. The range of supply pressures yielding bistable operation was found to be limited (from about 2 to 16 kN/m^2).

Fig. 58 gives the input characteristics, relating flow and pressure at each control ports. The characteristics are dependent on the output configuration (open or blocked). Furthermore it can be seen that again the device is not exactly symmetrical. Switching of the bistable occurs for control flow rates higher than expected.

A variation in the supply pressure between 2 to 16 kN/m^2 causes almost no variation on the ratio of the control to supply flow at switching. On the other hand, the effect of supply pressure on the control pressure at switching is illustrated in Fig.52. Again a strong non symmetricity is evident.

After these tests the bistable was disassembled and the etched plates examined.
No apparent asymmetry was noticed. On the other hand, because of the overetch, dimensions were slightly altered with respect to the nominal ones. Indeed the bistable tested was etched in a still $Fe\,Cl_3$ bath, and as explained in previous section, this does not minimize overetch. Thus nozzle width was 1.02 mm instead of 1 mm. This causes a reduction in the non-dimensional setback a/w_s and length L_w/w_s of the attachment wall. These etching

inaccuracies can account for the poor agreement between the results of the present tests and of the previous carried out on a large scale bistable model.

5.3 Conclusions and recommendations

The bistable tested was not symmetrical, and its performances were lower than expected.

Symmetricity could be obtained by alternating normally mounted and inverted etched plates.

On the other hand the over etch has to be compensated by a corresponding oversizing of the mask used to expose the photoresist.

APPENDIX A : SYSTEM OF EQUATIONS DESCRIBING THE JET TO WALL ATTACHMENT

A-1 The closed control case

A-1-1 At an arbitrary flow section

The eleven equations listed in section I-3.5.1 and derived in Ref.9 are given here below. Equations 6,7,12b,12c, 14 erroneously written in Ref.9 have here been suitably corrected.

Spread of the outer shear layer of the jet

It is assumed, as for a free jet, that

$$b_e = E_e \cdot X, \text{ with } E_e = 0{,}274 \tag{4}$$

Spread of the inner shear layer of the jet

It is assumed, as for a free jet, that

$$b_i = E_i \cdot X, \text{ with } E_i = 0{,}274 \tag{5a}$$

if $\ell_i > 0$, i.e. if the jet boundary does not touch the wall. Otherwise, Eq.(5a) is replaced by the identity

$$\ell_i = 0 \tag{5b}$$

and b_i is given by the available space between the jet and the attachment wall (see Eq.(7)).

Geometrical relation for the spacing between the outer jet edge and the wall

from Fig.(23)

$$(R + b_c + b_e + \ell_e)_N \cos(\alpha + \Phi_N) = (R + b_c + b_e + \ell_e)_{N-1} \cos(\alpha + \Phi_{N-1}) \tag{6}$$

Here suffixes N-1 and N refer to two adjacent flow sections, and Φ is the angle between the nozzle exit plane and any flow section.

Geometrical relation for the spacing between inner jet edge and attachment wall

Again from Fig.23

$$(R - b_c - b_i - \ell_i)_N \cos(\alpha - \Phi_N) = (R - b_c - b_i - \ell_i)_{N-1} \cos(\alpha - \Phi_{N-1}) \qquad (7)$$

Eqs 6 and 7 are here written in a simplified form with respect to that reported in Ref.9, where an unnecessary distinction between the case $R > 0$ and $R < 0$ as well as two errors in signs in the $R < 0$ case were made. This had no consequence on the results, because R was always positive.

Continuity equation for the outer half jet

Assuming that the jet centerline is a streamline, the mass conservation equation can be written as

$$Q_{s,e} = \left[\int_0^{b_c+b_e+\ell_e} u \, dy \right]_X$$

where $Q_{s,e} = R\, U_{max.e} (e^{W_s/2R} - 1)$ (8a)

is the flow rate emitted through the outer half of the supply nozzle. Because the velocity profile is not symmetric, this quantity differs from the analogous one ($Q_{s,i}$) relative to the inner half of the jet.

By using Eq.(1) and Eq.(3) for u, the integrals can be calculated. This leads to the expression :

$$U_{rme} = \frac{- U_{max.e}\, b_e \left[0{,}45 + \frac{R}{b_e} \left(e^{b_c/R} - 1 \right) \right] + Q_{s,e}}{\ell_e + 0.55\, b_e} \qquad (8)$$

Continuity equation for the inner half jet

The mass conservation condition is written as

$$Q_{si} = \left| \int_{-b_c - b_i - \ell_i}^{0} u \, dy \right|_X$$

where $Q_{si} = R\, U_{max.i} \left(1 - e^{-W_s/2R} \right)$ (9a)

is the flow rate emitted through the inner half of the supply nozzle.

This leads, with Eq.(1) and Eq.(3), to the expression

$$U_{rmi} = \frac{- U_{max.i}\, b_i \left[0.45 + \frac{R}{b_i} \left(1 - e^{-b_c/R} \right) \right] + Q_{s,i}}{\ell_i + 0.55\, b_i} \qquad (9b)$$

Bernoulli equation for the external flow

Because the flow in the region outside the curved outer boundary of the jet is irrotational and comes from the still atmosphere, the relative pressure in such region is given by

$$p_e = - \frac{\rho}{2} \, U_{rme}^2 / \cos^2 (\alpha + \phi) \qquad (10)$$

where U_{rme} is the component, normal to the flow section, of the velocity which is directed parallel to the outer wall.

Additional relation between $U_{max.e}$ and U_{rme}

This expression is obtained by equating the value of p_e given by Eq.(10) to the following one :

$$p_e = p_t - \frac{9}{2} U^2_{max.e} + \frac{9}{R} \int_{b_c}^{b_c+b_e} u^2 \, dy$$

obtained by using :

- Bernoulli's equation to predict the static pressure at the potential core edge, knowing the total pressure p_t of the supply flow.
- a momentum balance to predict the static pressure variation across the outer shear layer of the jet.

After evaluating the integral using Eq.(1) and Eq.(3), one gets

$$\frac{\rho}{2} U^2_{max.e} = p_t + \frac{\rho}{2} \frac{U^2_{rme}}{\cos^2(\alpha + \phi)} + \rho \frac{b_e}{R} \left[\frac{243}{270} (U_{max.e} - U_{rme})^2 + \right.$$

$$\left. + 0,9(U_{max.e} - U_{rme}) U_{rme} + U^2_{rme} \right] \qquad (11)$$

Momentum balance across the jet

Consider, in the inner half of the curved jet, the streamline dividing the supply flow from the flow that has been entrained in the jet. It originates obviously at the inner nozzle edge and terminates at the attachment point, and therefore bounds, in the closed control case, the recirculating bubble. The pressure p_i at the bubble boundary can be obtained from a momentum balance across the jet

$$p_e - p_i = \frac{\rho}{R} \int_{-(b_c+b_d)}^{b_c+b_e} U^2 \, dy \qquad (12a)$$

where the Y-coordinate of the dividing streamline, defined as $-(b_c + b_d)$ can be determined from a mass conservation condition

$$Q_{s,i} = \left| \int_{-(b_c+b_d)}^{0} u \, dy \right|_X \qquad (12b)$$

Again, using Eq.(1) and Eq.(3) to integrate these expressions, one gets, from the momentum balance :

$$p_e - p_i = \rho \frac{b_e}{R} \left[\frac{243}{770}(U_{max.e} - U_{rme})^2 + 0,9(U_{max.e} - U_{rme})U_{rme} + U_{rme}^2 \right]$$

$$+ \frac{\rho}{2} (U_{max.i}^2 - U_{max.e}^2)$$

$$+ \rho \frac{b_i}{R} \left[(U_{max.i} - U_{rmi})^2 (\eta_d - 1.6\eta_d^{2.5} + 1.5\eta_d^4 - \frac{8}{11} \eta_d^{5.5} + \right.$$

$$\left. + \frac{1}{7} \eta_d^7) + 2(U_{max.i} - U_{rmi})U_{rmi}(\eta_d - 0.4\eta_d^{2.5} + 0.25\eta_d^4) \right.$$

$$\left. + U_{rmi}^2 \eta_d \right] \qquad (12)$$

From the continuity equation defining $\eta_d = b_d/b_i$ (Eq.(12b)) one gets

$$R\, U_{max.i}(1 - e^{-b_c/R}) + U_{rmi}\, b_i\, \eta_d + (U_{max.i} - U_{rmi})b_i \cdot$$

$$\cdot (\eta_d - 0.8\eta_d^{2.5} + 0.25\eta_d^4) = Q_{si} \qquad (12c)$$

where Q_{si} is expressed by Eq.(9b).

Momentum conservation in the jet along X-direction

This condition, derived in Ref.9 by integrating the Navier-Stokes equation first along Y from the inner to the outer jet boundary - and then along X, can also be directly written in integral form as

$$\int_{-b_i-b_c}^{b_e+b_c} (p + \rho u^2)\,dy - \int_{-W_s/2}^{W_s/2} (p + \rho u^2)_{x=o}\,dy - \int_0^X \left[\frac{d(b_e + b_c)}{dx} \right.$$

$$\left. (p_e + \rho U_{rme}^2) + \rho U_{rme} (- v_e) \right] dx - \int_0^X \left[\frac{d(b_i + b_c)}{dx} \right.$$

$$\left. (p_i + \rho U_{rmi}^2) + \rho U_{rmi}\, v_i \right] dx = 0$$

where v_e and v_i, transversal velocity components at the outer and inner jet boundaries are given by

$$v_e = U_{rme}\, tg(\Phi + \alpha)$$

$$v_i = U_{rmi}\, tg(\Phi - \alpha)$$

and where the function p(y), static pressure in the jet, is given by a momentum balance in the Y-direction

$$p_e - p(y) = \frac{\rho}{R} \int_y^{b_e+b_c} u^2\, dy,$$

p_e being given by Eq.(10).

It is shown in Ref.9 that the third integral in the X-momentum equation as well as the term $\rho U_{rmi} v_i$ in the fourth integral, are one to two orders of magnitude smaller than the second integral in the same equation, and can thus be neglected.

Using Eq.(1) and Eq.(2) to evaluate the integrals, one can thus get the following relation

$$\rho b_e \left[\frac{243}{770} (U_{max.e} - U_{rme})^2 + 0.9 (U_{max.e} - U_{rme}) U_{rme} + U_{rme}^2 \right]$$

$$+ \rho b_i \left[\frac{243}{770} (U_{max.i} - U_{rmi})^2 + 0.9 (U_{max.i} - U_{rmi}) U_{rmi} + U_{rmi}^2 \right]$$

$$+ 2b_c p_t + \rho \frac{R}{4} (U_{max.i}^2 - U_{max.e}^2)$$

$$+ b_e p_e + \rho \frac{b_e^2}{R} \left[\frac{18771}{280280} (U_{max.e} - U_{rme})^2 + \frac{18}{70} (U_{max.e} - U_{rme}) U_{rme} + \frac{1}{2} U_{rme}^2 \right]$$

$$+ b_i p_i + \rho \frac{b_i^2}{R} \left[\frac{18771}{280280} (U_{max.i} - U_{rmi})^2 + \frac{18}{70} (U_{max.i} - U_{rmi}) U_{rmi} + \frac{1}{2} U_{rmi}^2 \right]$$

$$- W_s p_t - \rho \left[\frac{R}{4} (U_{max.i}^2 - U_{max.e}^2) \right]_{X=0} - \int_0^X (p_i + U_{rmi}^2) \frac{d(b_i + b_c)}{dx} dx = 0 \qquad (13)$$

where the last integral can be approximated as :

$$\int_0^X (p_i + \rho U_{rmi}^2) \frac{d(b_i + b_c)}{dx} dx = \sum_{j=1}^{N} \left[(p_{i.j} + \rho U_{rmi.j}^2)(b_{i.j} + b_{c.j} - b_{i.j-1} - b_{c.j-1}) R_j (\Phi_j - \Phi_{j-1}) \right]$$

Momentum conservation in the separation bubble

A control volume is defined, as bounded by two adjacent flow sections, the attachment wall and the dividing streamline. The momentum balance is written in the direction of the wall, neglecting the wall shear stresses, as follows

$$\left[J_f + J_r + p_i\,(\ell_i + b_i - b_d)\right]_{N-1} \cos(\Phi_{N-1} - \alpha) + \int_{X_{d.N-1}}^{X_{d.N}} p_i \sin(\alpha - \Phi)\, dx_d = \left[J_f + J_r + p_i(\ell_i + b_i - b_d)\right]_N \cos(\Phi_N - \alpha) - \int_{X_{d.N-1}}^{K_{d.N}} \tau_d \cos(\Phi - \alpha)\, dX_d \qquad (14a)$$

for the N-th control volume, and

$$p_i a_i \cos\alpha + \int_0^{X_{d.1}} p_i \sin(\alpha - \Phi)\, d X_d = \qquad (14b)$$

$$= \left[J_{f,1} + J_{r,1} + p_{i,1}(\ell_{i1} + b_{i1} - b_{d1})\right] \cos(\Phi_1 - \alpha) - \int_0^{X_{d.1}} \tau_d \cos(\Phi - \alpha)\, d X_d$$

for the first control volume.

These relation differ from those originally established in Ref.3, where the term $(\ell_i + b_i - b_d)$ was uncorrectly replaced by ℓ_i.

In these relations X_d is the length measured along the dividing streamline, and the momenta of the forward and reverse flows J_f and J_r are given by the relation

$$J_f + J_r = \int_{-b_c-b_i}^{-b_c-b_d} \rho u^2 \, dy + \int_{-b_c-b_i-\ell_i}^{-b_c-b_i} \rho U_{rmi}^2 \, dy =$$

$$= \rho b_i \left[(U_{max.i} - U_{rmi})^2 \left(\frac{243}{770} - \eta_d + 1.6\eta_d^{2.5} - 1.5\eta_d^4 + \frac{8}{11}\eta_d^{5.5} - \frac{1}{7}\eta_d^7 \right) + \right.$$

$$+ (U_{max.i} - U_{rmi}) U_{rmi} \left(0.9 - 2\eta_d + 1.6\eta_d^{2.5} - \frac{1}{2}\eta_d^4 \right)$$

$$\left. + U_{rmi}^2 (1 - \eta_d) \right] + \rho \ell_i U_{rmi}^2$$

obtained by using Eq.(3) for the velocity in the bubble.

The turbulent shear stress along the dividing streamline, τ_d is, according to Prandtl's constant diffusivity theory (Ref.7) and following Sawyer's assumption for curved jets (Ref.10) given by

$$\tau = \rho\varepsilon \left(\frac{\partial u}{\partial y} - K_2 \frac{u}{R} \right)$$

where the apparent viscosity ε is given by

$$\varepsilon = \frac{K_1}{E_i} b_i \, (U_{max.i} - U_{rmi})$$

and where Eq.(3) is again used for the velocity u.

Furthermore, the two integrals in Eq.(14) are approximated by expressing the differential term as

$$dX_d = (R - b_c - b_d)\, d\Phi$$

and by assuming p_i, τ_d, Φ, b_c and b_d to be given by the arithmetic average of their values at section N-1 and N. In Ref.9, an incorrect expression, with the term b_c missing was adopted in place of the previous relation.

Auxiliary relation for the potential core width

This relation will be used in the numerical computation to provide a good guess for the value of b_c, required to initiate an iteration process leading to the exact value of b_c. For this first guess, the potential core width will be assumed to be the same as that of a free jet, i.e.

$$b_c = \frac{W_s}{2}\left(1 - \frac{X}{5{,}77\ W_s}\right) \qquad (13a)$$

A-1-2At the first flow section

At the first flow section (X=0), the previously established system of twelve equations degenerates into 7 identities (deriving respectively from Eqs (4)(5)(6)(7)(13)(8) and (9) :

$$b_e = b_i = 0 \qquad \ell_i = a_i \qquad \ell_e = a_e \qquad b_c = W_s/2$$

$$U_{rme} = U_{rmi} = 0$$

and 4 equations only, one of the equations of the original system having disappeared. Indeed

- Eq.(2) remains unchanged,
- Eq.(10), which would lead to $p_e = 0$, is replaced by

$$p_e = - \frac{\rho}{2} v_e^2 \qquad (10')$$

where v_e, the entrainment velocity outside the jet, is given by the continuity equation

$$v_e = - \int_0^{b_c+b_e} \frac{\partial u}{\partial x} \, dy$$

which, using Eq.(1), (3) and (4) gives for X = 0

$$v_e = U_{max.e} \left(\frac{e^{W_s/2R}}{11.54} - 0.45E \right) \qquad (10")$$

- Eq.(11) reduces to Bernoulli equation at outer jet edge :

$$p_e = p_t - \frac{\rho}{2} U_{max.e}^2 \qquad (11')$$

- Eq.(12) reduces to

$$p_e - p_i = \frac{\rho}{2} \left(U_{max.i}^2 - U_{max.e}^2 \right)$$

which combined with Eq.(11'), yields

$$\frac{\rho}{2} U_{max.i}^2 = p_t - p_i \qquad (12')$$

- Eq.(14) loses its meaning and disappears.

Furthermore, it is convenient to replace Eqs (10', 10") by the following expression

$$R = -2W_s \Big/ \ell n \frac{p_t}{(p_t - p_i)\left[1 - \left(\frac{1}{11.54} - 0.45E\right)^2\right]} \qquad (10"')$$

obtained by combining together equations (2), (10' & 10"), (11'), (12').

Because the resulting system consists of four equations in five unknowns, an arbitrary value has to be given to one unknown. p_i was selected as the quantity to be fixed, because experimental results show that its ratio to p_t, total jet pressure, is approximately constant. Indeed, for the various combinations of attachment wall setback and angle used in bistable amplifiers, one has (Refs 4 and 9)

$$\left(\frac{p_i}{p_t}\right)_{X=0} \simeq -0.15$$

The following values have been used for the calculation :

α	a/W_s	p_i/p_t
10°	0.1	-0.165
	1	-0,150
	2	-0,115
15°	1	-0,165

A-2 The open control case

A-2-1 Initial control volume

The five equations listed in section I-3.5.2.1 and derived in Ref.9 are given here below. Eqs (16) and (19) erroneously written in Ref.9, have here been suitably corrected.

Momentum conservation in the separation bubble

This equation, which replaces Eq.(14b) written for the closed controls case, is :

$$p_i a_i \cos\alpha + \int_0^{X_{d,1}} p_i \sin(\alpha - \Phi)\, dX_d = \left[J_{f,1} + \int_{-b_c-b_i-\ell_i}^{-b_c-b_d} p(X,Y)dy \right]$$

$$\cos(\alpha - \Phi_1) - \int_0^{X_{d,1}} \tau_d \cos(\alpha - \Phi)dX_d + J_{c,i} \sin\alpha \quad (15)$$

where all the terms are calculated as in section A-1.1, except
- the control flow momentum $J_{c,i}$ which is derived from the experimental correlation $J_c = f(Q_c)$ established in Fig. 8 of Ref.4;
- the cross wise integral of pressure which is calculated using the value of pressure given by a momentum balance across the flow. Eq.(21a), with $n_a = 1$ and $b_a = b_i$ is thus obtained.

Continuity equation for the outer half jet

The mass conservation condition replacing Eq.(8) written for the closed controls case is

$$Q_{s,e} + Q_{ce} = \int_0^{b_c+b_e+\ell_e} u\, dy$$

where Q_{se} has already been defined(Eq.(8a)). Using Eq.(1) and Eq.(3) to evaluate the integrals, one gets

$$Q_{ce} - U_{rme}\ell_e = 0.45\, b_e U_{max.e} + 0.55\, b_e U_{rme} + RU_{max.e}(e^{b_c/R} - 1) - Q_{se} \qquad (16)$$

The second hand term also represents the volume flow entrained across the outer jet boundary $Q_{ent,e}$. This quantity is used in the program for computation of intermediate steps.

Continuity equation for the inner half jet

Again, the mass conservation condition replacing Eq.(9) written for the closed controls case, is :

$$Q_{si} + Q_{ci} = \int_{-b_c-b_i-\ell_i}^{o} u\, dy$$

where Q_{si} has already been defined (Eq.(9a)). Using Eq.(1) and (3) to evaluate the integrals, one gets

$$Q_{ci} - U_{rmi}\ell_i = 0.45\, b_i U_{max.i} + 0.55\, b_i U_{rmi} + RU_{max.i}(e^{b_c/R} - 1) - Q_{si} \qquad (17)$$

The second hand term also represents the volume flow entrained across the inner jet boundary $Q_{ent,i}$. This quantity is used in the program for the computation of intermediate steps.

Pressure loss in the outer control channel

By neglecting the dynamic head, the relative pressure outside of the curved outer boundary of the jet is given by the expression :

$$p_e = - \Delta p(Q_{ce}) \qquad (18a)$$

where $\Delta p = f(Q_{ce})$ is the pressure loss in the outer control channel, associated with the entrainment of the flow rate Q_{ce}.

In Ref.9 the following relation, derived from a numerical fit of experimental data is used :

$$\Delta p = 0.223\ V_{ce}^2 - 0.563.10^{-2}\ V_{ce}^4 + 0.14810^{-3}\ V_{ce}^6 - 0.206.10^{-5}\ V_{ce}^8$$

$$\text{where } V_{ce} = Q_{ce}/W_c \qquad (18b)$$

Pressure loss in the inner control channel

The relative pressure outside of the curved inner boundary of the jet is assumed in Ref.9 to be given by the expression

$$p_i + \frac{\rho}{2} \frac{U_{rmi}^2}{\cos^2(\alpha - \Phi)} = - \Delta p(Q_{ci}) - \Delta p_{rot} \qquad (19)$$

where the pressure loss $\Delta p = f(Q_{ci})$ in the inner control channel, is given as previously, by Eq.(18b) and where Δp_{rot} is the pressure drop associated with the change of $\frac{\pi}{2} + \alpha$ in the flow direction. In Ref.9, this term is approximately evaluated as

$$\Delta p_{rot} = 1.2 \frac{\pi/2 + \alpha}{\pi/2} \frac{\rho}{2} \left(\frac{Q_{ci}}{W_c}\right)^2$$

A-2-2 At any flow section downstream of the initial control volume

Out of the five equations listed in the previous paragraph, two (Eqs 18 and 19) disappear, as well as the two unknowns Q_{ce} and Q_{ci}, which have been calculated in the initial control volume. Furthermore, Eqs 16 and 17 still apply. Eq.(15) has to be modified to yield Eq.(21), as shown here below. One additional equation, replacing Eqs 12 or 12' for the previous cases, appears as Eq.(20).

Momentum balance across the jet

The pressure p_i at the bubble boundary can be obtained from a momentum balance across the jet.

$$p_e - p_i = \frac{\rho}{R} \int_{-(b_c+b_a)}^{b_c+b_e} u^2 \, dy \qquad (20)$$

where the y-coordinate of the attachment streamline, defined as $-(b_c + b_a)$, can be determined from a mass conservation condition similar to Eq.(12_b) :

$$Q_{si} + Q_{ci} = \left[\int_{-(b_c+b_a)}^{0} u \, dy \right] \qquad (20b)$$

Using Eq.(1) and Eq.(3) to integrate these expression, one gets, from Eq.(20) an expression similar to Eq.(12) where the quantity η_d is replaced by $\eta_a = b_a/b_i$. Similarly, Eq.(20b) leads to the expression defining η_a :

$$RU_{max.i}(1 - e^{-b_c/R}) + U_{rmi} b_i \eta_a + (U_{max.i} - U_{rmi}) b_i (\eta_a - 0.8\eta_a^{2.5} + 0.25\eta_a^4) =$$

$$= Q_{si} + Q_{ci} \qquad (20c)$$

Momentum conservation in the separation bubble

A control volume is defined, as bounded by two adjacent flow sections, the attachment wall and the dividing streamline. The momentum balance, written in the direction of the wall is, by neglecting the wall shear stresses

$$\left[J_f + J_r + \int_{-b_c-b_i-\ell_i}^{-b_c-b_d} p(y)\, dy \right]_{N-1} \cos(\Phi_{N-1} - \alpha) +$$

$$+ \int_{X_{d,N-1}}^{X_{d,N}} p(y_d) \sin(\alpha - \Phi)\, dX_d = \qquad (21)$$

$$= \left[J_f + J_r + \int_{-b_c-b_i-\ell_i}^{-b_c-b_d} p(y)\, dy \right]_N \cos(\Phi_N - \alpha) - \int_{X_{d,N-1}}^{X_{d,N}} \tau_d \cos(\Phi_N - \alpha)\, dX_d$$

where all the terms except the pressure integrals are calculated as in section A-1-1.

For evaluating the integrals in this expression, the static pressure p(y) in a cross section of the jet between the dividing streamline and the attachment streamline, is expressed using the transverse momentum balance

$$p(y) - p_i = \frac{\rho}{R} \int_{-b_c-b_a}^{y} u\, dy$$

p_i being the relative static pressure on the attachment streamline. It is furthermore assumed that the pressure $p(y)$ is, between the attachment streamline and the wall, independent of y and equal to p_i.

Then, using Eq.(1) and (3) to evaluate the velocity integral, the pressure integral in Eq.(21) becomes :

$$\int_{-b_c-b_i-\ell_i}^{-b_c-b_d} p(y)\,dy = p_i(b_i + \ell_i - b_a) + (b_d - b_a)\Bigg\{ p_i$$

$$- \rho\frac{b_i^2}{R}(U_{max.i} - U_{rmi})^2 \Bigg[\left| \frac{\eta^2}{2} - \frac{16}{35}\eta^{3.5} + \frac{3}{10}\eta^5 - \frac{16}{143}\eta^{6.5} + \frac{\eta^8}{56} \right|_{\eta_a}^{\eta_d}$$

$$-(\eta_d - \eta_a)(\eta_d - \frac{8}{5}\eta_d^{2.5} + \frac{3}{2}\eta_d^4 - \frac{8}{11}\eta_d^{5.5} + \frac{\eta_d^7}{11}) \Bigg]$$

$$+ 2(U_{max.i} - U_{rmi})U_{rmi} \Bigg[\left[\frac{\eta^2}{2} + \frac{8}{35}\eta^{3.5} + \frac{\eta^5}{20} \right]_{\eta_a}^{\eta_d}$$

$$- (\eta_d - \eta_a)(\eta_d - \frac{4}{5}\eta_d^{2.5} + \frac{\eta_d^4}{4}) \Bigg] + U_{rmi}^2(\eta_d - \eta_a)\eta_a \Bigg\} \qquad (21a)$$

where $\eta_d = b_d/b_i$, coordinate of the dividing streamline, is defined as in the closed controls case (Eq.(12c)) and where $\eta_a = b_a/b_i$, coordinate of the attachment streamline is given by Eq.(20c).

A-3 Additional relation for the length along the attachment wall

From geometrical considerations (Fig.21), it follows that

$$L_N = L_{N-1} + (R - b_c - b_i - \ell_i)_{N-1} \frac{\sin (\Phi_N - \Phi_{N-1})}{\cos (\Phi_N - \alpha)} \qquad (22)$$

APPENDIX B : THE COMPUTER PROGRAMS

The computer programs written by Bekaert (Ref.9) and their listings are given here below, for the two cases of closed and open controls. The non evident meaning of the variables used in the program is given in the list of symbols.

Input data to the programs is :

Geometric parameters

AI; AE; WS; WC; ALPHA

flow parameters

PTOT; PINT (closed controls case only)

constants

D11 (K_1=9.77); D22 (K_1=7.67); CONST (K_2=10)

XN=1.5 exponent of velocity profile

initial guess values

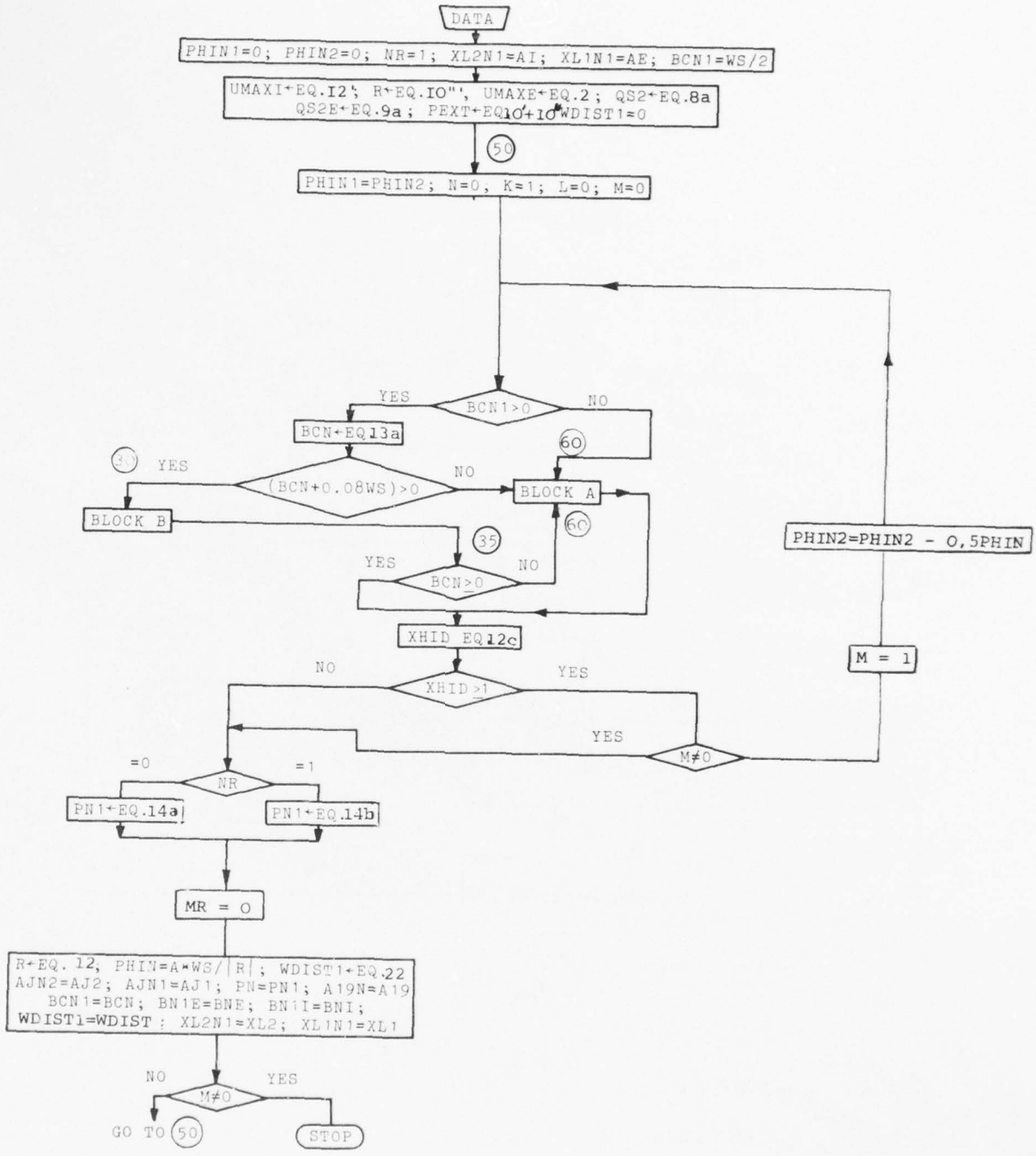
QCI, QCE (open controls case only)

PHIN : angular coordinate of second flow section

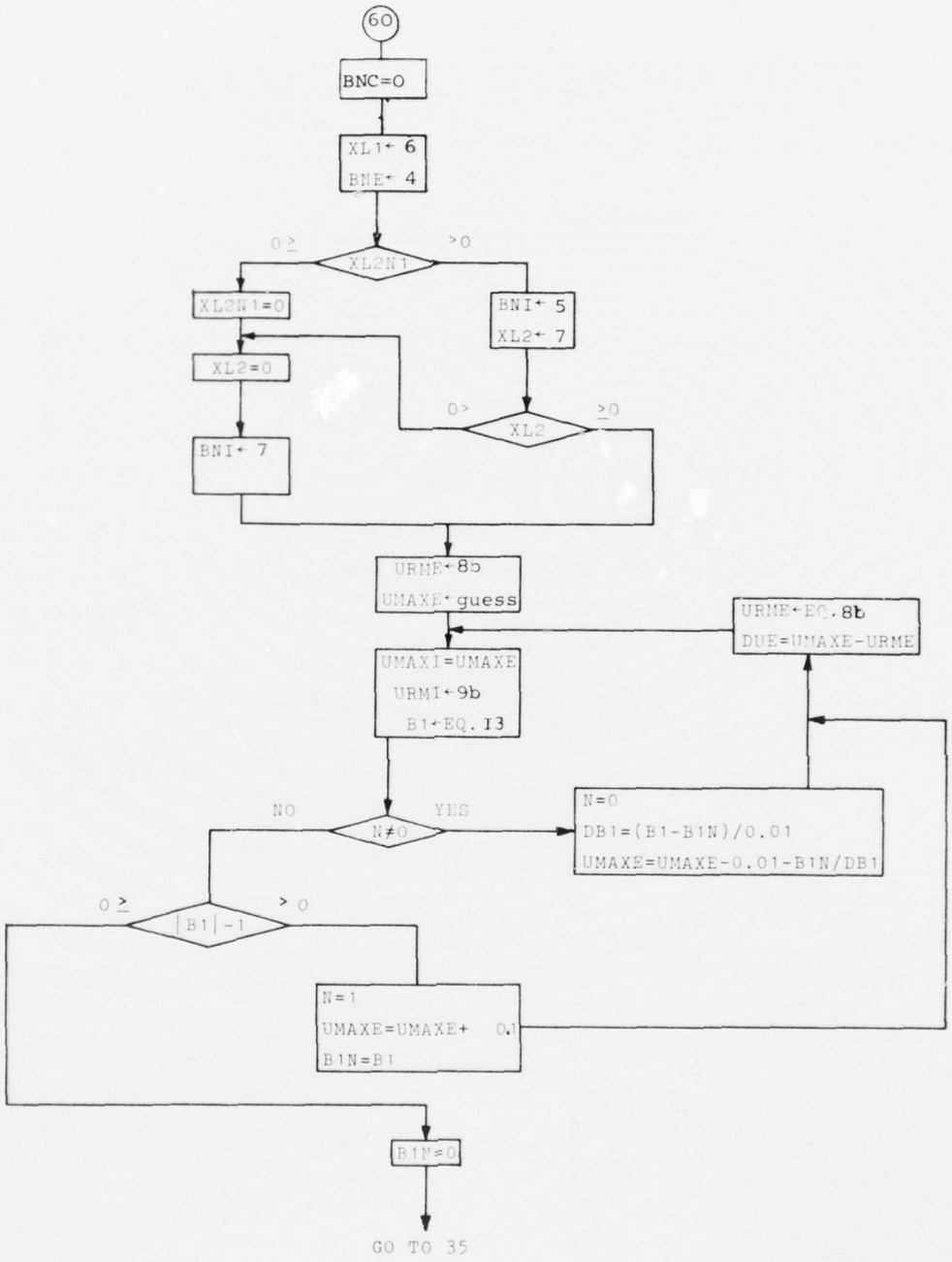
XHID : n_d (open controls case only)

ACC : accuracy criterion for stopping iterations.

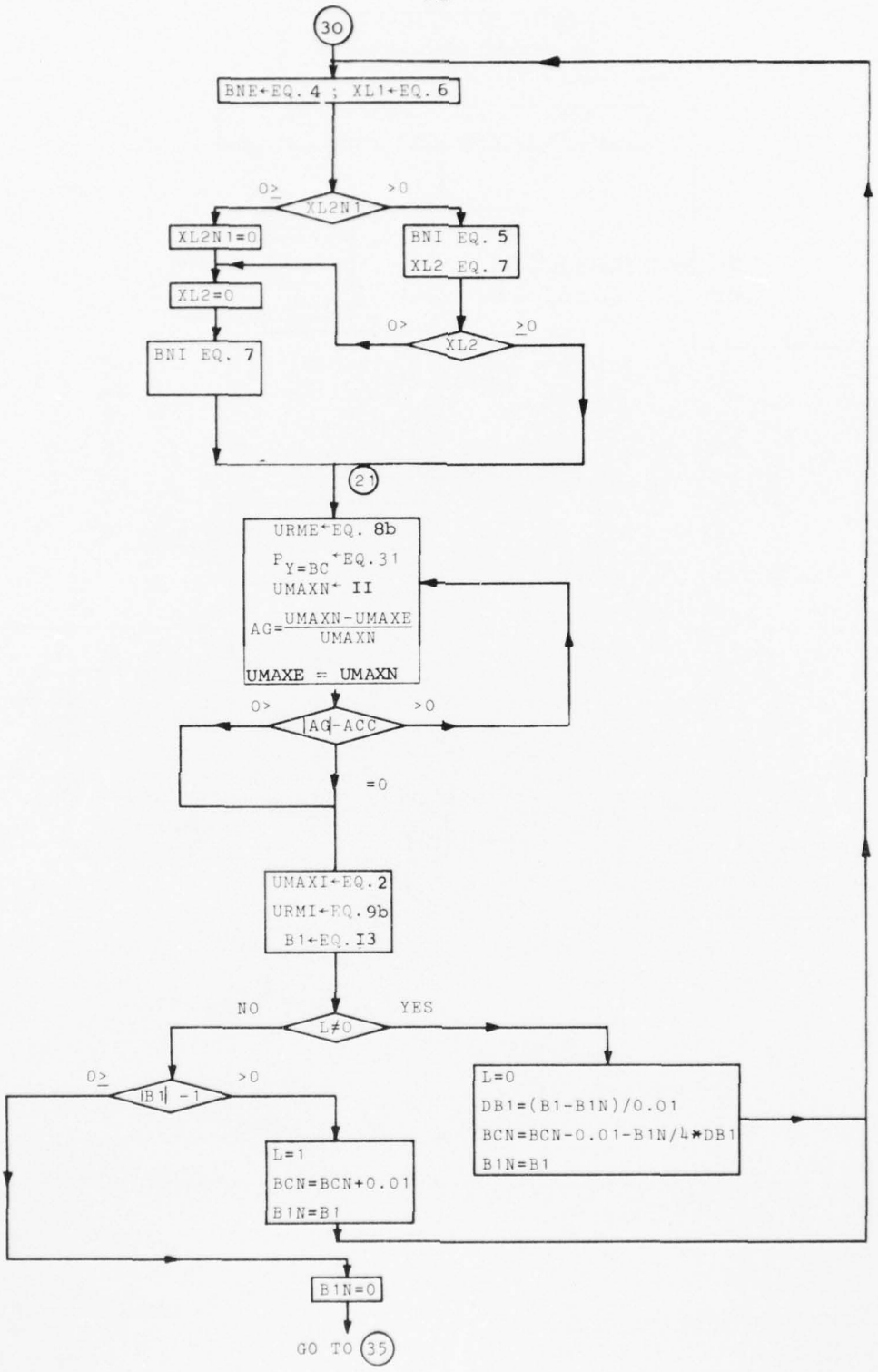
The numerical values of this input data that have been used for the present calculations are also given after the two program listings.



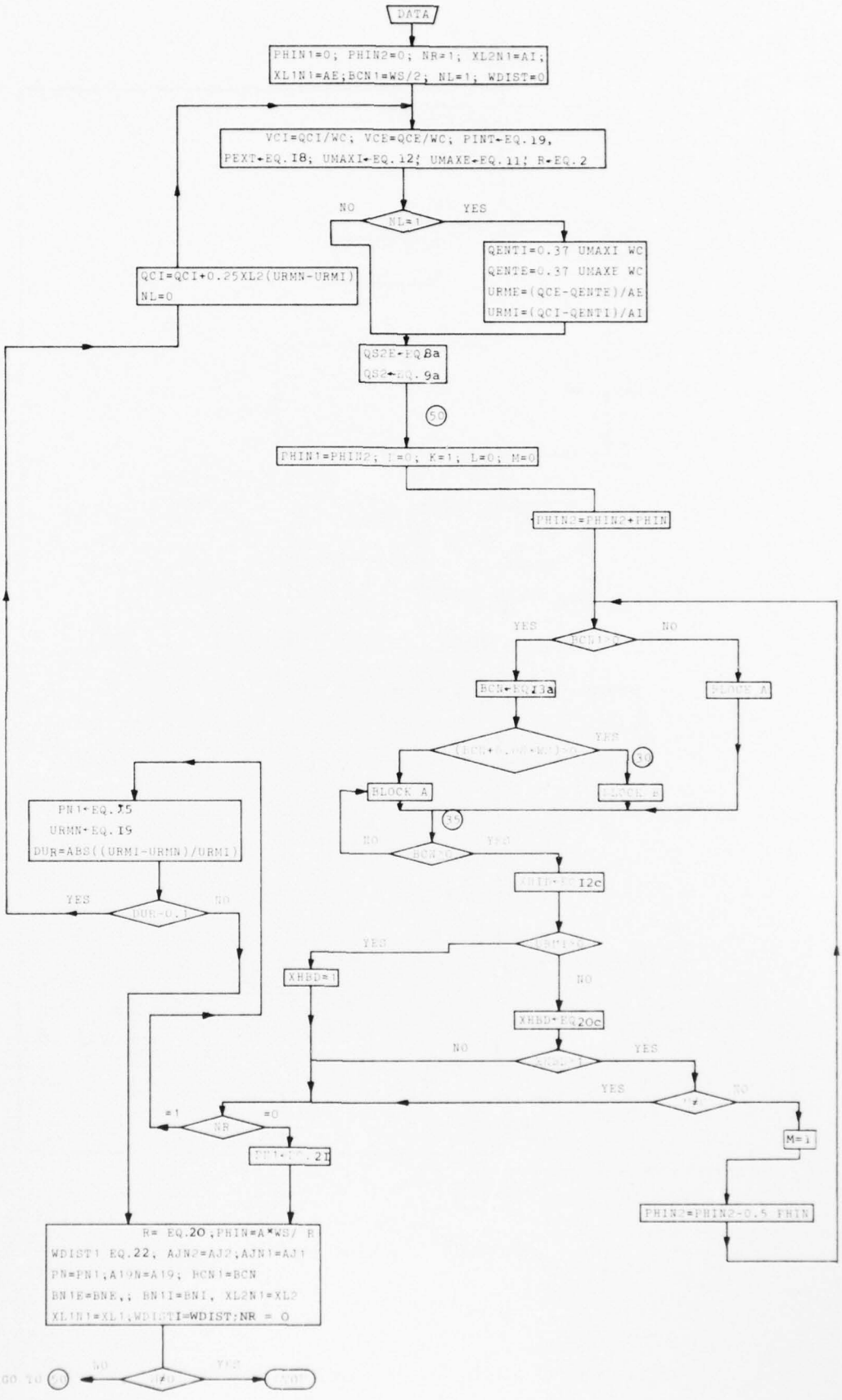
- FLOW CHART OF THE COMPUTER PROGRAM FOR THE CLOSED CONTROL CASE



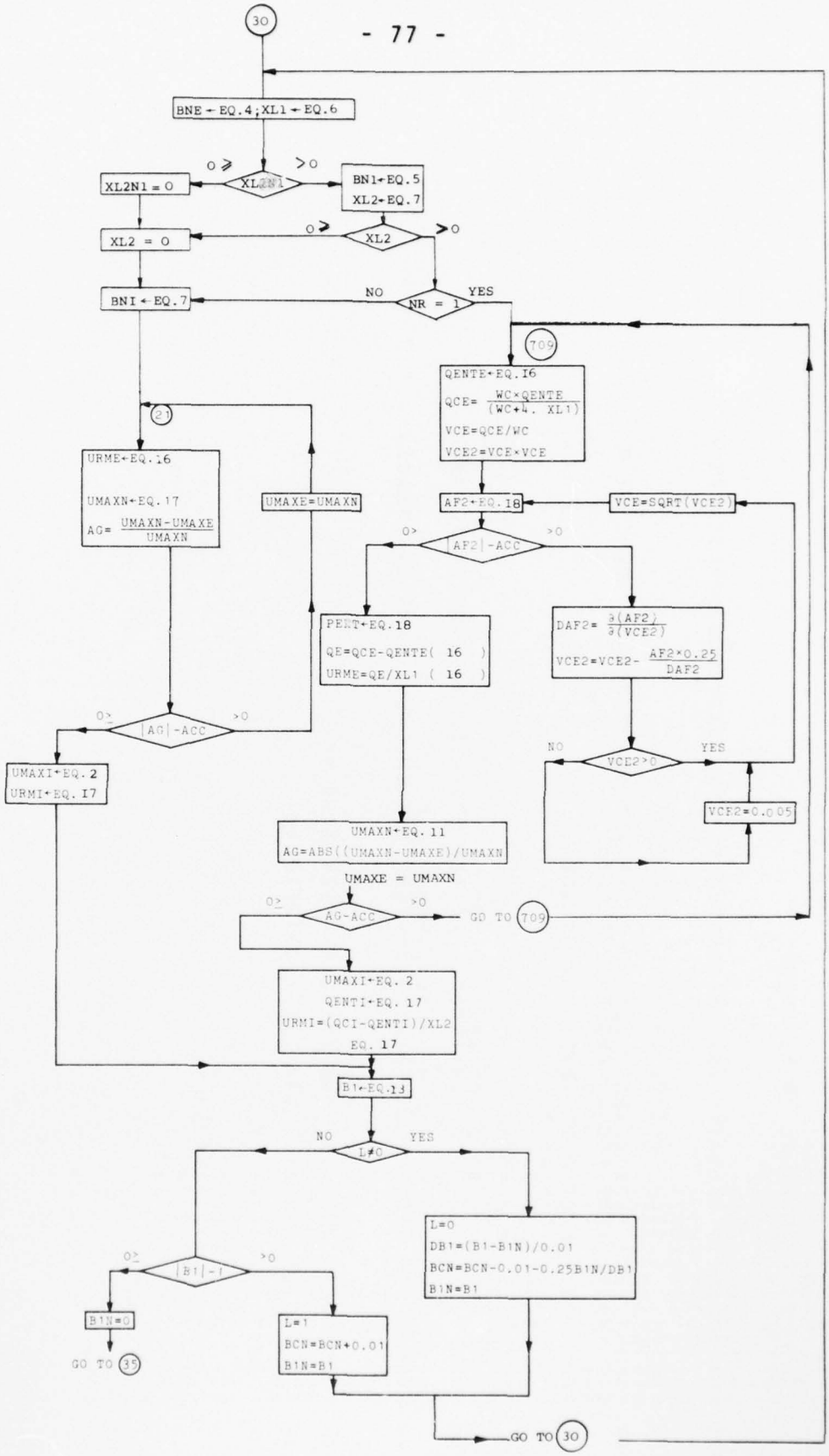
- FLOW CHART OF BLOCK A OF THE COMPUTER PROGRAM
FOR THE CLOSED AND OPEN CONTROL CASE



- FLOW CHART OF BLOCK B OF THE COMPUTER PROGRAM
FOR THE CLOSED CONTROL CASE



- FLOW CHART OF THE COMPUTER PROGRAM
FOR OPEN CONTROL CHANNEL OPERATION



- FLOW CHART OF BLOCK B FOR THE COMPUTER PROGRAM
FOR OPEN CONTROL CHANNEL OPERATION

```
%JOB,T240
%C/FORT/(BISTCC)
      1  CALL XTIME
         READ(105,2)AE,AI,WL,WS,WC,ALPHA
    2    FORMAT(6F6.0)
         IF(WS.EQ.0.)STOP
         WRITE(108,1000)
 1000  FORMAT(1H1,' VELOCITY AND PRESSURE FIELDS IN BISTABLE AMPLIFIERS'/
        12X,51(1H=)//)
         WRITE(108,1002)
 1002  FORMAT(' CLOSED CONTROL CHANNEL OPERATION')
         WRITE(108,1001)
 1001  FORMAT(//1X,'UNITS ARE : LENGTH MM, PRESSURE MM WATER, VELOCITY M/
        1SEC,'/13X,'TEMP DEG K, ANGLES RAD.'//)
         M=0
         READ(105,2)PTOT,PINT,TEMP,E,CONST,ACC
         READ(105,3)PHIN,XN,B
    3    FORMAT(3F6.0)
         READ(105,4)D11,D22
    4    FORMAT(2F10.0)
         WRITE(108,304) AE,AI,WL,WS,WC,ALPHA
  304  FORMAT(2X,2HAE,10X,2HAI,10X,2HWL,10X,2HWS,10X,2HWC,5X,10HALPHA(D
        1EG),2X,6F12.4)
         WRITE(108,204) PTOT,PINT,TEMP,E,CONST,ACC
  204  FORMAT(15X,4HPTOT,8X,4HPINT,8X,4HTEMP,11X,1HE,7X,5HCONST,9X,3HACC,
        1/10X,6F12.4/)
         XCO=B*WS
         WRITE(108,404) XN,B,XCO
  404  FORMAT(12X,2HXN,11X,1HB,10X,2HXC,/10X,3F12.4/)
         WRITE(108,104)D11,D22
  104  FORMAT(15X,4HEPS1,8X,4HEPS2,/10X,2F12.4/)
         WRITE(108,504)
  504  FORMAT(2X,51(1H*)///)
         D1=0.25/(D11*D11)
         D2=0.25/(D22*D22)
         ALPHA=ALPHA*0.0174533
         PHIN=PHIN*0.0174533
         RHO=0.125*TEMP/288.
         PHIN1=0.0
         PHIN2=0.0
         ZPS=0.5
         C1=1
         C2=2
         C3=3
         C4=4
         C5=5
         C6=6
         Q01=C3+C1
         Q02=XN*C2+C1
```

```
      QQ3=XN*C3+C1
      QQ4=XN*C4+C1
      QQ5=XN+C2
      QQ6=XN*C2+C2
      QQ7=XN*C3+C2
      QQ8=XN*C4+C2
      QQ9=XN*C2
      QQA=XN-C1
      ZZ1=C2/QQ1
      ZZ2=C1/QQ2
      XHID=0.35
      NR=1
      A1=C1-ZZ1+ZZ2
      A1D=ZZ1-ZZ2
      A11=C1-C4/QQ1+C6/QQ2-C4/QQ3+C1/QQ4
      A51=QQ1*QQ5
      A52=QQ2*QQ6
      A53=C4/(QQ3*QQ7)
      A54=C1/(QQ4*QQ8)
      A55=A11-ZP5+C4/A51-C6/A52+A53-A54
      A56=A1-ZP5+ZP5*A53-C1/A52
      UMAXI2=C2/RHO*(PTOT-PINT)
      UMAXI=SQRT(UMAXI2)
      A2=(-E*A1+0.5/B)**2
      A3=PTOT/((PTOT-PINT)*(C1-A2))
      R=-C2*WS/ALOG(A3)
      UMAXE=UMAXI*EXP(-WS/R)
      UMAXE2=UMAXE*UMAXE
      S=R*PHIN
      QS2=UMAXI*R*(C1-EXP(-WS/(2.*R)))
      QS2E=UMAXE*R*(EXP(WS/(2.*R))-1.)
      A57=WS*PTOT+R*RHO*(UMAXI2-UMAXE2)/4.
      SPIN=0.0
      QS2W=QS2*0.001
      WRITE(108,100)R,QS2W,UMAXE,UMAXI
  100 FORMAT(5X,3HR =,F10.4,5X,5HQS2 =,F10.4,' M3/SEC',5X,7HUMAXE =,
     1F10.4,5X,7HUMAXI =,F10.4/)
      BCH1=WS/2.
      BN1E=0.
      BN1I=0.
      XL1N1=AE
      XL2N1=AI
      WDIST1=(R-BCH1-BN1I-XL2N1)*SIN(PHIN)/COS(PHIN-ALPHA)
      XEI=E
      XEE=E
      PN=PINT
   50 PHIN1=PHIN2
      IF(R)171,162,172
  171 PHIN2=PHIN2-PHIN
 1171 A40=COS(PHIN1-ZP5*PHIN-ALPHA)
```

```
      GOTO 173
172   PHIN2=PHIN2+PHIN
1172  A40=COS(PHIN1+2P5*PHIN-ALPHA)
173   CONTINUE
      A22=COS(PHIN2-ALPHA)
      A4=COS(PHIN2+ALPHA)*COS(PHIN2+ALPHA)
      A7=COS(ALPHA-PHIN1)
      A8=COS(ALPHA+PHIN-PHIN1)
      A9=COS(ALPHA+PHIN1)
      A61=COS(ALPHA+PHIN2)
      A63=SIN(ALPHA+1.57079+PHIN1-PHIN)
      N=0
      K=1
      L=0
      B1N=0
      IF(BCN1)60,60,42
42    BCN=BCN1-2P5/B*PHIN*ABS(R)
      IF(BCN+0.2)60,60,30
 30   CONTINUE
      IF(R)31,162,32
32    BNE=BN1E+XEE*R*PHIN
      XL1=(R+BCN1*BN1E+XL1N1)*A9/A61-R-BCN-BNE
      IF(XL2N1)22,22,23
 23   BN1=BN1I+XE1*R*PHIN
      XL2=(-R+BCN1+BN1I+XL2N1)*A7/A22+R-BCN-BN1
      IF(XL2)24,25,25
22    XL2N1=0.0
24    XL2=0.0
      BN1=(-R+BCN1+BN1I+XL2N1)*A7/A22+R-BCN
      XE1=BN1/S
      IF(XE1-E)25,5,5
 5    XE1=E
      GOTO 23
31    BNE=BN1E+XEE*ABS(R)*ABS(PHIN)
      XL1=ABS(R)-BCN-BNE+(BCN1+BN1E+XL1N1-ABS(R))*A9/A63
      IF(XL2N1)34,34,36
36    BN1=BN1I+XE1*ABS(R)*ABS(PHIN)
      XL2=(ABS(R)+BCN1+BN1I+XL2N1)*A7/A9-ABS(R)-BCN-BN1
      IF(XL2)37,25,25
 34   XL2N1=0.0
 37   XL2=0.0
      BN1=(ABS(R)+BCN1+BN1I+XL2N1)*A7/A8-ABS(R)-BCN
      XE1=BN1/S
      IF(XE1-E)25,38,38
 38   XE1=E
      GOTO 36
25    CONTINUE
21    CONTINUE
      URME=(-UMAXE*BNE*A1-UMAXE*R*(EXP(BCN/R)-C1)+BS2E)/(XL1+A10*BNE)
      DUE=UMAXE-URME
```

```
      A5=ZP5*URME*URME/A4+BNE/R*(A11*DUE*DUE+C2*A1*DUE*URME+URME*URME)
      A30=C2*(A5+PTOT/RHO)
      UMAXN=SQRT(A30)
      A6=ABS((UMAXN-UMAXE)/UMAXN)
      UMAXE=UMAXN
      IF(A6-0.001)20,20,21
20    CONTINUE
      UMAXI=UMAXE*EXP(C2*BCN/R)
      URMI=(-UMAXI*BNI*A1-UMAXI*R*(D1-EXP(-BCN/R))+QS2)/(XL2+BNI*A10)
      DUI=UMAXI-URMI
      AJE=RHO*BNE*(DUE*DUE*A11+C2*DUE*URME*A1+URME*URME)
      BCJ=RHO*R*(UMAXI*UMAXI-UMAXE*UMAXE)/C4
      AJI=RHO*BNI*(DUI*DUI*A11+C2*DUI*URMI*A1+URMI*URMI)
      PEXT=-RHO*URME*URME*ZP5/A4
      A50=BNE*PEXT+BNI*PN
      APE=RHO/R*BNE*BNE*(-DUE*DUE*A55-C2*DUE*URME*A56-ZP5*URME*URME)
      API=RHO/R*BNI*BNI*(DUI*DUI*A55+C2*DUI*URMI*A56-ZP5*URMI*URMI)
      SPI=SPIN+(RHO*URMI*URMI+PN)*(BNI+BCN-BN1I-BCN1)
      B1=AJE+BCJ+AJI+A50+APE+API-A57+C2*PTOT*BCN-SPI
      IF(L)82,81,82
 81   A60=ABS(B1)-1.
      IF(A60)70,70,71
71    L=1
      BCN=BCN+0.01
      B1N=B1
      GOTO 30
82    L=0
      DB1=(B1-B1N)/0.01
      BCN=BCN-0.01-B1N/(C4*DB1)
      B1N=B1
      GO TO 30
70    B1N=0
      IF(BCN)60,35,35
60    BCN=0.0
      IF(R)151,162,152
 152  XL1=(R+BCN1+BN1E+XL1N1)*A9/A61-R-BN1E-XEE*R*PHIN
      IF(XL2N1)61,61,62
62    BNI=BN1I+XEI*R*PHIN
      XL2=(-R+BCN1+BN1I+XL2N1)*A7/A22+R-BNI
      IF(XL2)64,65,65
 61   XL2N1=0.0
 64   XL2=0.0
      BNI=(-R+BCN1+BN1I+XL2N1)*A7/A22+R
      XEI=BNI/S
      IF(XEI-E)65,66,66
 66   XEI=E
      GOTO 62
151   BNE=BN1E+XEE*ABS(R)*ABS(PHIN)
      XL1=ABS(R)-BNE+(BCN1+BN1E+XL1N1-ABS(R))*A9/A63
      IF(XL2N1)154,154,156
```

```
156   BNI=BN1I+KEI*PHIN*ABS(R)
      XL2=(ABS(R)+BCN1+BN1I+XL2N1)*A7/A8-ABS(R)-BNI
      IF(XL2)157,65,65
154   XL2N1=0.0
157   XL2=0.0
      BNI=(ABS(R)+BCN1+BN1I+XL2N1)*A7/A8-ABS(R)
      XEI=BNI/S
      IF(XEI-E)65,158,158
158   XEI=E
      GOTO 156
65    CONTINUE
      BNE=BN1E+KEE*PHIN*ABS(R)
      DUE=DUE*SQRT((C6*WS)/S)
      URME=(QS2-BNE*DUE*A1)/(XL1+BNE)
      UMAXE=DUE+URME
      GOTO 63
 94   URME=(QS2E-UMAXE*BNE*A1)/(XL1+BNE*A10)
      DUE=UMAXE-URME
63    UMAXI=UMAXE
      URMI=(QS2-UMAXI*BNI*A1)/(XL2+BNI*A10)
      DUI=UMAXI-URMI
      AJE=RHO*BNE*(DUE*DUE*A11+C2*DUE*URME*A1+URME*URME)
      AJI=RHO*BNI*(DUI*DUI*A11+C2*DUI*URMI*A1+URMI*URMI)
      PEXT=-RHO*URME*URME*ZP5/A4
      A50=BNE*PEXT+BNI*PN
      APE=RHO/R*BNE*BNE*(-DUE*DUE*A55-C2*DUE*URME*A56-ZP5*URME*URME)
      API=RHO/R*BNI*BNI*(DUI*DUI*A55+C2*DUI*URMI*A56-ZP5*URMI*URMI)
      SPI=SPIN+(RHO*URMI*URMI+PN)*(BNI-BN1I)
      B1=AJE+AJI+A50+APE+API-A57-SPI
      IF(N)86,87,86
87    A70=ABS(B1)-1
      IF(A70)95,95,89
89    N=1
      UMAXE=UMAXE+0.1
      B1N=B1
      GOTO 94
86    N=0
      DB1=(B1-B1N)/0.1
      UMAXE=UMAXE-0.1-B1N/DB1
      B1N=B1
      GOTO 94
95    CONTINUE
35    CONTINUE
      IF(BCN)131,131,132
131   A13=0.0
      GOTO 133
132   A13=R*UMAXE*EXP(BCN/R)*(EXP(BCN/R)-C1)
 133  A12=XHID-C2/QQ1*XHID**QQ1+XHID**QQ2/QQ2
      F1=A13+DUI*BNI*A12+URMI*BNI*XHID-QS2
      F11=ABS(F1)
```

```
      IF(F11-0.01)27,27,26
   26 DF1=DUI*BNI*(C1-C2*XN*XHID**XN/QQ1+C2*XN*XHID**QQ9/QQ2)+URMI*BNI
      XHID=XHID-F1/DF1*ZP5
      GOTO 133
   27 CONTINUE
      IF(XHID-1.)2027,2027,1027
 1027 IF(M)2027,701,2027
 2027 CONTINUE
      A18=XHID**QQ1/QQ1
      A17=XHID**QQ2/QQ2
      A15=XHID-C4*A18+C6*A17-C4*XHID**QQ3/QQ3+XHID**QQ4/QQ4
      A16=XHID-C2*A18+A17
      AJ1=(RHO*BNI*(DUI*DUI*(A11-A15)+C2*DUI*URMI*(A1-A16)+URMI*URMI*(C1
     1-XHID)))*A22
      AJ2=URMI*URMI*RHO*A22*XL2
      A20=C1-XHID**XN
      A21=(-C2*XN*XHID**QQA*A20*DUI)/BNI-CONST/R*(DUI*A20*A20+URMI)
      IF(BCN)150,150,140
  150 D1=D2
      GOTO 160
  140 D1=D1
  160 TN=RHO*BNI*DUI*D1/XEI*A21
      TN=ABS(TN)
      IF(R)181,162,182
  181 A23=-R+BCN+BNI*XHID
      A150=SIN(ALPHA-PHIN1+ZP5*PHIN)
      GOTO 183
  182 A23=R-BCN-BNI*XHID
      A150=SIN(ALPHA-PHIN1-ZP5*PHIN)
  183 CONTINUE
      A19=A22*(XL2+BNI*(C1-XHID))
      IF(NR)29,29,28
   28   NR=0
      A80=TN*A23*PHIN*A40
      PN1=(-AJ1-AJ2+A80+PINT*XL2N1*COS(ALPHA)+PINT*A23*PHIN*A150)/A19
      PNM1=PINT
      GOTO 40
   29 A80=ZP5*(TN+TN1)*A23*PHIN*A40
      PN1=(AJN1+AJN2+PNM1*A19N-AJ1-AJ2+A80+PN*A23*A150*ABS(PHIN))/A19
      PNM1=PN
   40 CONTINUE
      WRITE(108,9000) URMI,UMAXI,UMAXE,URME,XL2
 9000 FORMAT(//1X,7HURMI   =,F12.6,5X,7HUMAXI =,F12.6,5X,7HUMAXE =,F12.6,
     15X,7HURME   =,F12.6,5X,7HXL2    =,F12.6)
      WRITE(108,9001) BNI,BCN,XL1,BNE,XEI
 9001 FORMAT(1X,7HBNI    =,F12.6,5X,7HBCN    =,F12.6,5X,7HXL1    =,F12.6,
     15X,7HBNE    =,F12.6,5X,7HXEI    =,F12.6)
      WRITE(108,9002) A80,PN1,XHID
 9002 FORMAT(1X,7HA80    =,F12.6,5X,7HPN1    =,F12.6,5X,7HXHID   =,F12.6)
      AJE=RHO*BNE*(DUE*DUE*A11+C2*DUE*URME*A1+URME*URME)
```

```
      AJBC=ZP5*RHO*(UMAXI*UMAXI-UMAXE*UMAXE)*R
      AJPI=RHO*BNI*(DUI*DUI*A15+C2*DUI*URMI*A16+URMI*URMI*KHID)
      PEXT=-RHO*URME*URME*ZP5/A4
      R=(AJE+AJBC+AJPI)/(PEXT-PN1)
      PHIN=(ZP5*WS)/ABS(R)
      BCN1=BCN
      BN1E=BNE
      BN1I=BNI
      XL1N1=XL1
      XL2N1=XL2
      TN1=TN
      AJN2=AJ2
      AJN1=AJ1
      PN=PN1
      A19N=A19
      S=S+PHIN*ABS(R)
      SPIN=SPI
      IF(R)161,162,163
  163 WDIST=((R-BCN1-BN1I-XL2N1)*SIN(PHIN)/COS(PHIN2-ALPHA))+WDIST1
      GOTO 164
  161 WDIST=(-R+BCN1+BN1I+XL2N1)*SIN(PHIN)/COS(ALPHA+PHIN-PHIN1)+WDIST1
  164 CONTINUE
      WRITE(108,909) PHIN1,PHIN2,R,PEXT
  909 FORMAT(1X,7HPHIN1 =,F12.6,5X,7HPHIN2 =,F12.6,5X,7HR      =,F12.6,
     15X,7HPEXT  =,F12.6)
      WRITE(108,908)WDIST,WDIST1,S
  908 FORMAT(1X,7HWDIST =,F12.6,5X,7HWDIST1=,F12.6,5X,7HS      =,F12.6)
      WDIST1=WDIST
      IF(M)9999,192,9999
  192 IF(PN1-100.)50,9999,9999
  701 M=1
      WRITE(108,8888)
 8888 FORMAT(/' LAST SLICE IS DEVIDED IN TWO PARTS'/)
      IF(R)702,703,704
  703 WRITE(108,1703)
 1703 FORMAT(1X,' R EQUALS ZERO'//)
 9999 CALL XTIME
      GO TO 1
  702 PHIN2=PHIN2+PHIN*0.5
      GO TO 1171
  704 PHIN2=PHIN2-PHIN*0.5
      GO TO 1172
  162 CONTINUE
      END
%EOD
%C/LINKDX/SG,FR,CL,SL,UL,(BISTCC)
%C/BIB/REP,GI.EP
%C/BIB/INC,GI.EP
```

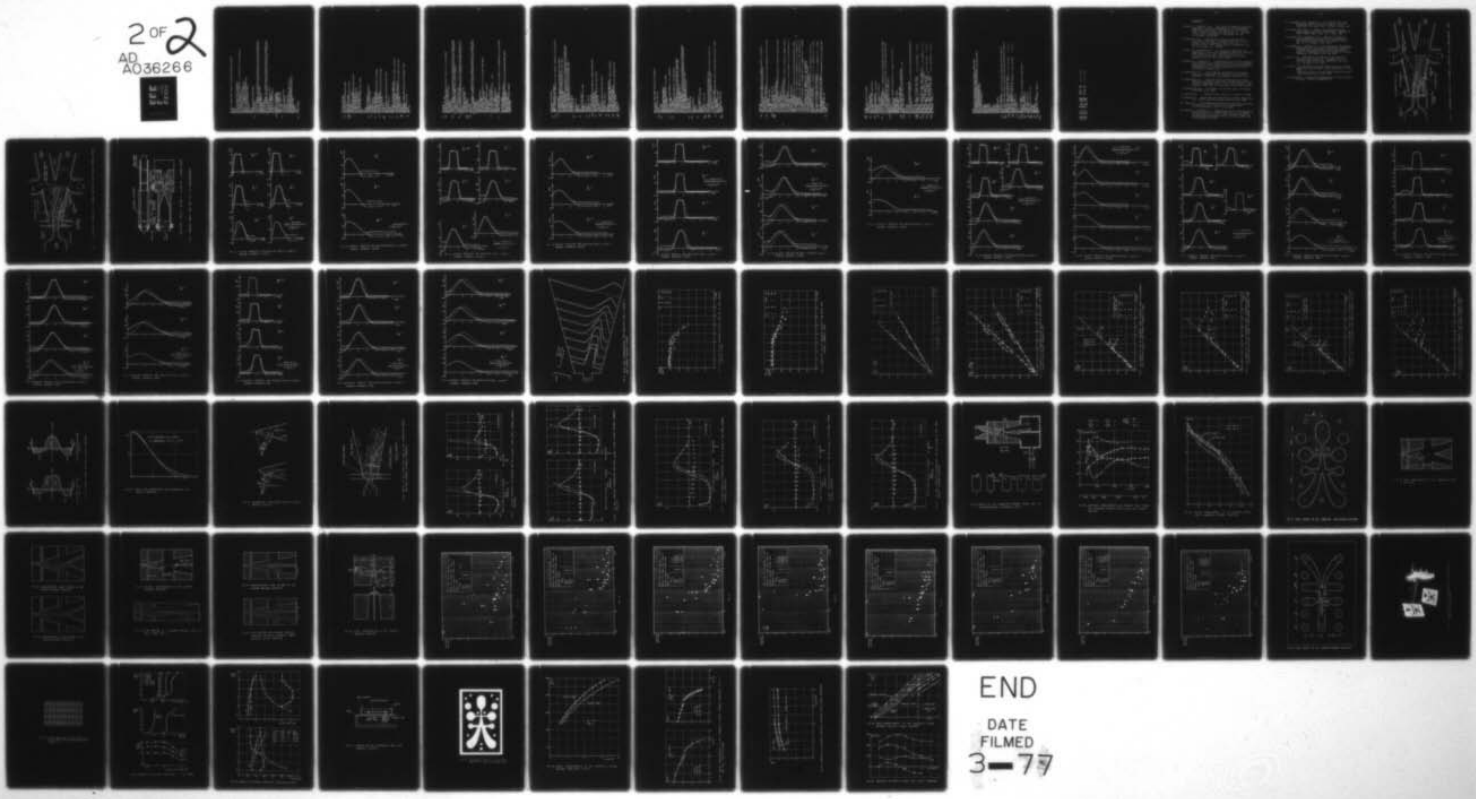
```
%JOB,T240
%C/BISTCC/
  5.0   5.0    35.    2.5    2.5    10.
  100.   -9.7  288.   .2746  10.     .01
  1.5   1.5     5.77
  9.77          7.67
  2.5   2.5     35.    2.5    2.5    10.
  100.  -15.0  288.   .2746  10.     .01
  1.5   1.5     5.77
  9.77          7.67
  0.25  0.25    35.    2.5    2.5    10.
  100.  -16.5  288.   .2746  10.     .01
  1.5   1.5     5.77
  9.77          7.67
  2.5   2.5     35.    2.5    2.5    15.
  100.  -14.5  288.   .2746  10.     .01
  1.5   1.5     5.77
  9.77          7.67
```

```
%JOB,T100
%C/FORT/(BISTCD)
      1  CALL XTIME
         READ(105,2)AE,AI,WL,WS,WC,ALPHA
    2    FORMAT(6F6.0)
         IF(WS.EQ.0.)STOP
         WRITE(108,1000)
 1000  FORMAT(1H1,' VELOCITY AND PRESSURE FIELDS IN BISTABLE AMPLIFIERS'/
        12X,51(1H=)//)
         WRITE(108,1002)
 1002  FORMAT(' OPEN CONTROL CHANNEL OPERATION')
         WRITE(108,1001)
 1001  FORMAT(//1X,'UNITS ARE : LENGTH MM, PRESSURE MM WATER, VELOCITY M/
        1SEC,'/13X,' TEMP DEG K, ANGLES RAD., VOLUME FLOW 1.E-3 M3/SEC'//)
         READ(105,3)PTOT,QCI,QCE,TEMP,E,CONST,D11,D22
 3       FORMAT(8F6.0)
         READ(105,4)XN,B,XNID,ACC
  4      FORMAT(4F6.0)
         WRITE(108,304) AE,AI,WL,WS,WC,ALPHA
  304   FORMAT(/17X,2HAE,10X,2HAI,10X,2HWL,10X,2HWS,10X,2HWC,5X,10HALPHA(D
        1EG),/10X,6F12.4/)
         WRITE(108,204) PTOT, QCI,TEMP,E,CONST,ACC
  204   FORMAT(15X,4HPTOT,8X,4HQCI ,8X,4HTEMP,11X,1HE,7X,5HCONST,9X,3HACC,
        1/10X,6F12.4/)
         WRITE(108,404) XN,B,QCE
  404   FORMAT(17X,2HXN,11X,1HB,9X,3HQCE,/10X,3F12.4/)
         WRITE(108,605)D11,D22
  605   FORMAT(15X,4HEPS1,8X,4HEPS2,/10X,2F12.4/)
         WRITE(108,520)
  520   FORMAT(2X,51(1H*)///)
         D1=0.25/(D11*D11)
         D2=0.25/(D22*D22)
         ALPHA=ALPHA*0.0174533
         PHIN=PHIN*0.0174533
         RHO=0.125*TEMP/288.
         PHIN1=0.0
         PHIN2=0.0
         ZP5=0.5
         C1=1.
         C2=2.
         C3=3.
         C4=4.
         C5=5.
         C6=6.
         BCH1=WS/2
         BH1E=0.
         BH1I=0.
         XL1N1=AE
         XL2N1=AI
```

AD-A036 266 VON KARMAN INST FOR FLUID DYNAMICS RHODE-SAINT-GENESE--ETC F/G 9/5
STUDY OF THE SWITCHING MECHANISM IN BISTABLE AMPLIFIERS WITH AP--ETC(U)
NOV 76 M CARBONARO DA-ERO-75-G-073

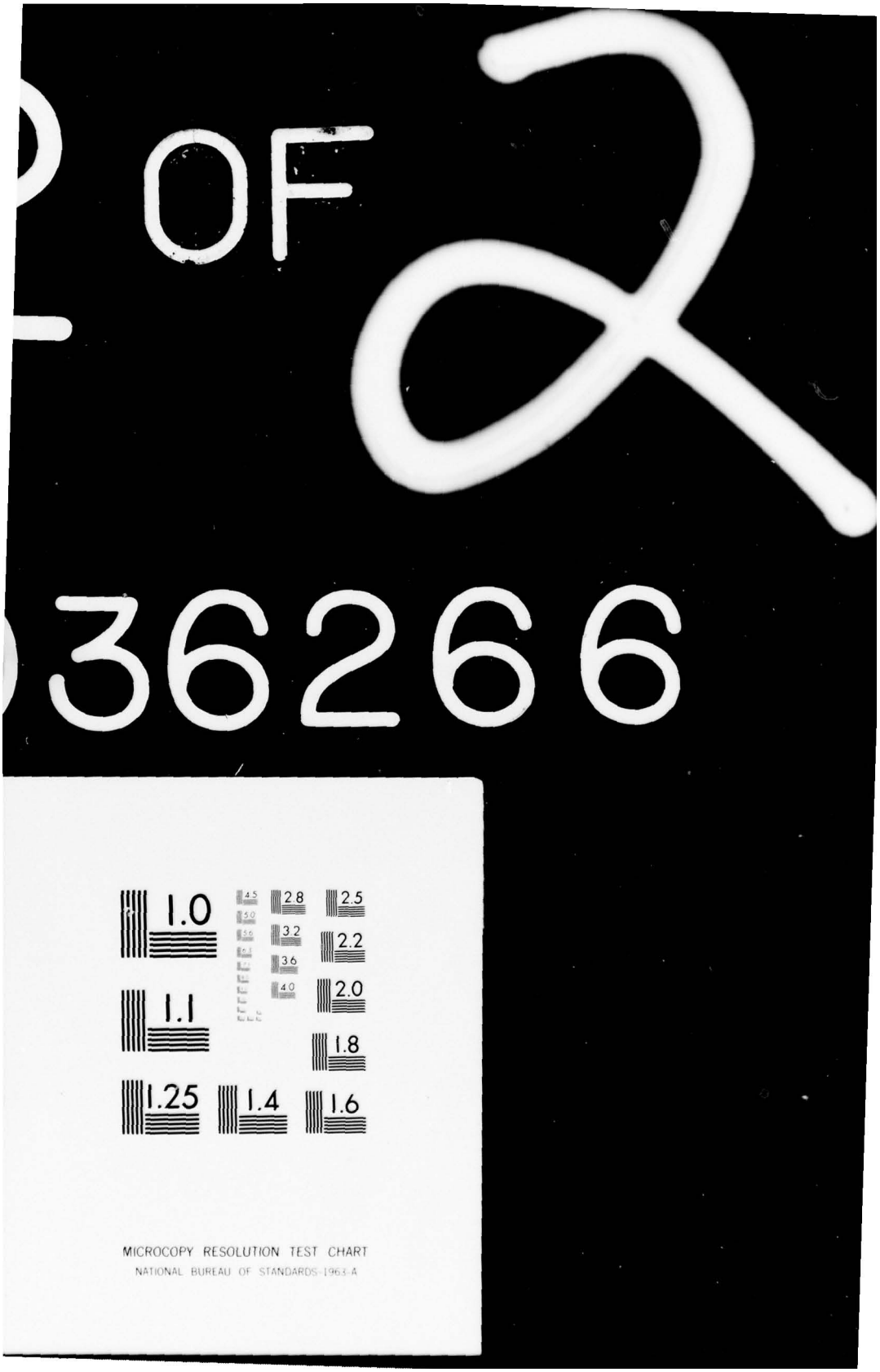
UNCLASSIFIED NL

2 OF 2
AD A036266



END

DATE FILMED
3-77


OF
36266
1.0
1.1
1.25
1.4
1.6
1.8
2.0
2.2
2.5
2.8
3.2
3.6
4.0
4.5
5.0
5.6
6.3
MICROCOPY RESOLUTION TEST CHART
NATIONAL BUREAU OF STANDARDS-1963-A

```
      WDIST1=(R-BCN1-BN1I-XL2N1)*SIN(PHIN)/COS(PHIN-ALPHA)
      XEI=E
      XEE=E
      NR=1
      A1=C1-C2/(XN+C1)+C1/(C2*XN+C1)
      A10=C2/(XN+C1)-C1/(C2*XN+C1)
      A11=C1-C4/(XN+C1)+C6/(C2*XN+C1)-C4/(C3*XN+C1)+C1/(C4*XN+C1)
      A51=(XN+C1)*(XN+C2)
      A52=(C2*XN+C1)*(C2*XN+C2)
      A53=C4/((C3*XN+C1)*(C3*XN+C2))
      A54=C1/((C4*XN+C1)*(C4*XN+C2))
      A55=A11-ZP5+C4/A51-C6/A52+A53-A54
      A56=A1-ZP5+ZP5*A53-C1/A52
      WDIST=0.0
      NL=1
      BK1=4.
      TGA=SIN(ALPHA)/COS(ALPHA)
721   VCI=QCI/WC
      VCI2=VCI*VCI
      PINT=-0.496182E-1-0.222789*VCI2+0.563274E-2*VCI2**2-0.148242E-3*VC
     1I2**3+0.206558E-5*VCI2**4-0.138133E-7*VCI2**5+0.354175E-10*VCI2**6
      UMAXI2=C2/RHO*(PTOT-PINT)
      UMAXI=SQRT(UMAXI2)
      VCE=QCE/WC
      VCE2=VCE*VCE
      PEXT=-0.496182E-1-0.222789*VCE2+0.563274E-2*VCE2**2-0.148242E-3*VC
     1E2**3+0.206558E-5*VCE2**4-0.138133E-7*VCE2**5+0.354175E-10*VCE2**6
     2+0.496182E-1
      UMAXE2=2./RHO*(PTOT-PEXT)
      UMAXE=SQRT(UMAXE2)
      R=-WS/ALOG(UMAXE/UMAXI)
      SPI=0.
      IF(NL)511,511,519
 519  QENTE=0.37*UMAXE*WC
      QENTI=0.37*UMAXI*WC
      URME=(QCE-QENTE)/AE
      URMI=(QCI-QENTI)/AI
511   CONTINUE
      TPHIN=WC/(R-AI-WC*TGA)
      PHIN=ATAN(TPHIN)
      S=R*PHIN
      CO2=EXP(WS*ZP5/R)
      QS2=UMAXI*R*(C1-EXP(-WS/(2.*R)))
      QS2E=UMAXE*R*(EXP(WS/(2.*R))-1.)
      A57=WS*PTOT+R*RHO*(UMAXI2-UMAXE2)/4.
      DUE=UMAXE-URME
      PH=PINT
      SPIN=0.0
      M=0
50    PHIN1=PHIN2
```

```
      IF(R)171,162,172
171   PHIN2=PHIN2-PHIN
1171  A40=COS(PHIN1+2P5*PHIN-ALPHA)
      GOTO 173
172   PHIN2=PHIN2+PHIN
1172  A40=COS(PHIN1+2P5*PHIN-ALPHA)
173   CONTINUE
      A22=COS(PHIN2-ALPHA)
      A4=COS(PHIN2+ALPHA)*COS(PHIN2+ALPHA)
      A7=COS(ALPHA-PHIN1)
      A8=COS(ALPHA+PHIN-PHIN1)
      A9=COS(ALPHA+PHIN1)
      A61=COS(ALPHA+PHIN2)
      A63=SIN(ALPHA+1.57079+PHIN1-PHIN)
      N=0
      K=1
      L=0
      B1N=0.
      IF(BCN1)60,60,42
42    BCN=BCN1-2P5/B*PHIN*ABS(R)
      IF(BCN-0.03)60,60,30
 30   CONTINUE
      CO4=EXP(BCN/R)
      IF(R)31,162,32
32    BNE=BN1E+KEE*R*PHIN
      XL1=(R+BCN1+BN1E+XL1N1)*A9/A61-R-BCN-BNE
      IF(XL2N1)22,22,23
 23   BNI=BN1I+KE1*R*PHIN
      XL2=(-R+BCN1+BN1I+XL2N1)*A7/A22+R-BCN-BNI
      IF(XL2)24,25,25
22    XL2N1=0.0
24    XL2=0.0
      BNI=(-R+BCN1+BN1I+XL2N1)*A7/A22+R-BCN
      KEI=BNI/S
      IF(KEI-E)25,5,5
 5    KEI=E
      GOTO 23
31    BNE=BN1E+KEE*ABS(R)*ABS(PHIN)
      XL1=ABS(R)-BCN-BNE+(BCN1+BN1E+XL1N1-ABS(R))*A9/A63
      IF(XL2N1)34,34,36
36    BNI=BN1I+KE1*ABS(R)*ABS(PHIN)
      XL2=(ABS(R)+BCN1+BN1I+XL2N1)*A7/A8-ABS(R)-BCN-BNI
      IF(XL2)37,25,25
 34   XL2N1=0.0
 37   XL2=0.0
      BNI=(ABS(R)+BCN1+BN1I+XL2N1)*A7/A8-ABS(R)-BCN
      KEI=BNI/S
      IF(KEI-E)25,38,38
 38   KEI=E
      GOTO 36
```

```
25    CONTINUE
      IF(NR)21,21,709
709   QENTE=UMAXE*(A1*E*S+R*(EXP(BCN/R)-CD2))+(C1-A1)*E*S*URNE
      CD5=WC/XL1*C1/SQRT(BK1)
      QCE=(WC*QENTE)/(WC+4.*XL1)
      VCE=QCE/WC
      VCE2=VCE*VCE
802     AF2=-0.496182E-1-0.222789*VCE2+0.563274E-2*VCE2**2-0.148242E-3*VC
     1E2**3+0.206558E-5*VCE2**4-0.138133E-7*VCE2**5+0.354175E-10*VCE2**6
     2+0.5*RHO*((VCE*WC-QENTE)/XL1)**2+0.496182E-1
      BF2=ABS(AF2)
      IF(BF2-0.02)800,800,801
801   DAF2=-0.22279+0.011265*VCE2-0.4447E-3*VCE2**2+0.8262E-5*VCE2**3-0.
     169D6E-7*VCE2**4+0.2125E-9*VCE2**5+0.5*RHO*WC*(WC-QENTE*VCE2**-0.5)
     2/XL1**2
      VCE2=VCE2-AF2/DAF2*0.25
      IF(VCE2)805,805,806
805   VCE2=0.0005
806   VCE=SQRT(VCE2)
      GOTO 802
800   CONTINUE
      PEXT=-0.496182E-1-0.222789*VCE2+0.563274E-2*VCE2**2-0.148242E-3*VC
     1E2**3+0.206558E-5*VCE2**4-0.138133E-7*VCE2**5+0.354175E-10*VCE2**6
     2+0.496182E-1
      QCE=VCE*WC
      QE=QCE-QENTE
      URNE=QE/XL1
      CD3=-ZP5*URNE*URNE/A4
      DUE=UMAXE-URNE
      A5=CD3+BNE/R*(A11*DUE*DUE+C2*A1*DUE*URNE+URNE*URNE)
      A3D=C2*(A5+PTOT/RHO)
      UMAXN=SQRT(A3D)
      A6=ABS((UMAXN-UMAXE)/UMAXN)
      UMAXE=UMAXN
      IF(A6-ACC)714,714,709
714   UMAXI=UMAXE*EXP(C2*BCN/R)
      QEN=UMAXI*(A1*E*S+R*(1./CD2-1./CD4))
      B6=(1.-A1)*E*S
      URNI=(QCI-QEN)/(B6+XL2)
      QENTI=QEN+B6*URNI
      IF(URNI)715,716,716
21    URNE=(-UMAXE*BNE*A1-UMAXE*R*(EXP(BCN/R)-C1)+QS2E+QCE)/(XL1+A1D*BNE
     1)
      DUE=UMAXE-URNE
      PEXT=-RHO*URNE*URNE*ZP5/A4
      A5=-PEXT/RHO+BNE/R*(A11*DUE*DUE+C2*A1*DUE*URNE+URNE*URNE)
      A3D=C2*(A5+PTOT/RHO)
      UMAXN=SQRT(A3D)
      A6=ABS((UMAXN-UMAXE)/UMAXN)
      UMAXE=UMAXN
```

```
      IF(A6-0.001)20,20,21
20    CONTINUE
      UMAXI=UMAXE*EXP(C2*BCN/R)
715   URMI=(-UMAXI*BNI*A1-UMAXI*R*(C1-EXP(-BCN/R))+QS2+QCI)/(XL2+BNI*A10
     1)
716   DUI=UMAXI-URMI
      AJE=RHO*BNE*(DUE*DUE*A11+C2*DUE*URME*A1+URME*URME)
      BCJ=RHO*R*(UMAXI*UMAXI-UMAXE*UMAXE)/C4
      AJI=RHO*BNI*(DUI*DUI*A11+C2*DUI*URMI*A1+URMI*URMI)
      A50=BNE*PEXT+BNI*PN
      APE=RHO/R*BNE*BNE*(-DUE*DUE*A55-C2*DUE*URME*A56-ZP5*URME*URME)
      API=RHO/R*BNI*BNI*(DUI*DUI*A55+C2*DUI*URMI*A56-ZP5*URMI*URMI)
      SPI=SPIN+(RHO*URMI*URMI+PN)*(BNI+BCN-BNII-BCN1)
      B1=AJE+BCJ+AJI+A50+APE+API-A57+C2*PTOT*BCN-SPI
      A60=ABS(B1)-0.5
      IF(A60)70,70,71
71    IF(L)82,81,82
81    L=1
      BCN=BCN+0.01
      B1N=B1
      GOTO 30
82    L=0
      DB1=(B1-B1N)/0.01
      BCN=BCN-0.01-B1N/(15.*DB1)
      B1N=B1
      GO TO 30
70    B1N=0.
      IF(BCN)60,35,35
60    BCN=0.0
      IF(R)151,162,152
 152  XL1=(R+BCN1+BN1E+XL1N1)*A9/A61-R-BN1E-KEE*R*PHIN
      IF(XL2N1)61,61,62
62    BNI=BN1I+KEI*R*PHIN
      XL2=(-R+BCN1+BN1I+XL2N1)*A7/A22+R-BNI
      IF(XL2)64,65,65
 61   XL2N1=0.0
 64   XL2=0.0
      BNI=(-R+BCN1+BN1I+XL2N1)*A7/A22+R
      XEI=BNI/S
      IF(XEI-E)65,66,66
 66   XEI=E
      GOTO 62
151   BNE=BN1E+KEE*ABS(R)*ABS(PHIN)
      XL1=ABS(R)-BNE+(BCN1+BN1E+XL1N1-ABS(R))*A9/A63
      IF(XL2N1)154,154,156
156   BNI=BN1I+KEI*PHIN*ABS(R)
      XL2=(ABS(R)+BCN1+BN1I+XL2N1)*A7/A8-ABS(R)-BNI
      IF(XL2)157,65,65
154   XL2N1=0.0
157   XL2=0.0
```

```
      BNI=(ABS(R)+BCN1+BN1I+XL2N1)*A7/A8-ABS(R)
      XEI=BNI/S
      IF(XEI-E)65,158,158
158   XEI=E
      GOTO 156
65    CONTINUE
      BNE=BN1E+XEE*PHIN*ABS(R)
      DUE=DUE*SQRT((C6*WS)/S)
      URNE=(QS2+QCE-BNE*DUE*A1)/(XL1+BNE)
      UMAXE=DUE+URNE
      GOTO 63
94    URNE=(QS2E+QCE-UMAXE*BNE*A1)/(XL1+BNE*A1D)
      DUE=UMAXE-URNE
63    UMAXI=UMAXE
      URNI=(QS2+QCI-UMAXI*BNI*A1)/(XL2+BNI*A1D)
      DUI=UMAXI-URNI
      AJE=RHO*BNE*(DUE*DUE*A11+C2*DUE*URNE*A1+URNE*URNE)
      AJI=RHO*BNI*(DUI*DUI*A11+C2*DUI*URNI*A1+URNI*URNI)
      PEXT=-RHO*URNE*URNE*ZP5/A4
      A5D=BNE*PEXT+BNI*PN
      APE=RHO/R*BNE*BNE*(-DUE*DUE*A55-C2*DUE*URNE*A56-ZP5*URNE*URNE)
      API=RHO/R*BNI*BNI*(DUI*DUI*A55+C2*DUI*URNI*A56-ZP5*URNI*URNI)
      SPI=SPIN+(RHO*URNI*URNI+PN)*(BNI-BN1I)
      B1=AJE+AJI+A5D+APE+API-A57-SPI
      IF(N)86,87,86
87    A7D=ABS(B1)-1
      IF(A7D)35,35,89
89    N=1
      UMAXE=UMAXE+0.1
      B1N=B1
      GOTO 94
86    N=0
      DB1=(B1-B1N)/0.1
      UMAXE=UMAXE-0.1-B1N/DB1
      B1N=B1
      GOTO 94
35    IF(BCN)131,131,132
131   A13=0.0
      GOTO 133
132   A13=R*UMAXE*EXP(BCN/R)*(EXP(BCN/R)-C1)
133   A12=XHID-C2/(XN+C1)*XHID**(XN+C1)+XHID**(C2*XN+C1)/(C2*XN+C1)
      F1=A13+DUI*BNI*A12+URNI*BNI*XHID-QS2
      F11=ABS(F1)
      IF(F11-0.01)27,27,26
 26   DF1=DUI*BNI*(C1-C2*XN*XHID**XN/(XN+C1)+C2*XN*XHID**(C2*XN)/(C2*XN+
     1C1))+URNI*BNI
      XHID=XHID-F1/DF1*ZP5
      GOTO 133
27    IF(URNI)906,905,905
905   XHBD=1.
```

```
      GOTO 903
906   B12=XHBD-C2/(XN+C1)*XHBD**(XN+C1)+XHBD**(C2*XN+C1)/(C2*XN+C1)
      BF1=A13+DUI*BNI*B12+URMI*BNI*XHBD-QS2-QCI
      BF11=ABS(BF1)
      IF(BF11-ACC)510,510,904
904   DB1=DUI*BNI*(C1-C2*XN*XHBD**XN/(XN+C1)+C2*XN*XHBD**(C2*XN)/(C2*XN+
     1C1))+URMI*BNI
      XHBD=XHBD-BF1/DB1*ZP5
      GOTO 906
 510  IF(XHBD-0.98)903,501,501
501   IF(M)903,502,903
903   A18=XHID**(XN+C1)/(XN+C1)
      A17=XHID**(C2*XN+C1)/(C2*XN+C1)
      A15=XHID-C4*A18+C6*A17-C4*XHID**(C3*XN+C1)/(C3*XN+C1)+XHID**(C4*XN
     1+C1)/(C4*XN+C1)
      A16=XHID-C2*A18+A17
      D18=XHBD**(XN+C1)/(XN+C1)
      D17=XHBD**(C2*XN+C1)/(C2*XN+C1)
      D15=XHBD-C4*D18+C6*D17-C4*XHBD**(C3*XN+C1)/(C3*XN+C1)+XHBD**(C4*XN
     1+C1)/(C4*XN+C1)
      D16=XHBD-C2*D18+D17
      AJ1=(RHO*BNI*(DUI*DUI*(A11-A15)+C2*DUI*URMI*(A1-A16)+URMI*URMI*(C1
     1-XHID)))*A22
      AJ2=URMI*URMI*RHO*A22*KL2
      A20=C1-XHID**XN
      A21=(-C2*XN*XHID**(XN-C1)*A20*DUI)/BNI-CONST/R*(DUI*A20*A2 +URMI)
      DXHI=XHBD-XHID
      P11=0.5*XHBD**2-16./35.*XHBD**3.5+0.3*XHBD**5-16./143.*XHBD**6.5+1
     1./56.*XHBD**8
      P12=0.5*XHID**2-16./35.*XHID**3.5+0.3*XHID**5-16./143.*XHID**6.5+1
     1./56.*XHID**8
      P13=(XHBD-8./5.*XHBD**2.5+1.5*XHBD**4-8./11.*XHBD**5.5+1./7.*XHBD*
     1*7)*DXHI
      P14=0.5*XHBD**2-8./35.*XHBD**3.5+1./20.*XHBD**5
      P15=0.5*XHID**2-8./35.*XHID**3.5+1./20.*XHID**5
      P16=(XHBD-0.8*XHBD**2.5+0.25*XHBD**4)*DXHI
      P17=0.5*(XHBD**2-XHID**2)-XHBD*DXHI
      P1=-RHO*BNI/R*(DUI*DUI*(P11-P12-P13)+2.*DUI*URMI*(P14-P15-P16)+
     1URMI*URMI*P17)*BNI*A22
      D20=XHID-8./5.*XHID**2.5+1.5*XHID**4.-8./11.*XHID**5.5+1./7.*XHID
     1**7.
      D21=XHID-0.8*XHID**2.5+0.25*XHID**4.
      D22=XHBD-8./5.*XHBD**2.5+1.5*XHBD**4.-8./11.*XHBD**5.5+1./7.*XHBD
     1**7.
      D23=XHBD-0.8*XHBD**2.5+0.25*XHBD**4.
      DPH=-RHO*BNI/R*(DUI*DUI*(D20-D22)+2.*DUI*URMI*(D21-D23)+URMI*URMI
     1*(XHID-XHBD))
      IF(BCN)150,150,140
150   D1=D2
      GOTO 160
```

```
140   D1=D1
160   TN=RHO*BNI*DUI*D1/XEI*A21
      TN=ABS(TN)
      IF(R)181,162,182
181   A23=-R+BCN+BNI*XHID
      A15D=SIN(ALPHA-PHIN1+ZP5*PHIN)
      GOTO 183
182   A23=R-BCN-BNI*XHID
      A15D=SIN(ALPHA-PHIN1-ZP5*PHIN)
 183  CONTINUE
      A19=A22*(XL2+BNI*(C1-XHID))
      IF(NR)29,29,28
28    A8D=TN*A23*PHIN*A4D
      JCI=0.412338-3.3896*QCI+1.16508*QCI**2-0.04087*QCI**3+0.942E-3*QCI
     1**4-0.7827E-5*QCI**5
      PN1=(-AJ1-AJ2+A8D+PINT*XL2N1*COS(ALPHA)+(PINT+DPN)*A23*PHIN*A15D
     1-JCI*RHO*SIN(ALPHA)-PI)/A19
      WRITE(108,2280)AJ1,AJ2,XHID,QENTI
2280  FORMAT(4F12.6)
      PNM1=PN1
      URMN2=(PINT-PN1)*2/RHO-((QCI/WC)**2*(1.+ALPHA/1.57)*1.2*1.3)
      AUR=ABS(URMN2)
      URMN=SQRT(AUR)
      DURM=(URMI-URMN)/URMI
      DUR=ABS(DURM)
      IF(DUR-0.01)400,400,1400
1400   QCIN=QCI+XL2*(URMN-URMI)*0.25*URMN2/AUR
      WRITE(108,2400) QCI,QCIN,URMN,URMI,PN1,PINT,QCE
2400  FORMAT(1X,7F12.6)
      ML=0
      QCI=QCIN
      GOTO 721
 29   A41=ZP5*(TN+TN1)*A23*PHIN*A4D
      PN1=(AJN1+AJN2+PN   *A19N+PIN1-AJ1-AJ2+A41+(PN+DPN)*A23*A15D*ABS(PH
     1IN)-PI)/A19
      PNM1=PN
      GO TO 40
 400  WRITE(108,9400) QCI,QCE,PINT,PEXT
9400  FORMAT(1X,7HQCI    =,F12.6,5X,7HQCE    =,F12.6,5X,7HPINT   =,F12.6,
     15X,7HPEXT   =,F12.6)
40    CONTINUE
      WRITE(108,9000) URMI,UMAXI,UMAXE,URME,XL2
9000  FORMAT(//1X,7HURMI  =,F12.6,5X,7HUMAXI =,F12.6,5X,7HUMAXE =,F12.6,
     15X,7HURME   =,F12.6,5X,7HXL2    =,F12.6)
      WRITE(108,9001) BNI,BCN,XL1,BNE,XEI
9001  FORMAT(1X,7HBNI    =,F12.6,5X,7HBCN    =,F12.6,5X,7HXL1    =,F12.6,
     15X,7HBNE    =,F12.6,5X,7HXEI    =,F12.6)
      WRITE(108,9002) A8D,PN1,XHID,XHBD
9002  FORMAT(1X,7HA8D    =,F12.6,5X,7HPN1    =,F12.6,5X,7HXHID   =,F12.6,
     15X,7HXHBD   =,F12.6)
```

```
      NR=0
      AJE=RHO*BNE*(DUE*DUE*A11+C2*DUE*URNE*A1+URNE*URNE)
      AJBC=ZP5*RHO*(UMAXI*UMAXI-UMAXE*UMAXE)*R
      AJPI=RHO*BNI*(DUI*DUI*D15+C2*DUI*URNI*D16+URNI*URNI*KHBD)
      PEXT=-RHO*URNE*URNE*ZP5/A4
      R=(AJE+AJBC+AJPI)/(PEXT-PN1)
      PHIN=(ZP5*WS)/ABS(R)
      PIN1=PI
      BCN1=BCH
      BN1E=BNE
      BN1I=BNI
      XL1N1=XL1
      XL2N1=XL2
      TN1=TN
      PN=PN1
      AJN2=AJ2
      AJN1=AJ1
      A19N=A19
      S=S+PHIN*ABS(R)
      SPIN=SPI
      IF(R)161,162,163
  163 WDIST=((R-BCN1-BN1I-XL2N1)*SIN(PHIN)/COS(PHIN2-ALPHA))+WDIST1
      GOTO 164
  161 WDIST=(-R+BCN1+BN1I+XL2N1)*SIN(PHIN)/COS(ALPHA+PHIN-PHIN1)+WDIST1
  164 CONTINUE
      WRITE(108,909) PHIN1,PHIN2,R,PEXT
  909 FORMAT(1X,7HPHIN1 =,F12.6,5X,7HPHIN2 =,F12.6,5X,7HR      =,F12.6,
     15X,7HPEXT   =,F12.6)
      WRITE(108,908)WDIST,WDIST1,S
  908 FORMAT(1X,7HWDIST =,F12.6,5X,7HWDIST1=,F12.6,5X,7HS      =,F12.6)
      WDIST1=WDIST
      IF(M)1111,192,1111
 1111 CALL XTIME
      GO TO 1
  502 M=1
      WRITE(108,8888)
 8888 FORMAT(/' LAST SLICE IS DEVIDED IN TWO PARTS'/)
      IF(R)503,162,504
  503 PHIN2=PHIN2+PHIN*0.5
       GOTO 1171
  504 PHIN2=PHIN2-PHIN*0.5
      GOTO 1172
  192 IF(PN1-100.)193,1111,1111
  193 CONTINUE
      GOTO 50
  162 CONTINUE
      WRITE(108,1703)
 1703 FORMAT(1X,' R EQUALS ZERO'//)
      END
%EOD
```

```
2.5   2.5    40.     2.5    2.5     10.
100.  10.     0.65    288.   0.274   10.     9.77   7.67
1.5   5.77    0.35  0.01
2.5   2.5    40.     2.5    2.5     15.
100.  10.     0.65    288.   0.274   10.     9.77   7.67
1.5   5.77    0.35  0.01
```

REFERENCES

1. Moses H.L., Comparin R.A. : "The effect of geometric and fluid parameters on static performance of wall-attachment-type fluid amplifiers". Proceedings of the "Fluidics State of the Art Symposium", HDL, Wash. D.C., 30 Sept-3 Oct. 1974, republished in AGARDograph 215, ed. J. Kirshner, pp 229-248.

2. Drzewiecki T.M. : "The design of fluidic turbulent wall attachment flip-flops". Proceedings of the "Fluidics State of the Art Symposium", HDL, Wash. D.C., 30 Sept.-3 Oct. 1974, republished in AGARDograph 215, ed. J. Kirshner, pp. 249-292.

3. Goto J.M., Drzewiecki T.M. : "An analytical model for the response of fluidic wall attachment amplifiers". HDL-TR-1598, Fluidics 32, Hary Diamond Labs, Wash. D.C. (AD-747761), June 1972, also published in Fluidics Quarterly, Vol.5, N°1, January 1973.

4. Bekaert G., Carbonaro M. : "Experimental study of the switching characteristics of bistable amplifier in the turbulent flow regime". Final technical report to US Army European Research Office, contract number DAJA-37-73-C-1212 (AD-782892), January 1974.

5. Riethmuller M.L. : "Laser doppler velocimetry" VKI Lecture Series on "Measurements of unsteady fluid dynamics phenomena", VKI-LS-73, VKI Brussels, 27-31 Jan. 1975.

6. Riethmuller M.L. : "Analysis of the output data of a laser doppler velocimeter" AGARD Conf. on Applications of non-intrusive instrumentation in fluid flow research. Fluid Dynamics Panel Symp. 3-5 May 1976, IS St Louis, France.

7. Abramovitch G.N. : "The theory of turbulent jets", MIT Press, Cambridge, Mass. 1963.

8. Schlichting : "Boundary layer theory", Mc Graw-Hill, 1960.

9. Bekaert, G. : "Attachment and switching in bistable amplifiers", Ph.D. Thesis, Louvain-la-Neuve, Belgium, Feb. 1976.

10. Sawyer R.A. : "Two-dimensional re-attaching jet flows including the effect of jet curvature on the entrainment". J. Fluid Mechanics, Vol.7, P & 4, 1963.

11. Bekaert G., Carbonaro M. : "Experimental study of the switching characteristics of bistable amplifiers in the laminar and turbulent flow regime". Final Technical Report to US Army European Research Office, Contract number DAJA-37-74-C-2689, July 1975.

12. Drzewiecki T.M., Manion F.M. : "The laminar flip flop" Proceedings of the "Fluidics state of the art symposium", HDL, Wash. D.C., 30 Sept.-3 Octo. 1974.

13. Manion F.M., Mon G. : "Design and staging of laminar proportional amplifiers". HDL-TR-1608, Fluerics 33, Harry Diamond Labs., Wash. D.C., Sept. 1972.

14. Manion F.M., Drzewiecki T.M. : "Analytical design of laminar proportional amplifiers". Proceedings of the "Fluidics State of the Art Symposium", HDL, Wash. D.C., 30 Sept.-3 Oct. 1974.

15. Sarpkaya T., Kirshner J.M. : "The comparative performance characteristics of vented and unvented, cusped and straight and curved walled bistable amplifiers", paper f3. Proceedings of the 3rd Cranfield Fluidics Conference, ed. BHRA, Turin, May 1968.

16. Cox L.S. : "Fabrication of fluidics or the search for unconventional practices". Proceedings of the "Fluidics State of the Art Symposium", HDL, Wash. D.C., 30 Sept.-3 Oct. 1974.

17. Anon.: "An introduction to photo-fabrication using Kodak photo-sensitive resists". Kodak publication N° P-79, 1970.
"Chemical milling with Kodak photo-sensitive resits" Kodak publication N° P-131, 1968.

18. Buekenhout L. (ELCOMAT-CMF raghenoplein 21, 2800 Mechelen, Belgium). Personal communications.

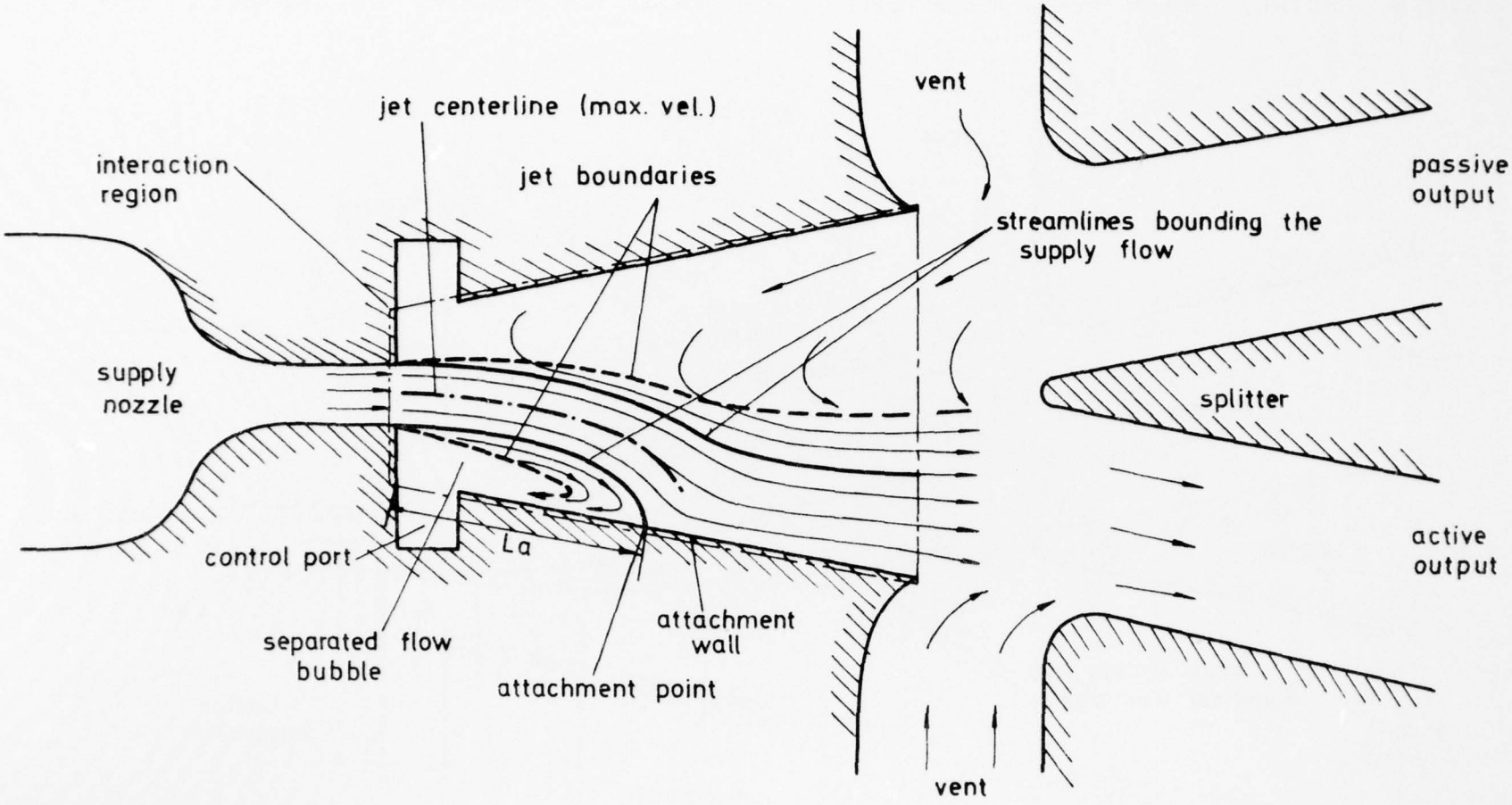


FIG. 1 a STREAMLINE PATTERN IN A BISTABLE AMPLIFIER WITH CLOSED CONTROL PORTS

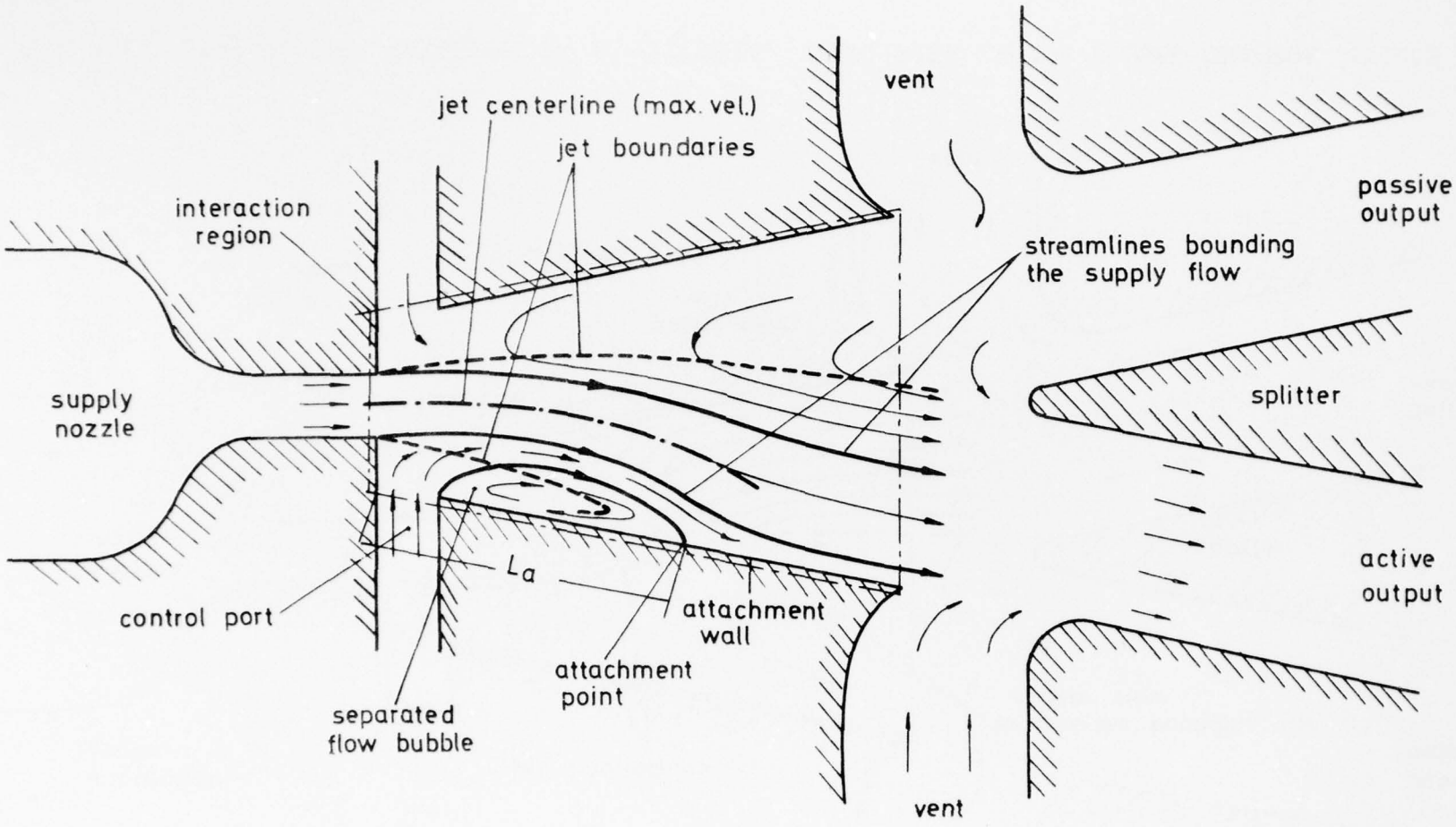
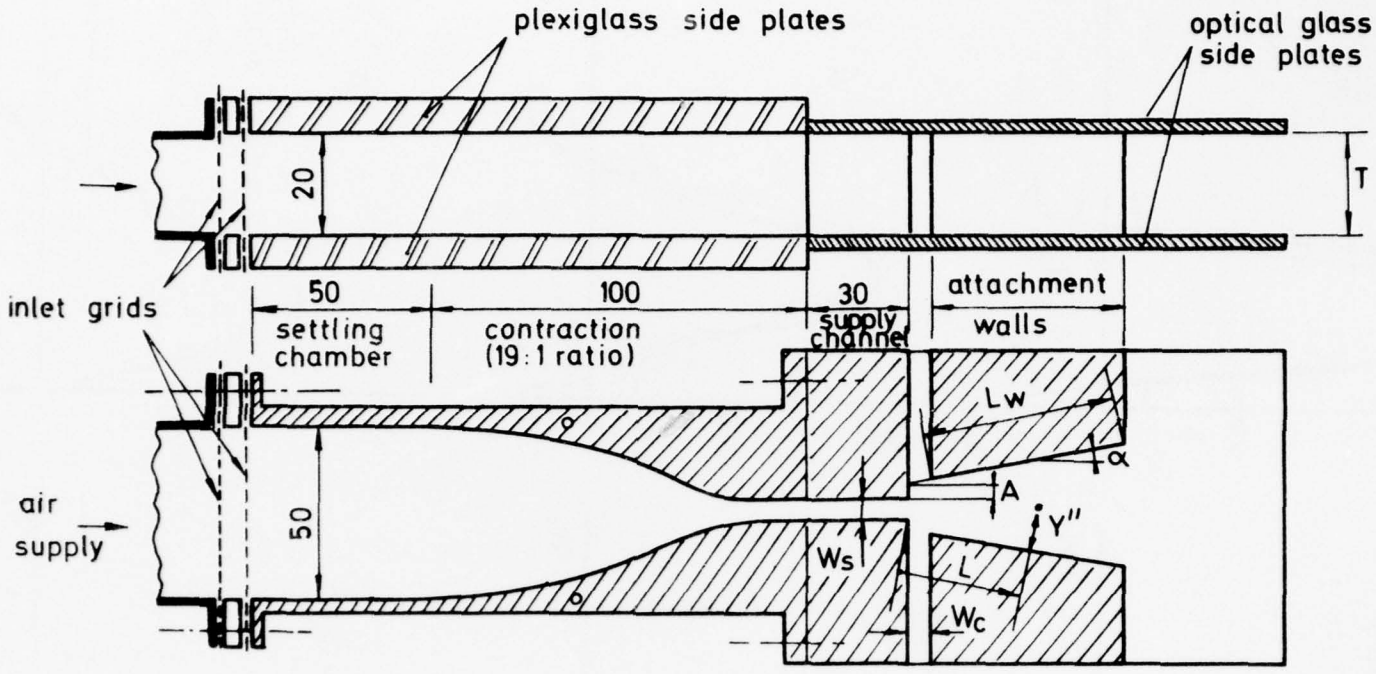


FIG. 1 b STREAMLINE PATTERN IN A BISTABLE AMPLIFIER WITH OPEN CONTROL PORTS.



$W_s = 2{\cdot}5$ mm, $T/W_s = 8$, $W_c/W_s = 1$, $L_w/W_s = 17$, $\alpha, A/W_s$ = variable

FIG. 2 BISTABLE MODEL USED FOR THE LDV MEASUREMENTS

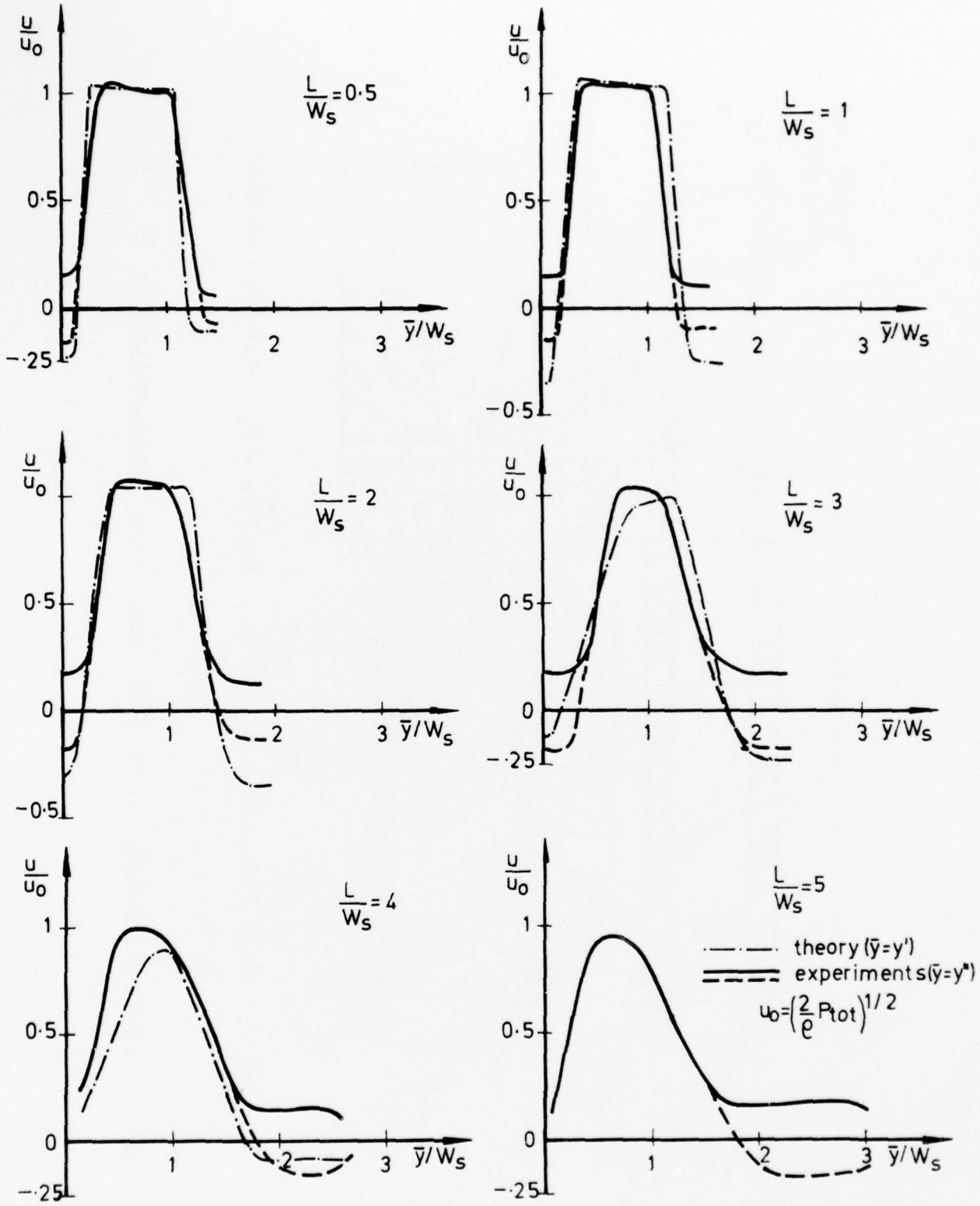


FIG. 3a VELOCITY PROFILES FOR AR=8; α=10°; A/W_s = 0·1; L_W/W_s =17
CONTROL CHANNELS CLOSED

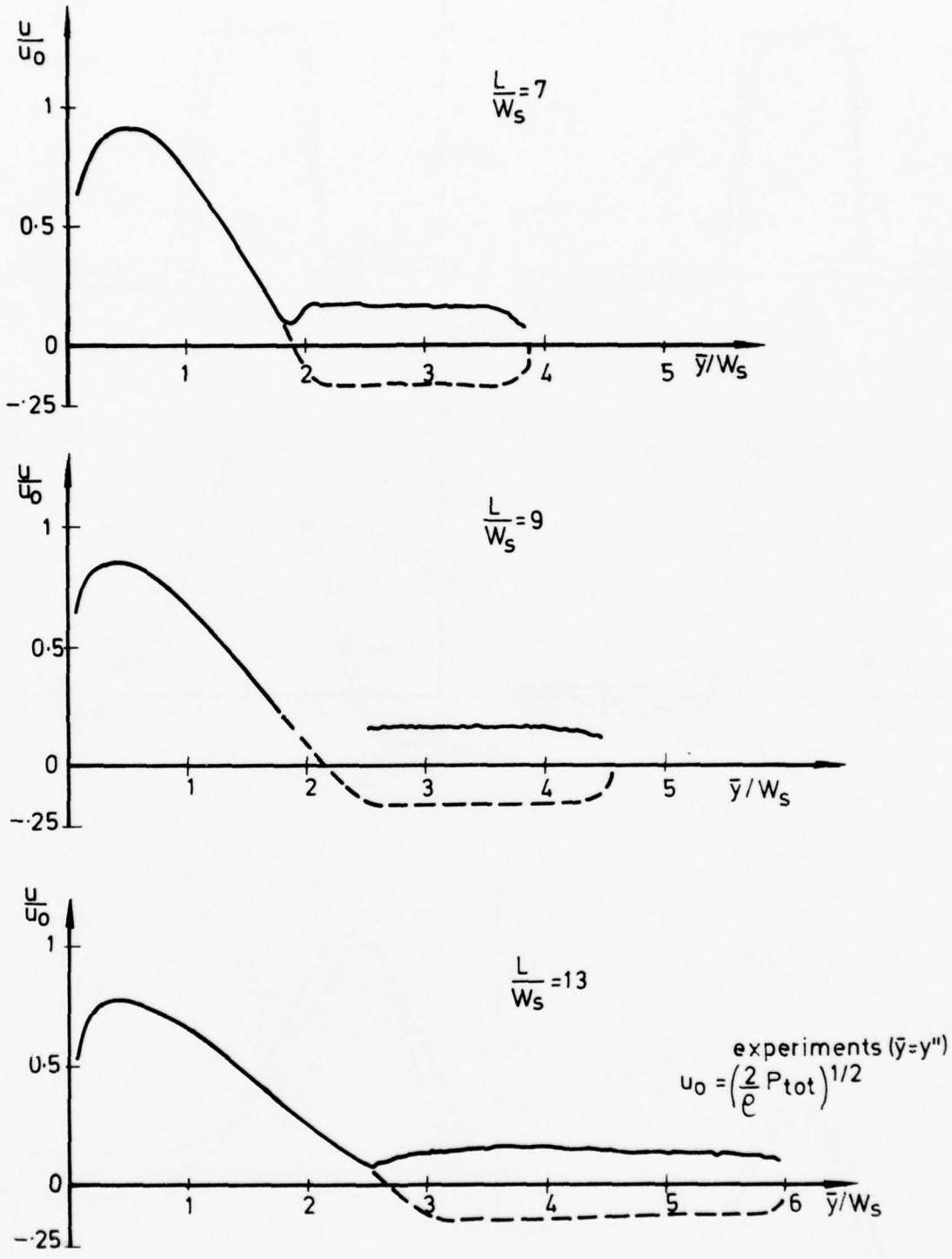


FIG. 3 b VELOCITY PROFILES FOR AR = 8, α=10°; A/Ws = 0·1; Lw/Ws = 17
CONTROL CHANNELS CLOSED

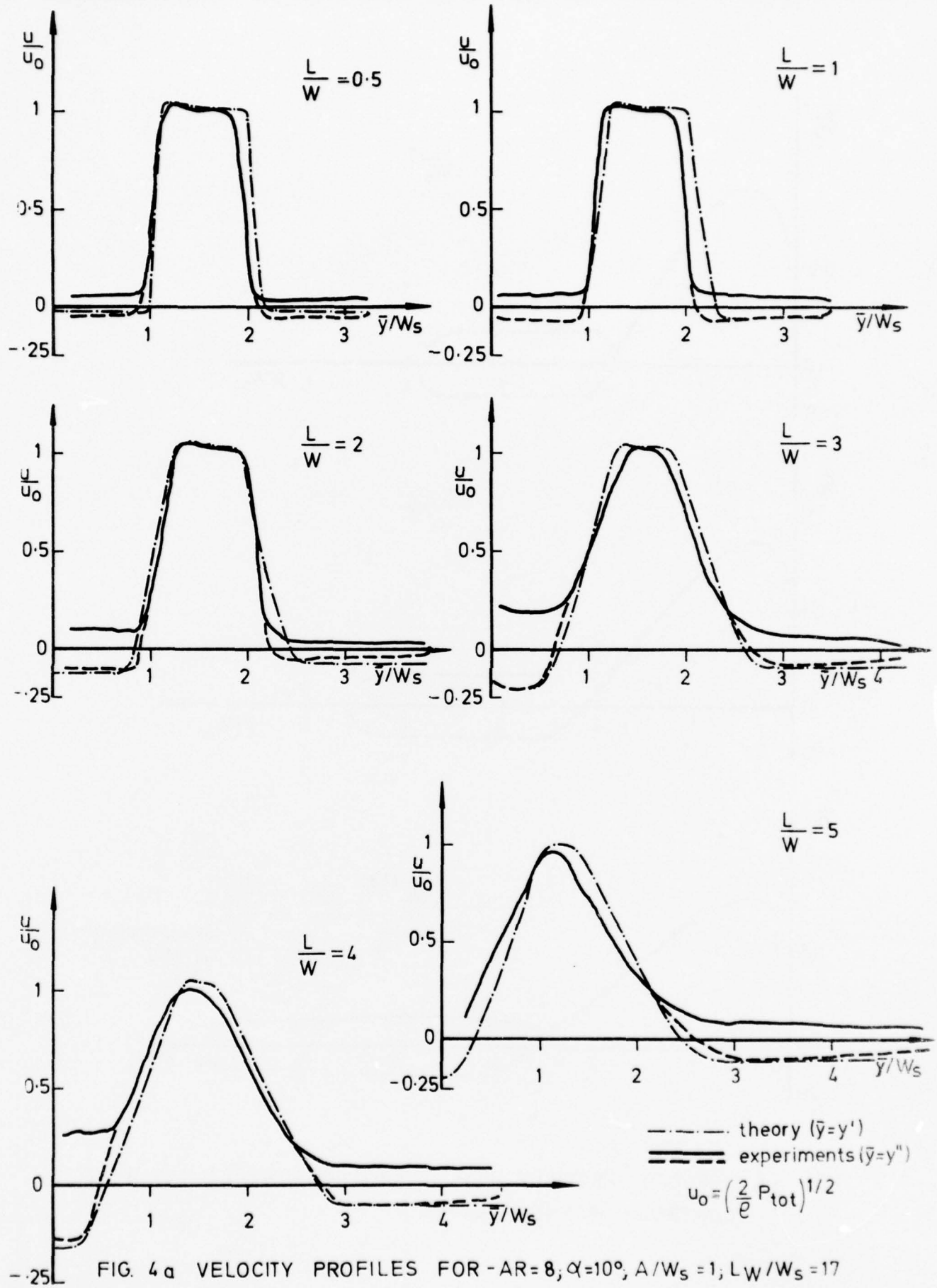


FIG. 4a VELOCITY PROFILES FOR - AR = 8; α = 10°, A/W_s = 1; L_W/W_s = 17
CONTROL CHANNELS CLOSED

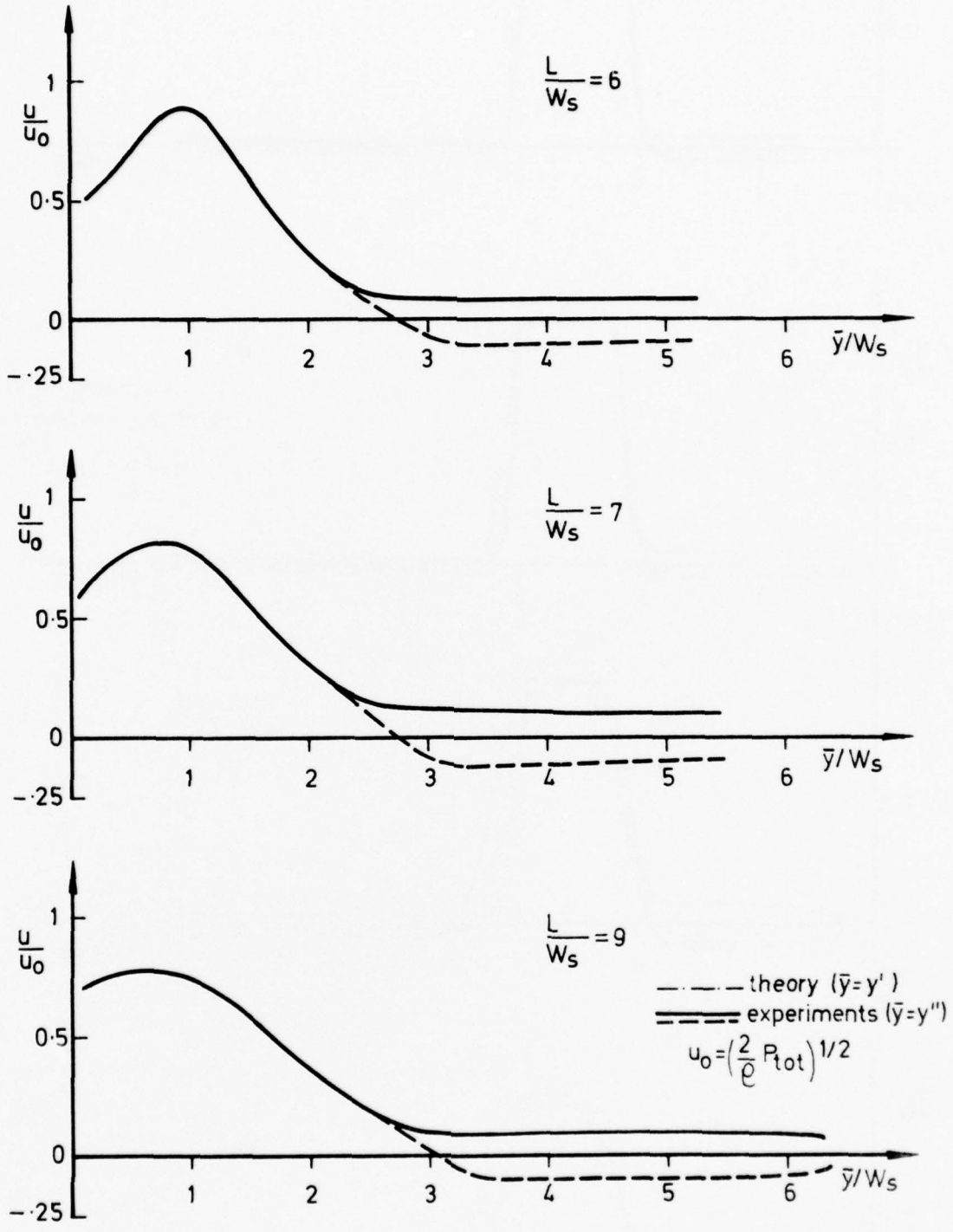


FIG. 4 b VELOCITY PROFILES FOR AR=8; α=10°; A/Ws=1; Lw/Ws=17
CONTROL CHANNELS CLOSED

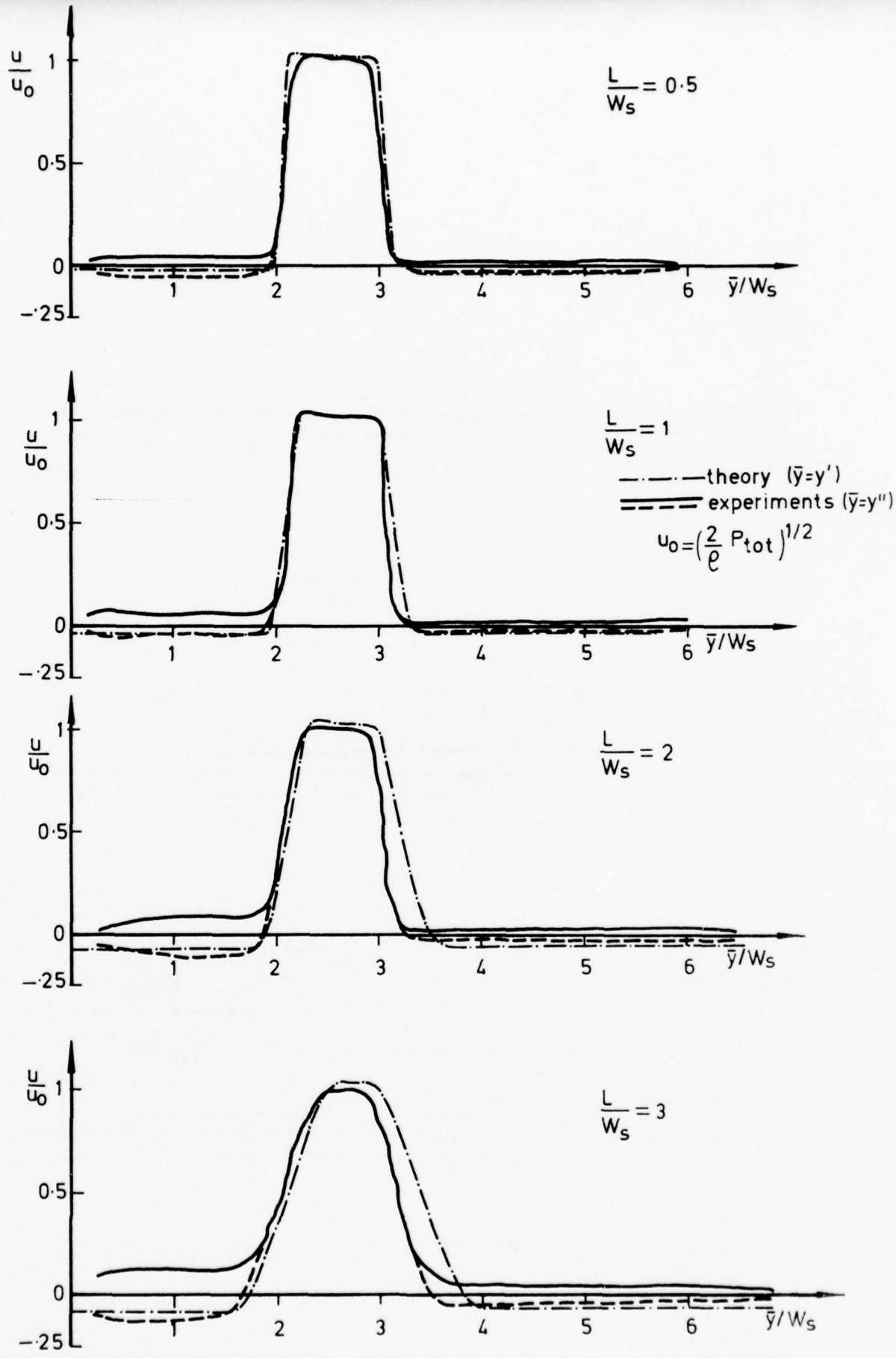


FIG. 5a VELOCITY PROFILES FOR AR=8; α=10°; A/Ws = 2; Lw/Ws = 17
CONTROL CHANNELS CLOSED

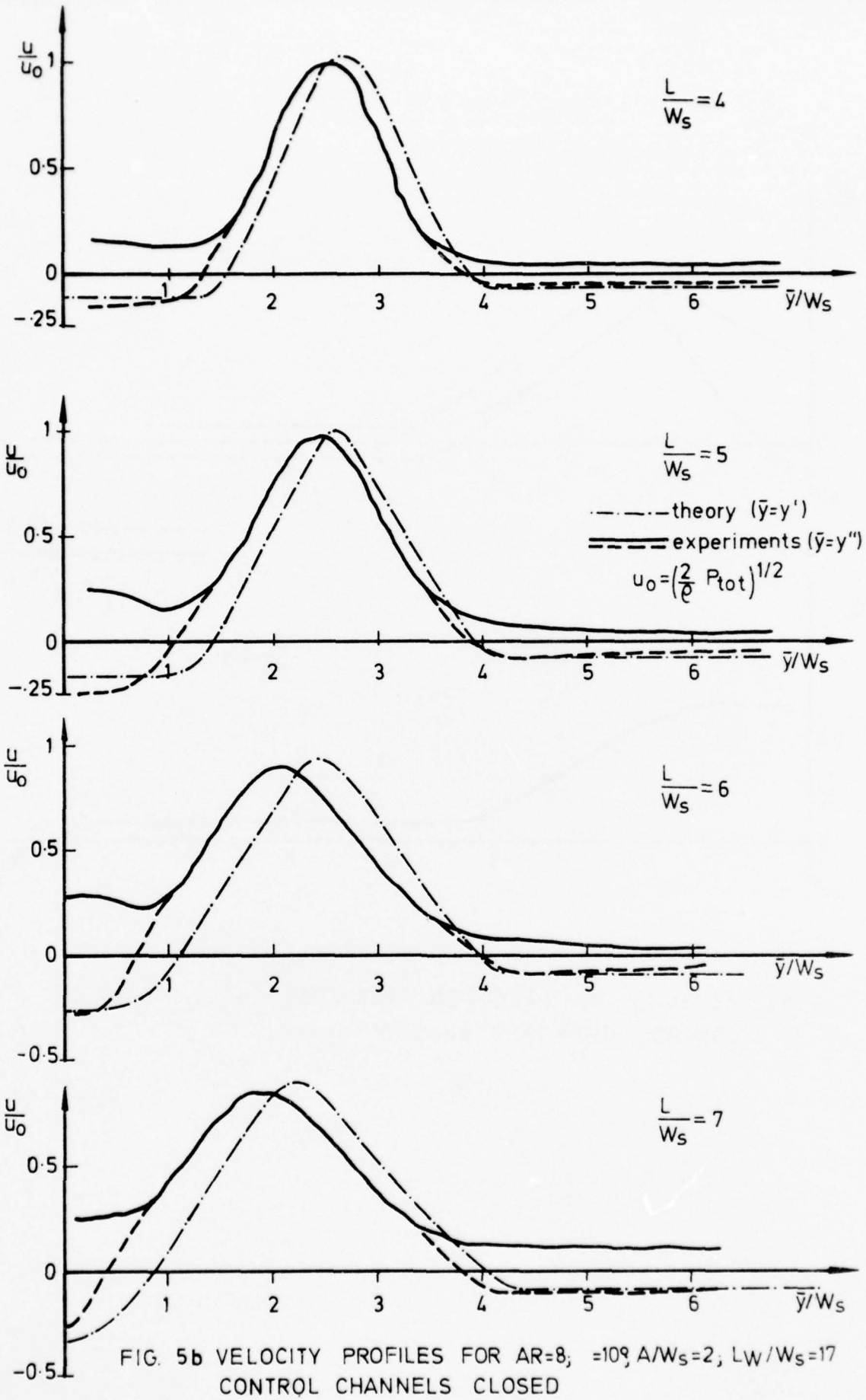


FIG. 5b VELOCITY PROFILES FOR AR=8; =10°, A/Ws=2; Lw/Ws=17
CONTROL CHANNELS CLOSED

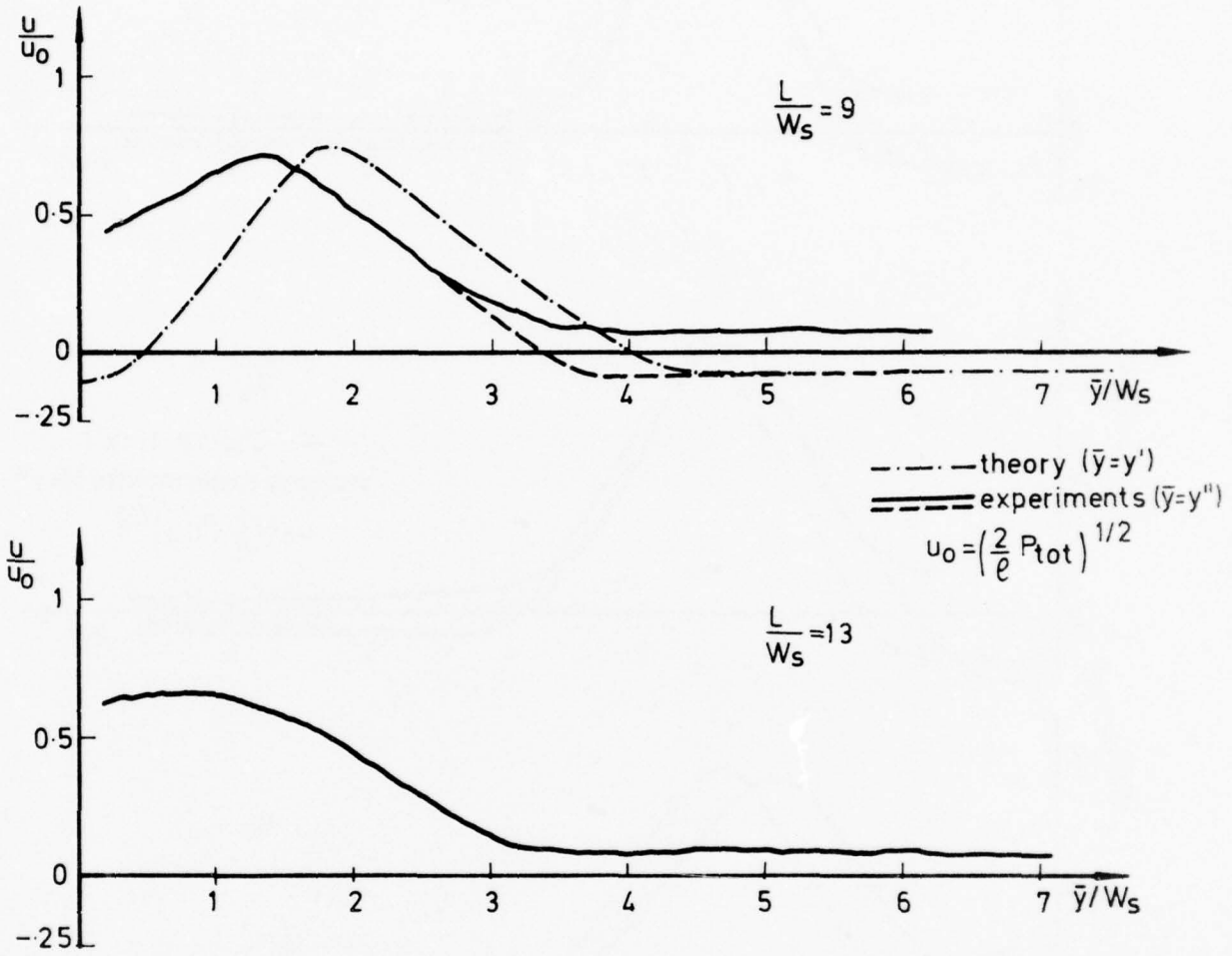


FIG. 5c VELOCITY PROFILES FOR AR=8, α=10°; A/W_s=2; L_W/W_s =17
CONTROL CHANNELS CLOSED

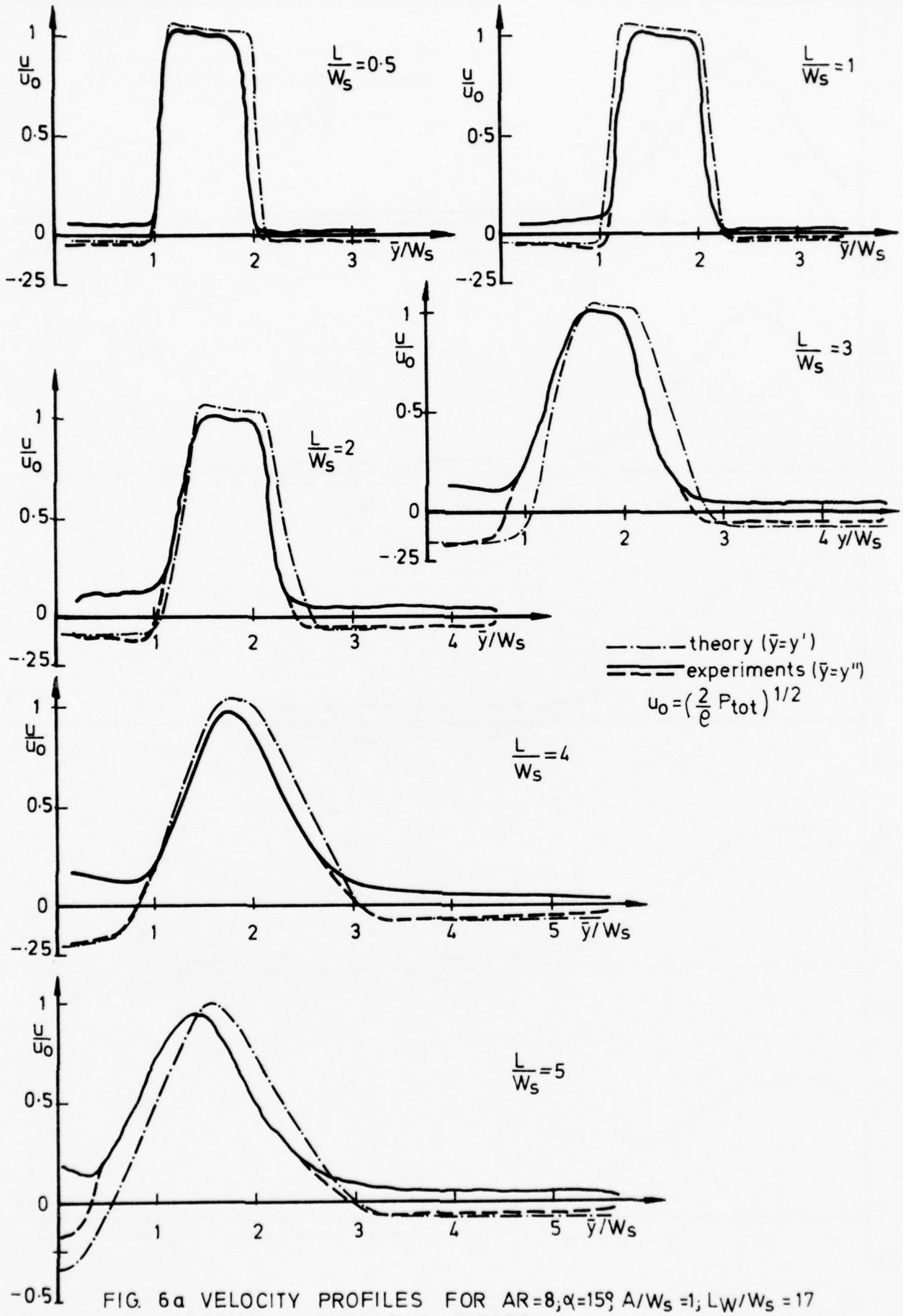


FIG. 6a VELOCITY PROFILES FOR AR=8; α=15°; A/Ws =1; Lw/Ws = 17
CONTROL CHANNELS CLOSED

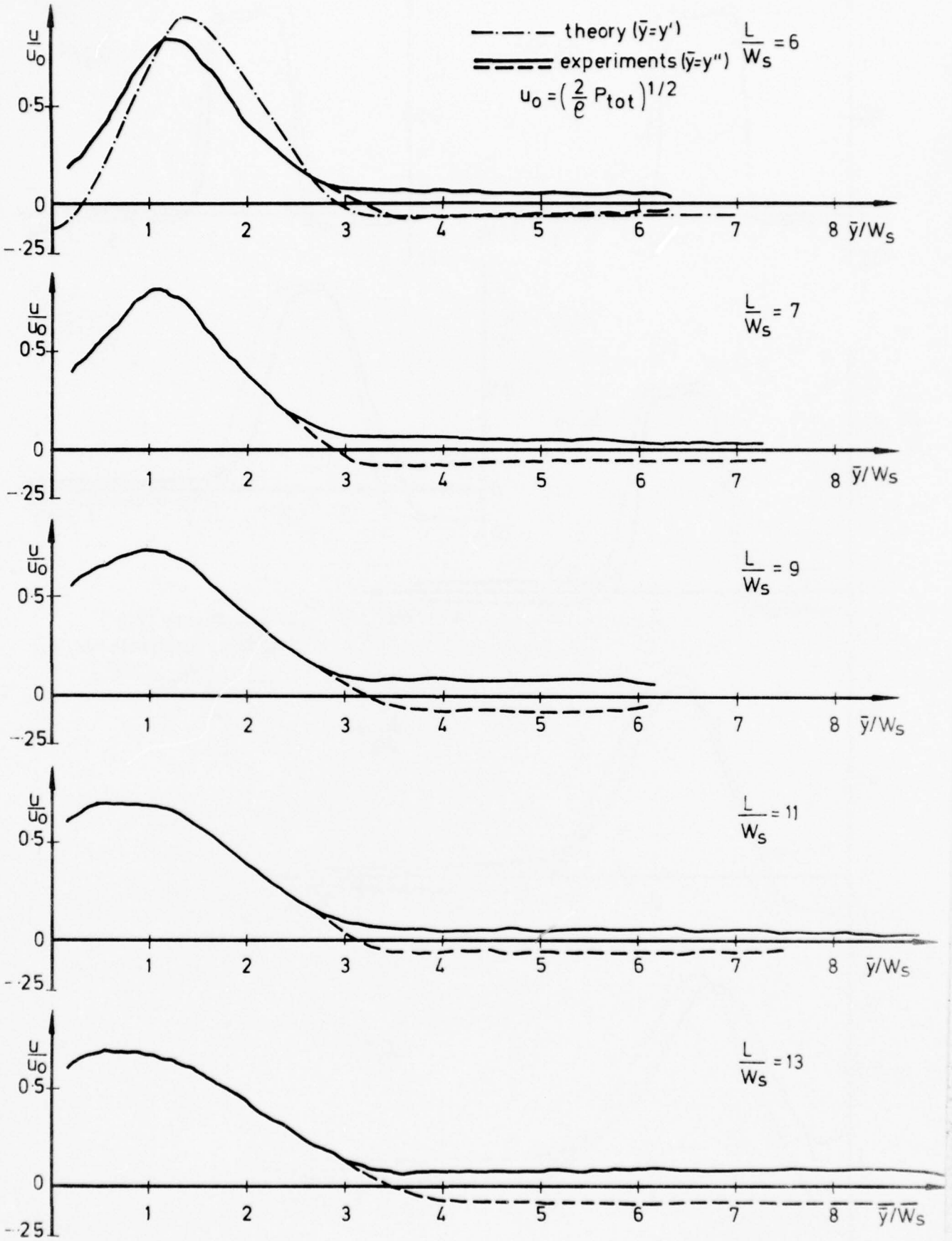


FIG. 6 b VELOCITY PROFILES FOR AR=8; α=15°; A/W_s =1; L_W/W_s =17
CONTROL CHANNELS CLOSED

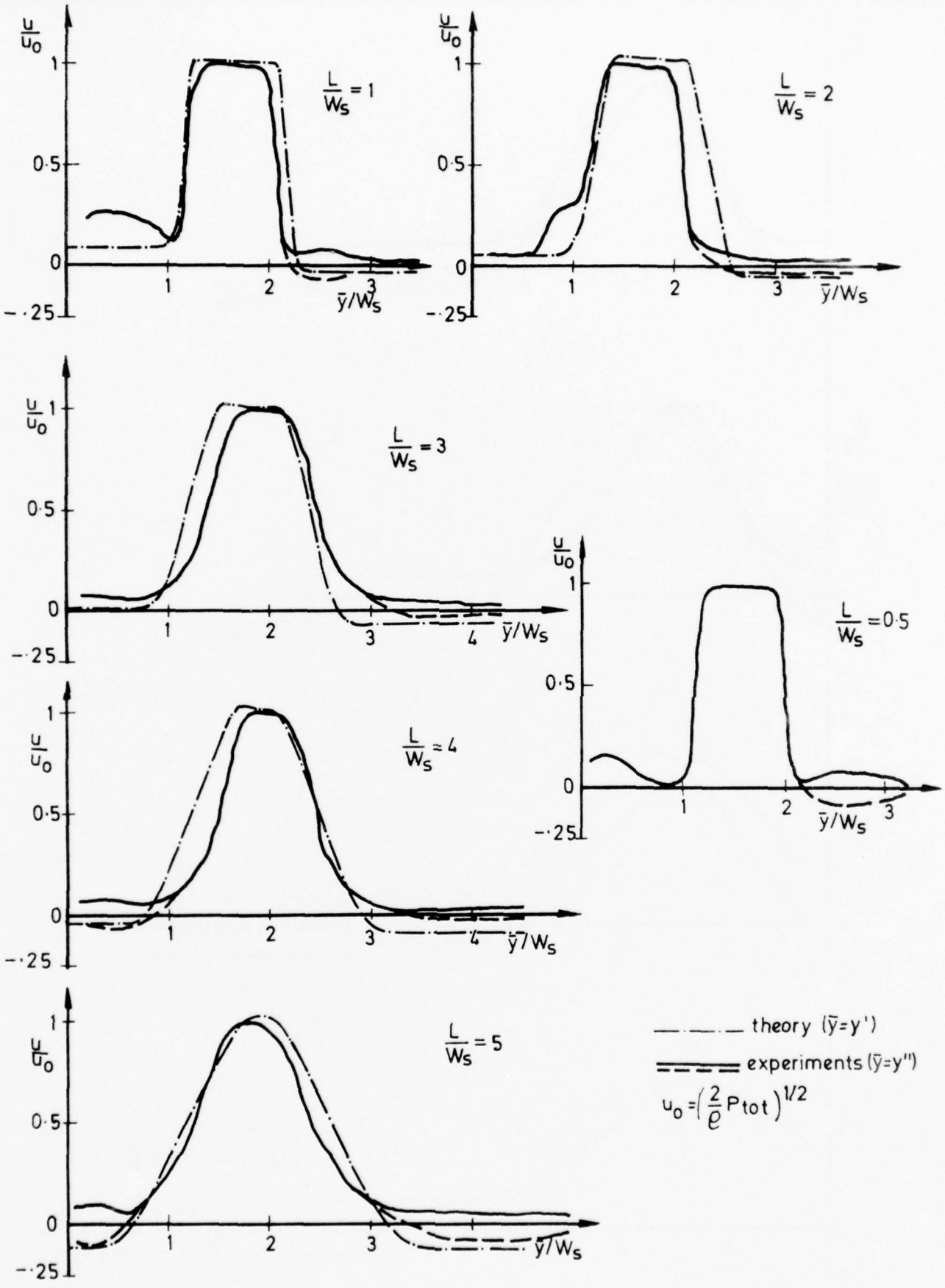


FIG. 7a VELOCITY PROFILES FOR AR = 8, $\alpha = 10°$, $A/W_s = 1$, $L_W/W_s = 17$
CONTROL CHANNELS OPEN

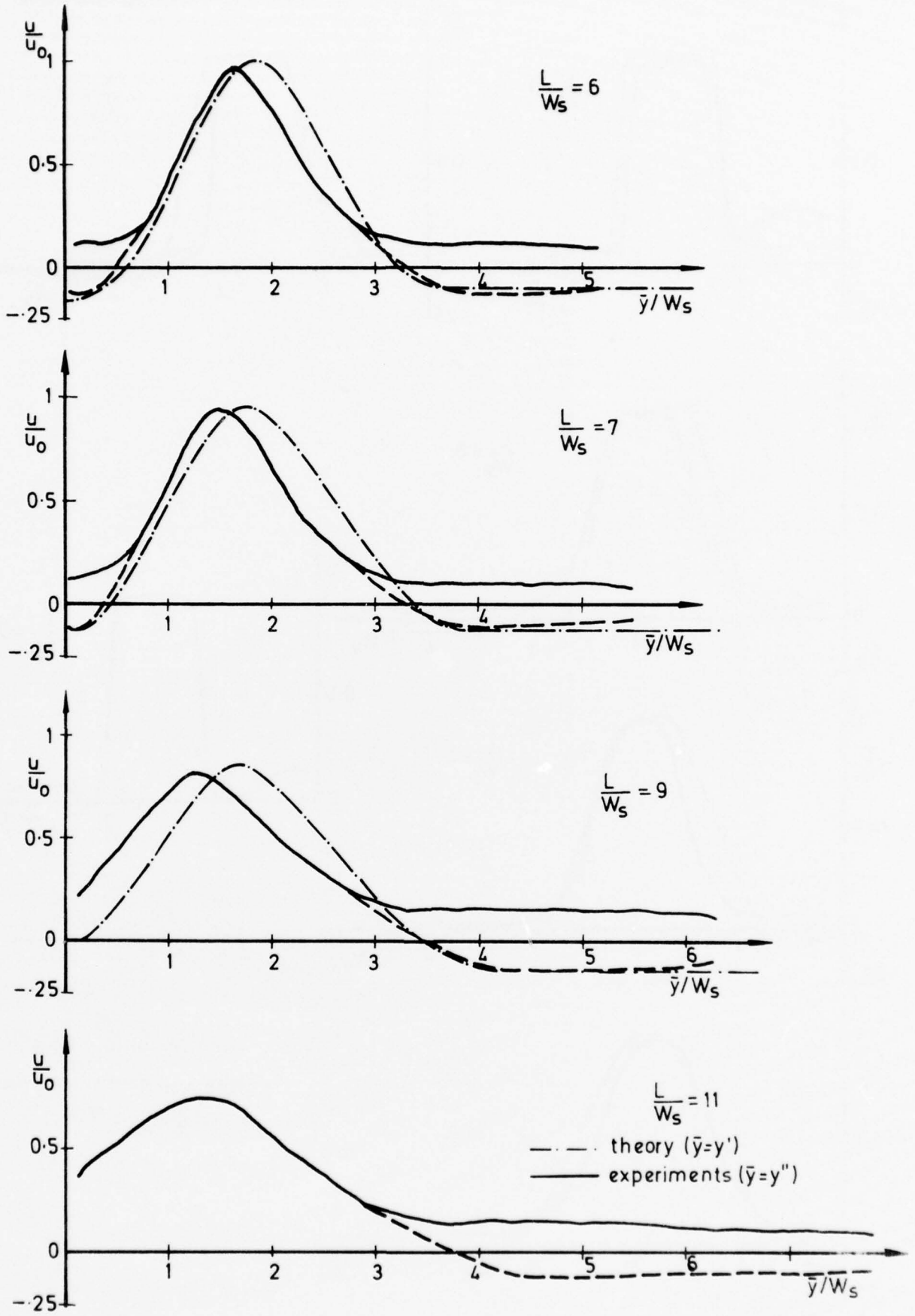


FIG 7b VELOCITY PROFILES FOR AR = 8, $\alpha = 10°$, $A/W_s = 1$, $L_W/W_s = 17$
CONTROL CHANNELS OPEN

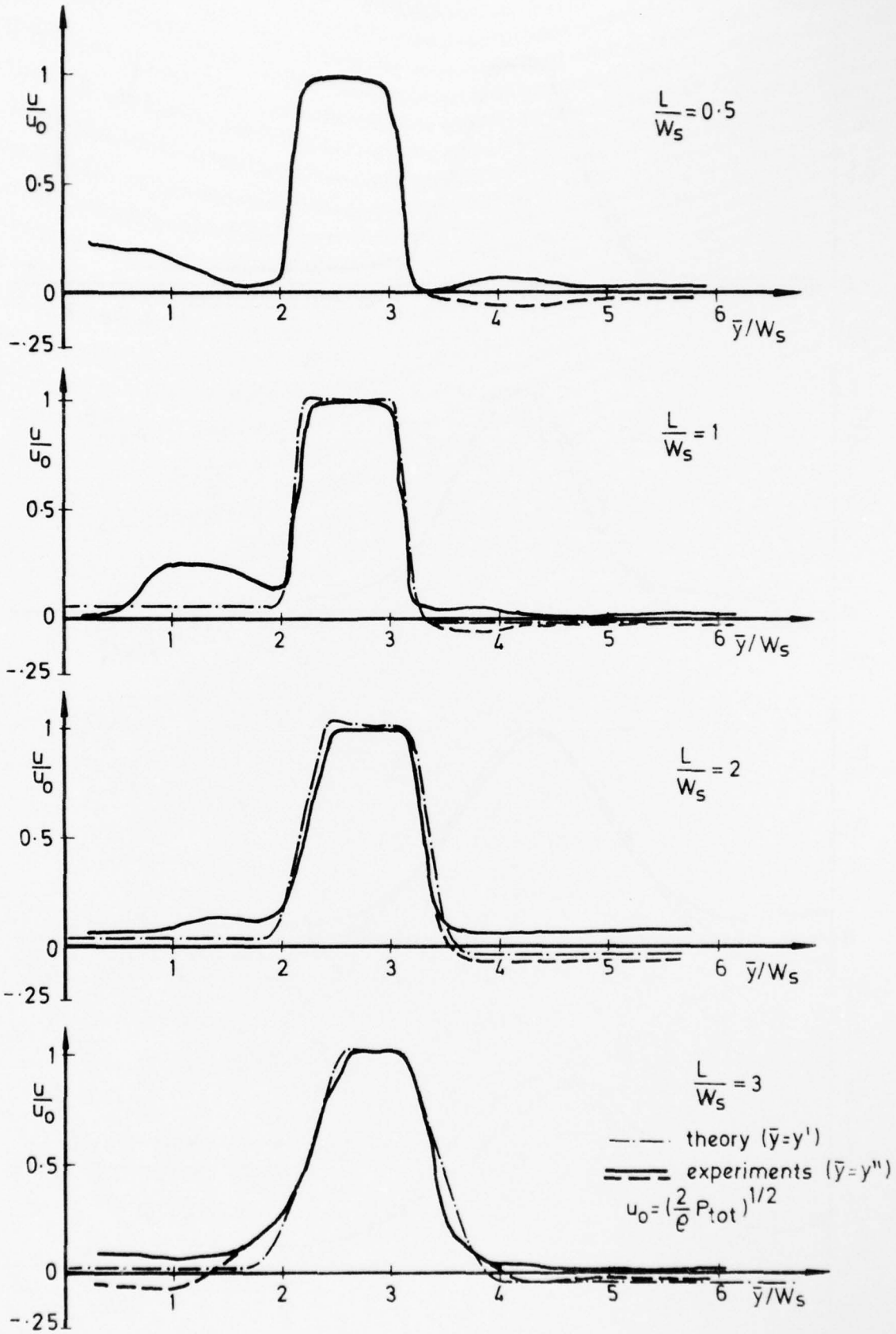


FIG. 8a VELOCITY PROFILES FOR AR = 8, $\alpha = 10°$, $A/W_s = 2$, $L_W/W_s = 17$
CONTROL CHANNELS OPEN

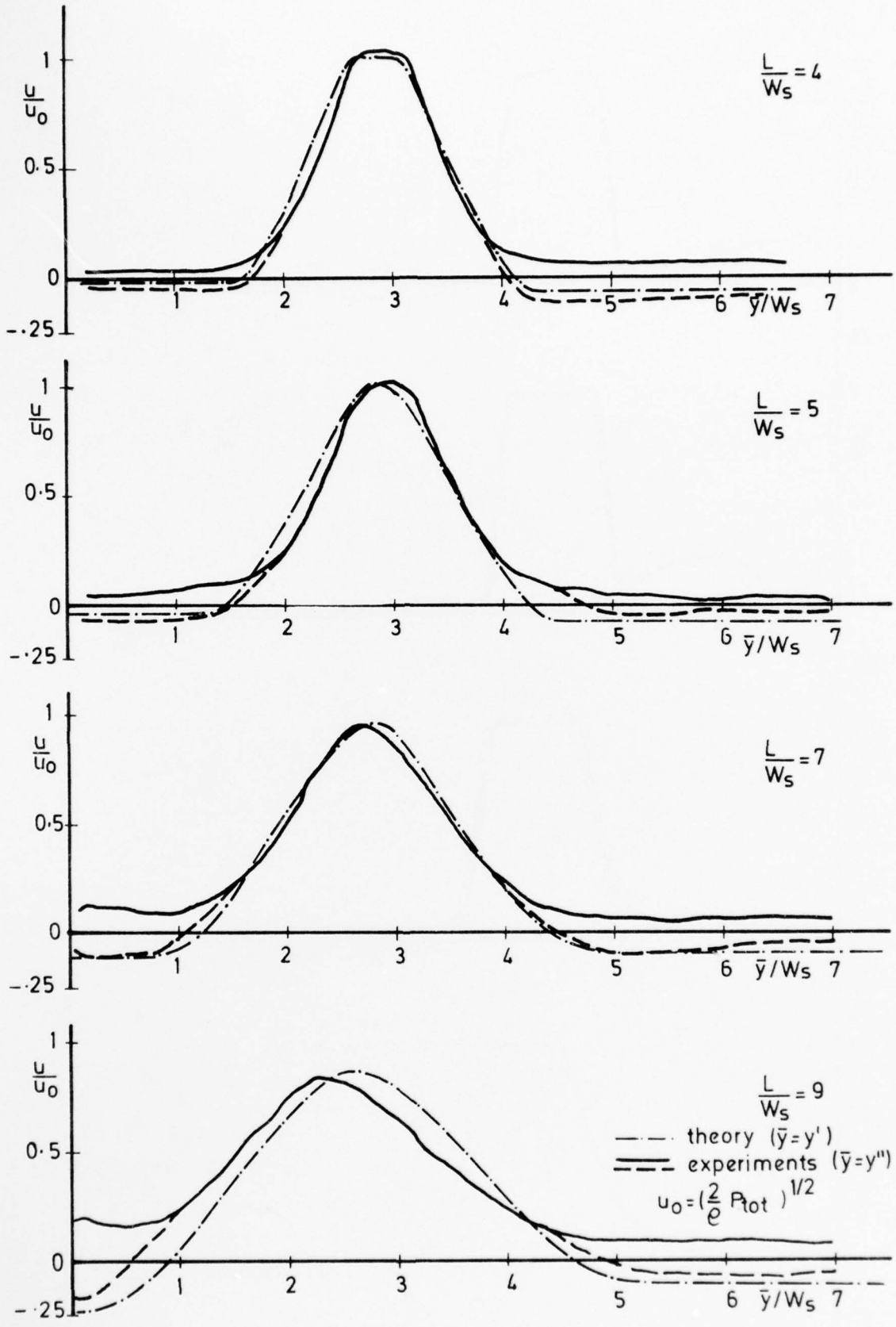


FIG. 8b VELOCITY PROFILES FOR AR = 8, α=10°, $A/W_s = 2$, $L_W/W_s = 17$
CONTROL CHANNELS OPEN

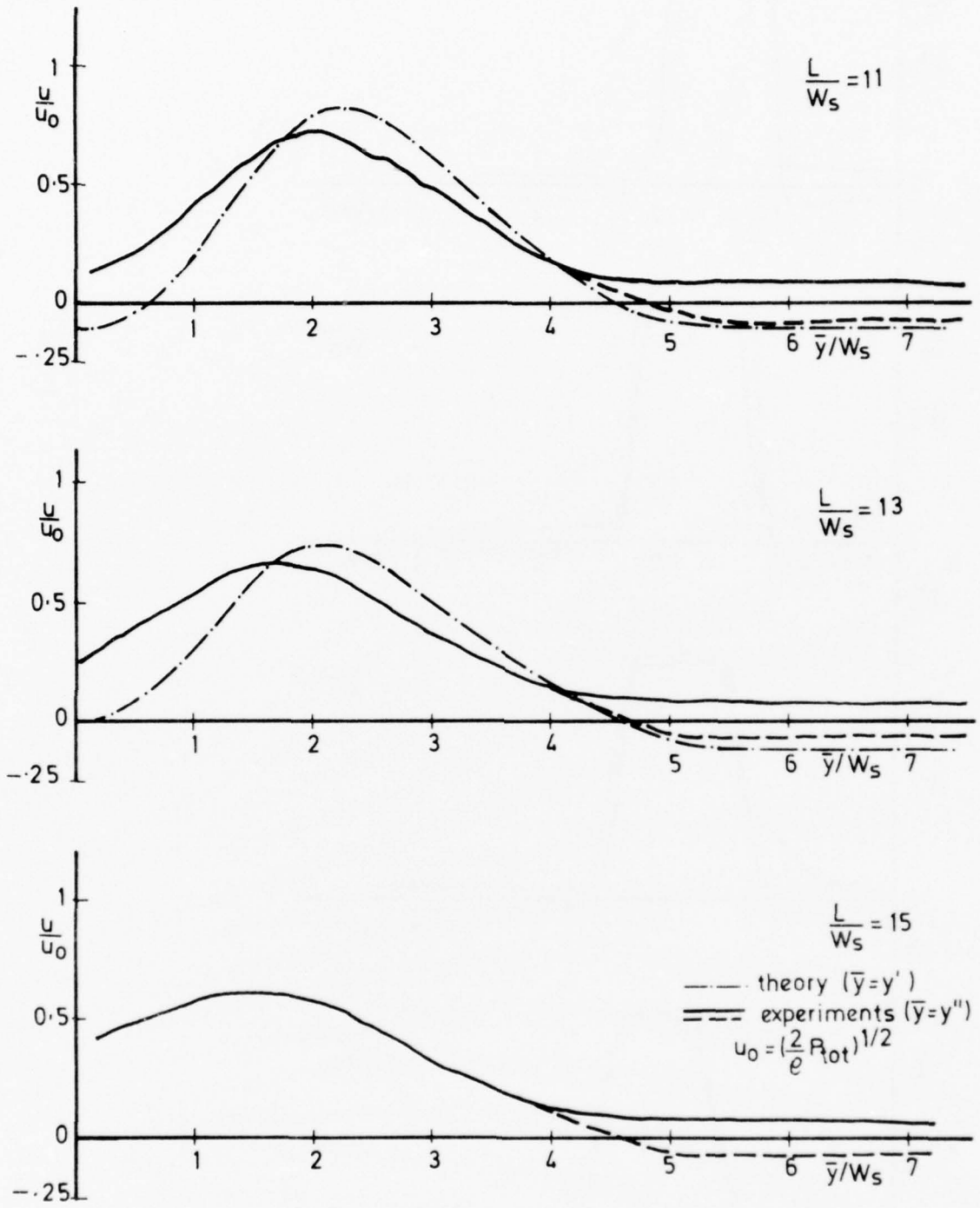


FIG. 8 c VELOCITY PROFILES FOR AR= 8, α=10°, $A/W_s = 2$, $L_W/W_s = 17$
CONTROL CHANNELS OPEN

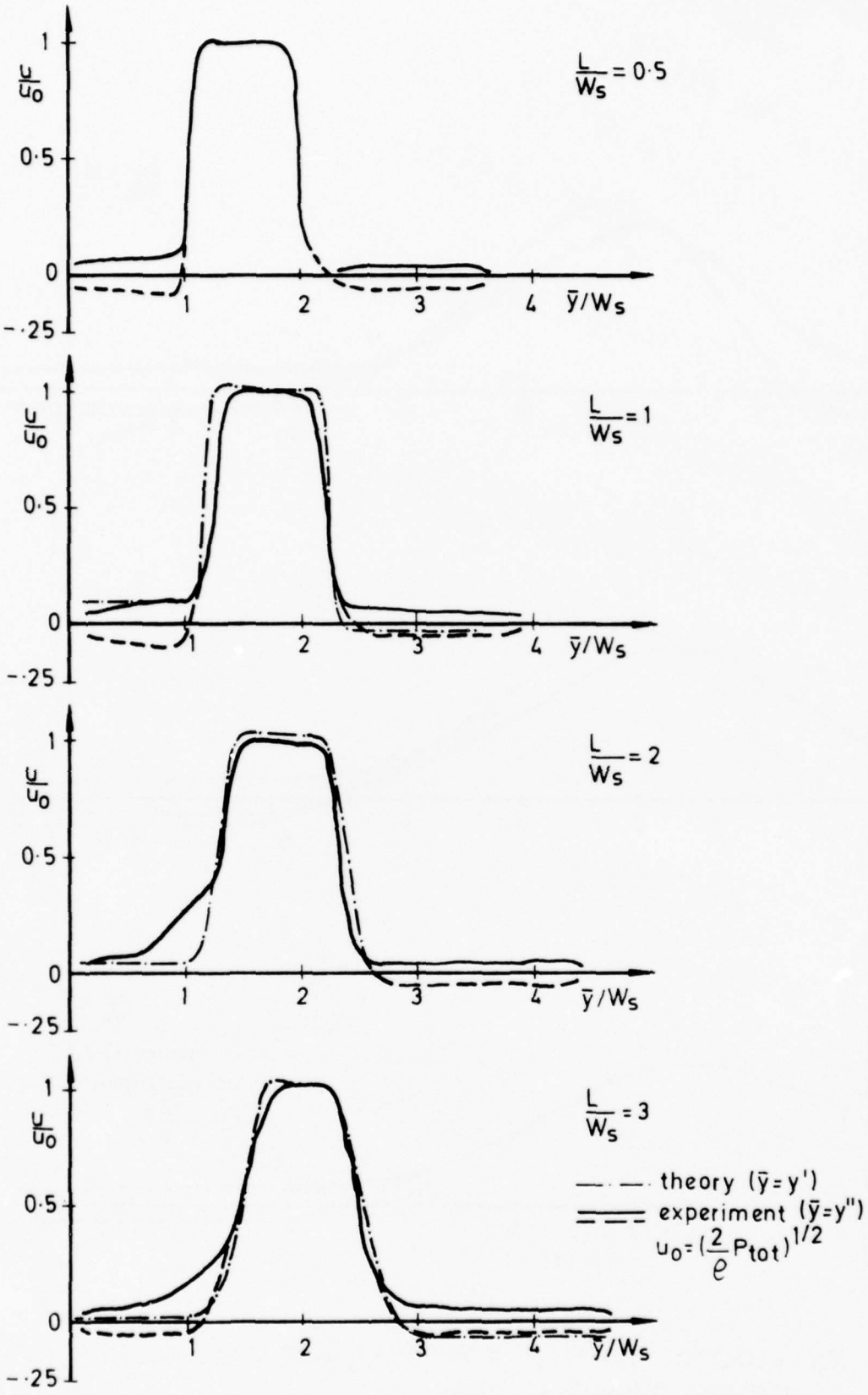


FIG. 9a VELOCITY PROFILES FOR AR = 8, α = 15, A/W_s = 1, L_W/W_s = 17
CONTROL CHANNELS OPEN

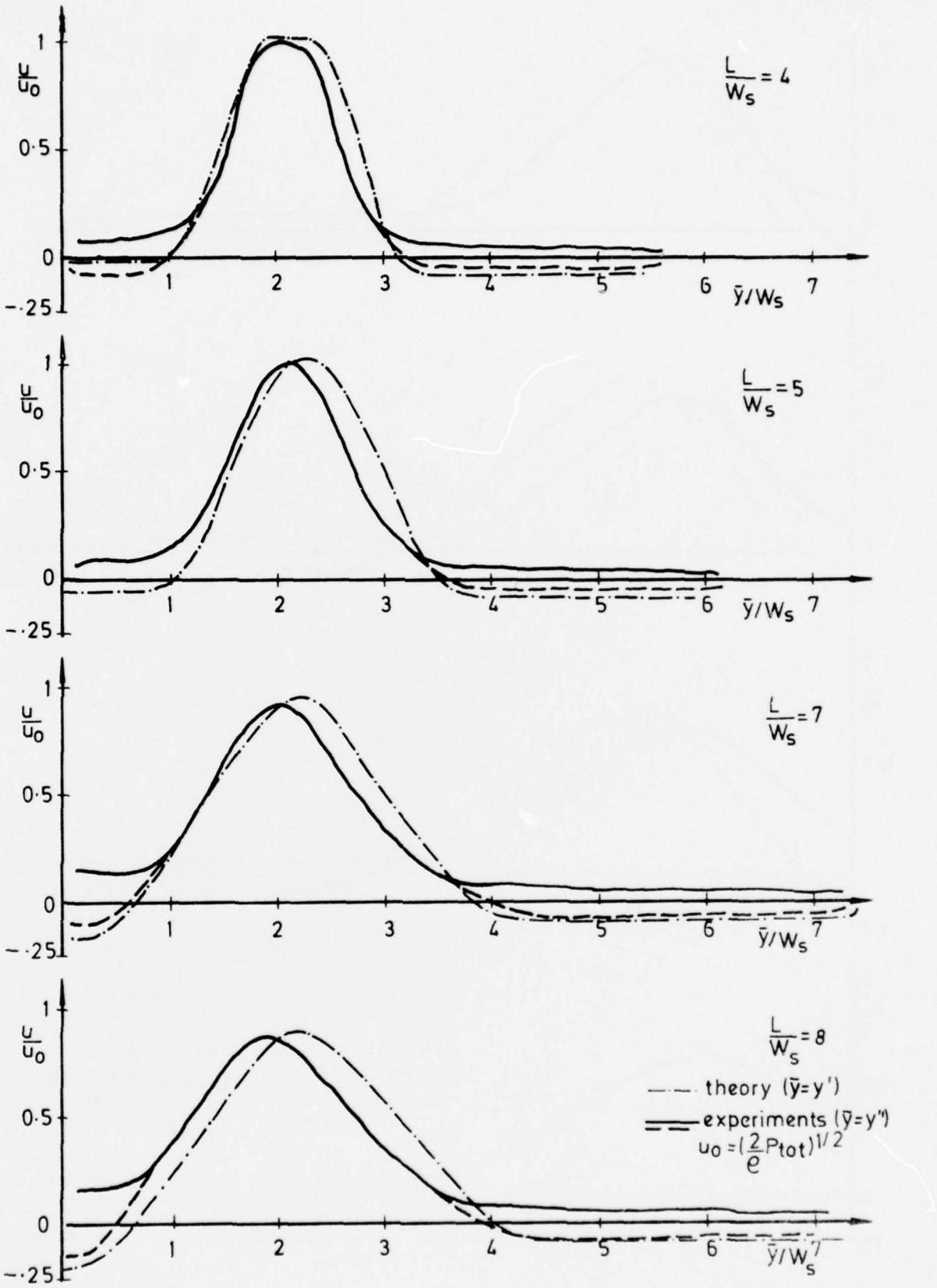


FIG 9b VELOCITY PROFILES FOR AR = 8, $\alpha = 15°$, $A/W_s = 1$, $L_W/W_s = 17$
CONTROL CHANNELS OPEN

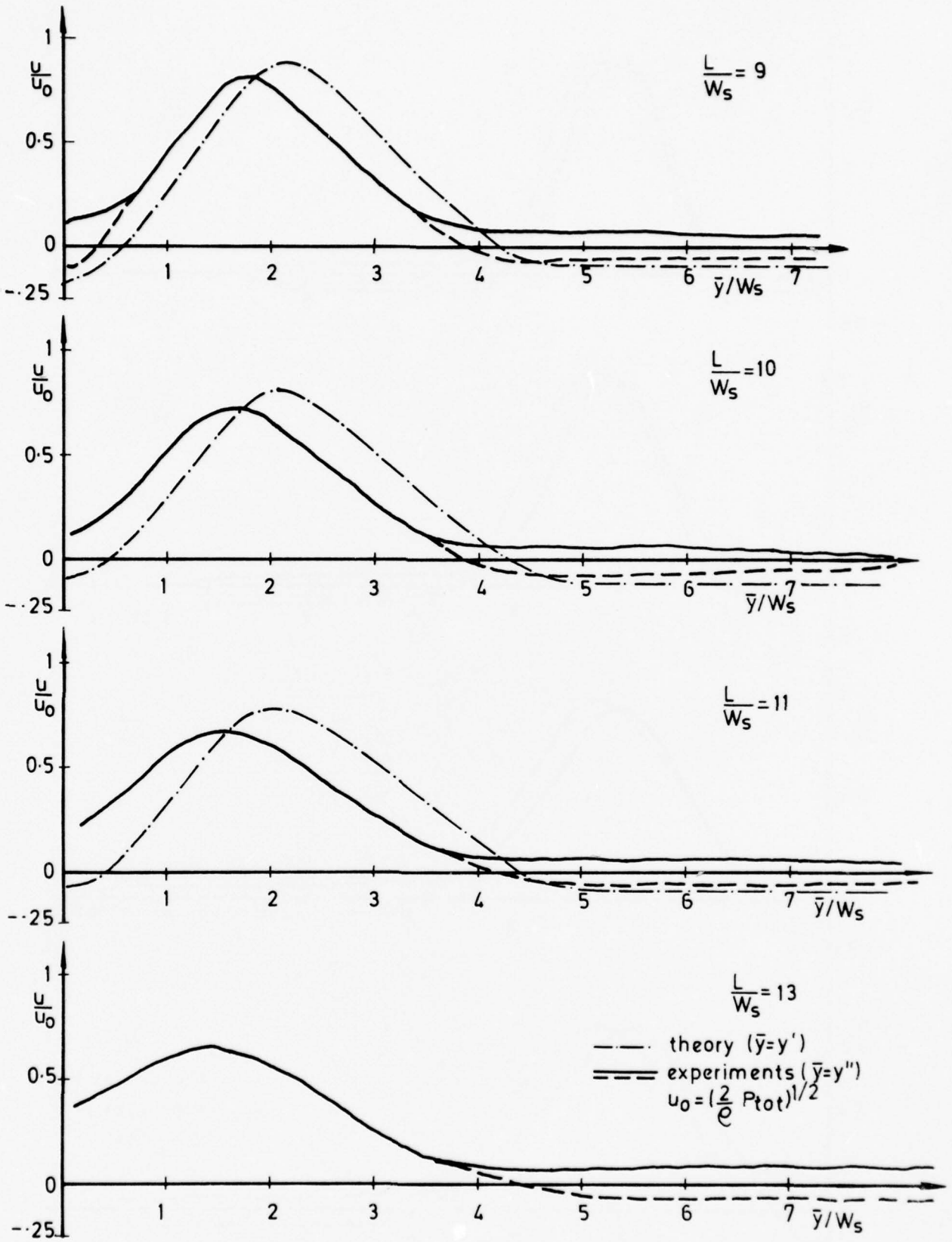


FIG. 9c VELOCITY PROFILES FOR AR=8, α=15°, A/Ws=1, Lw/Ws=17
CONTROL CHANNELS OPEN

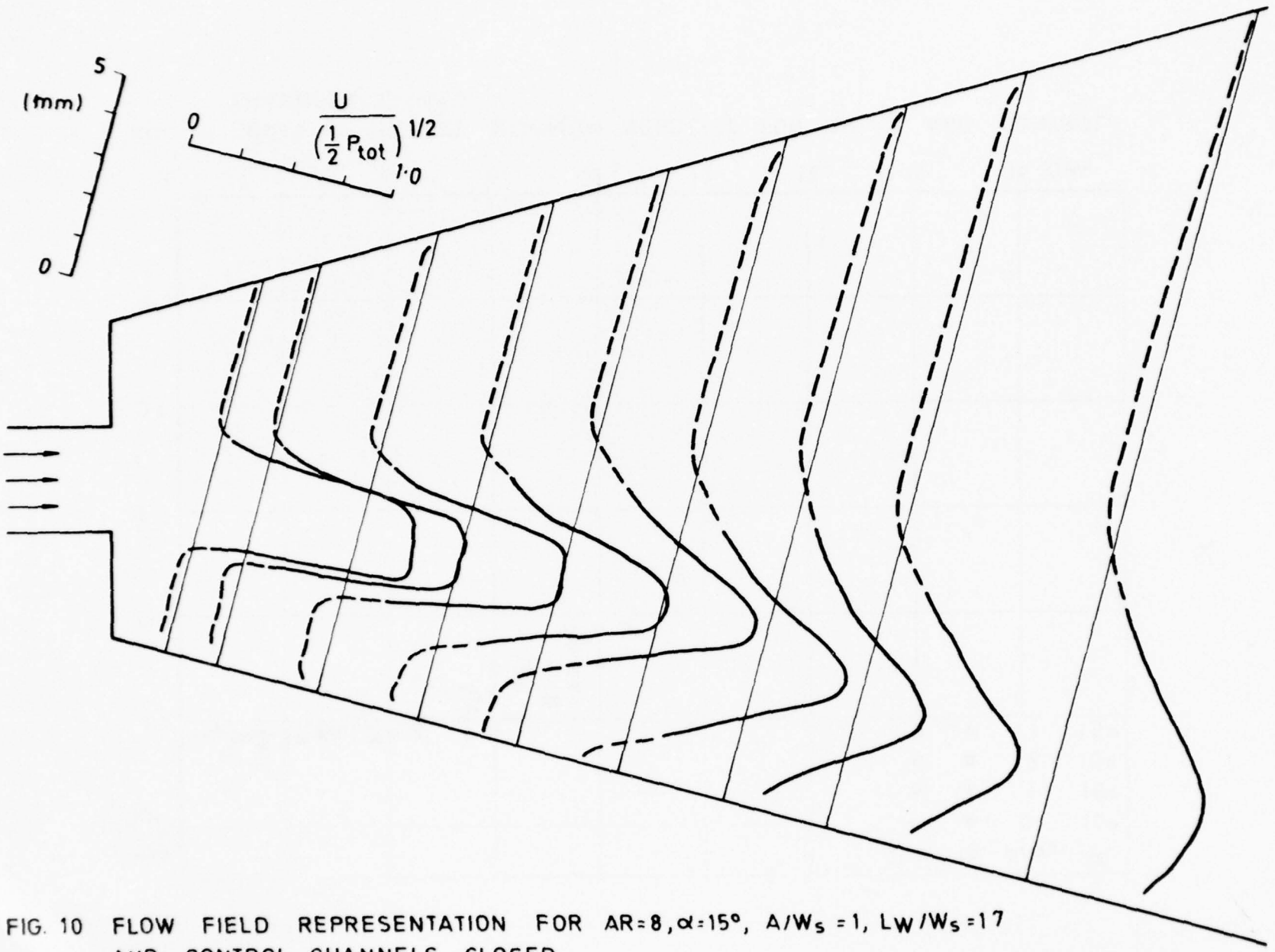


FIG. 10 FLOW FIELD REPRESENTATION FOR AR=8, α=15°, A/W_S = 1, L_W/W_S = 1·7 AND CONTROL CHANNELS CLOSED

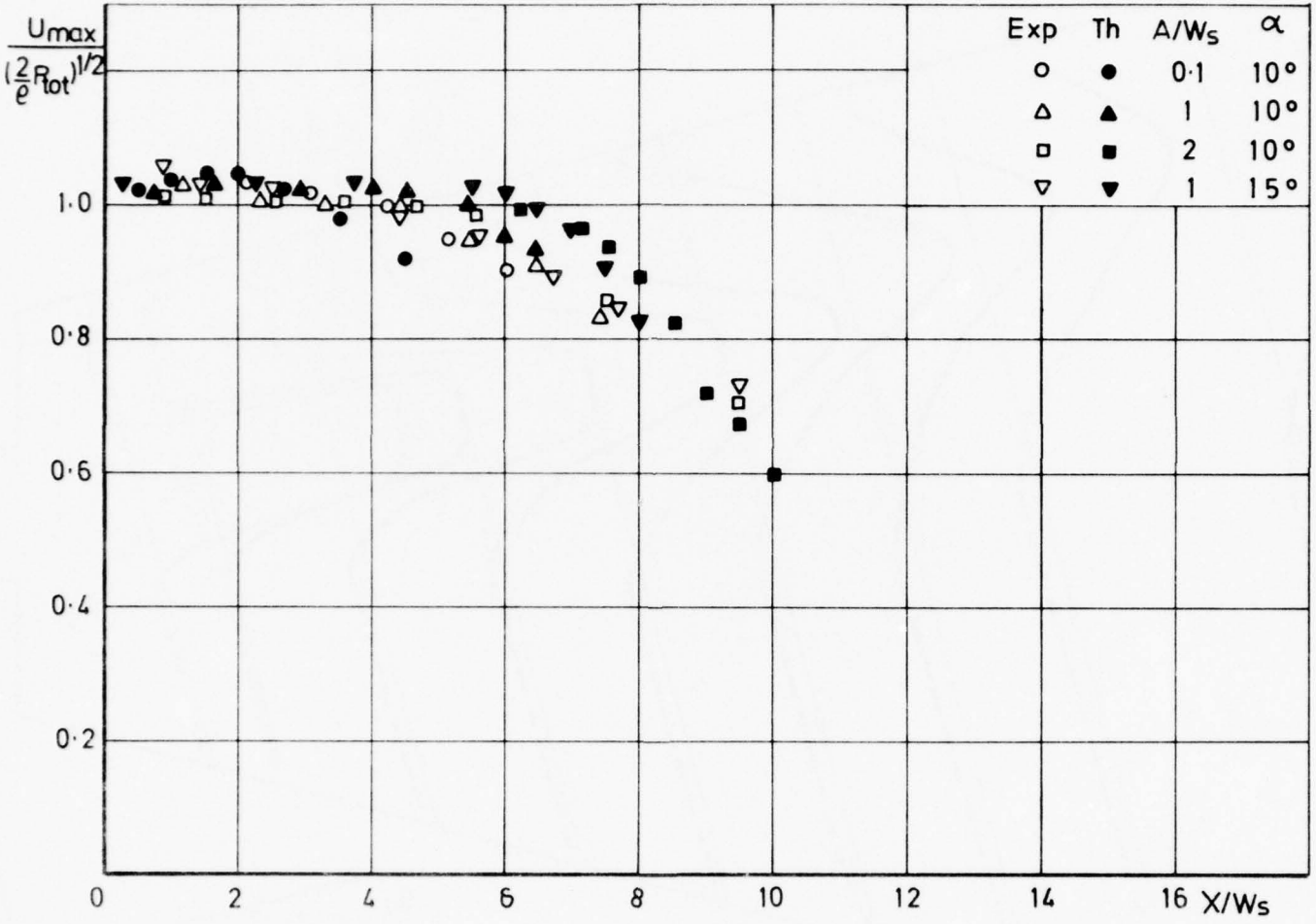


FIG. 11 DECAY OF THE JET MAXIMUM VELOCITY FOR AR = 8 AND CONTROL CHANNELS CLOSED

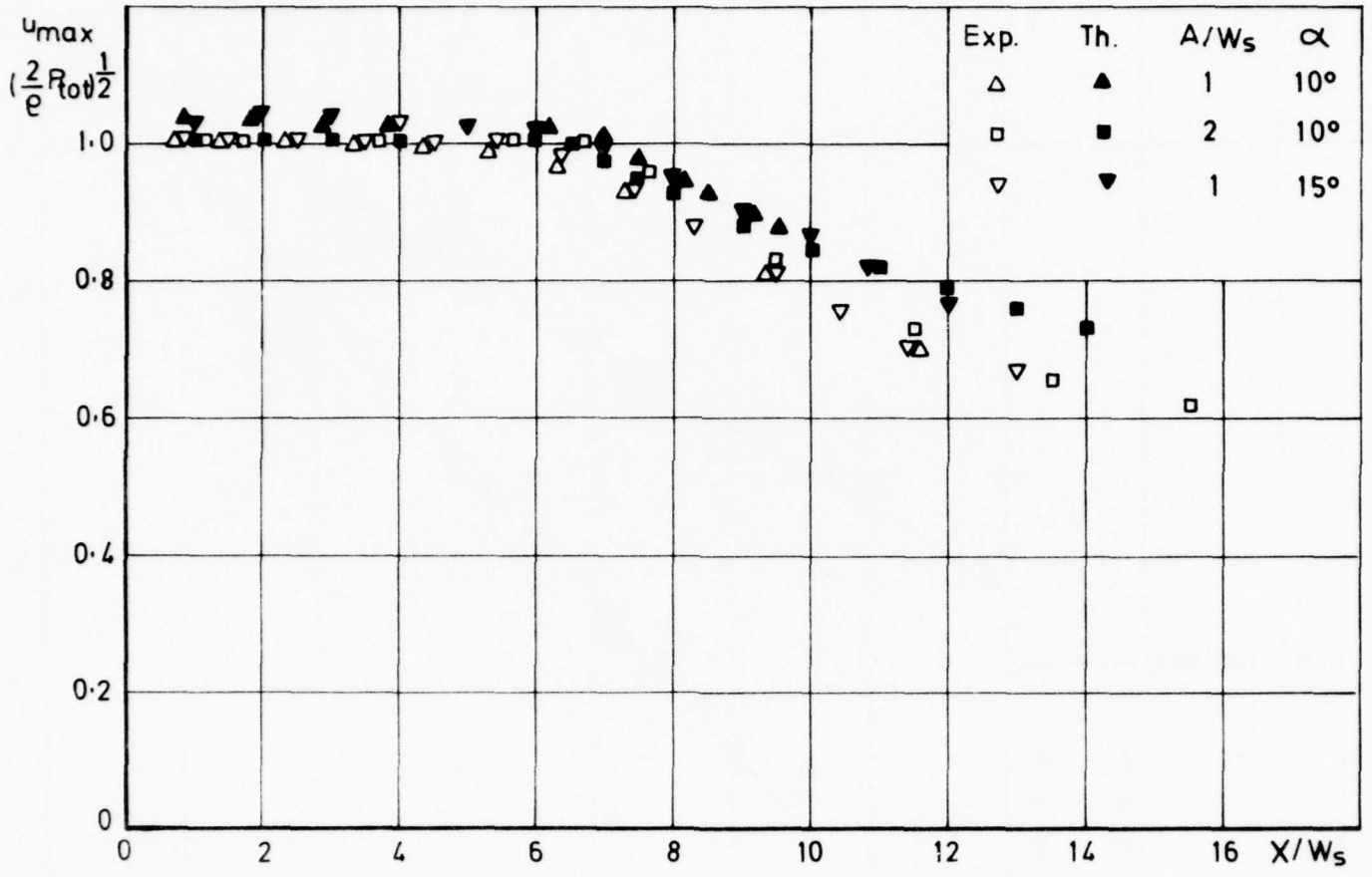


FIG. 12 DECAY OF THE JET MAXIMUM VELOCITY FOR AR=8 AND CONTROL CHANNELS OPEN

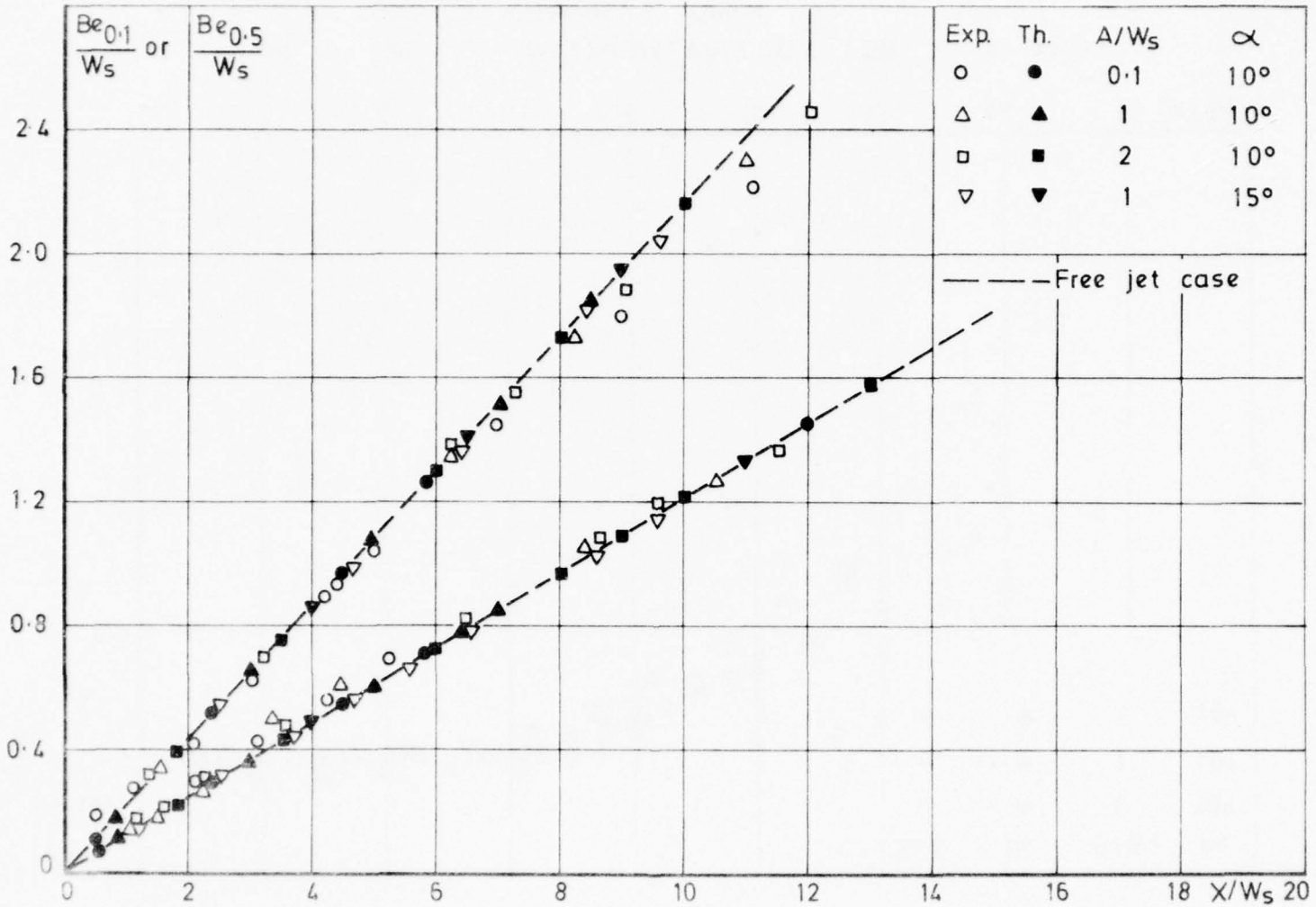


FIG. 13 THE GROWTH OF THE BOUNDARY LAYER ALONG THE UNATTACHED SIDE FOR AR=8, L_W/W_s =17 AND CONTROL CHANNELS CLOSED

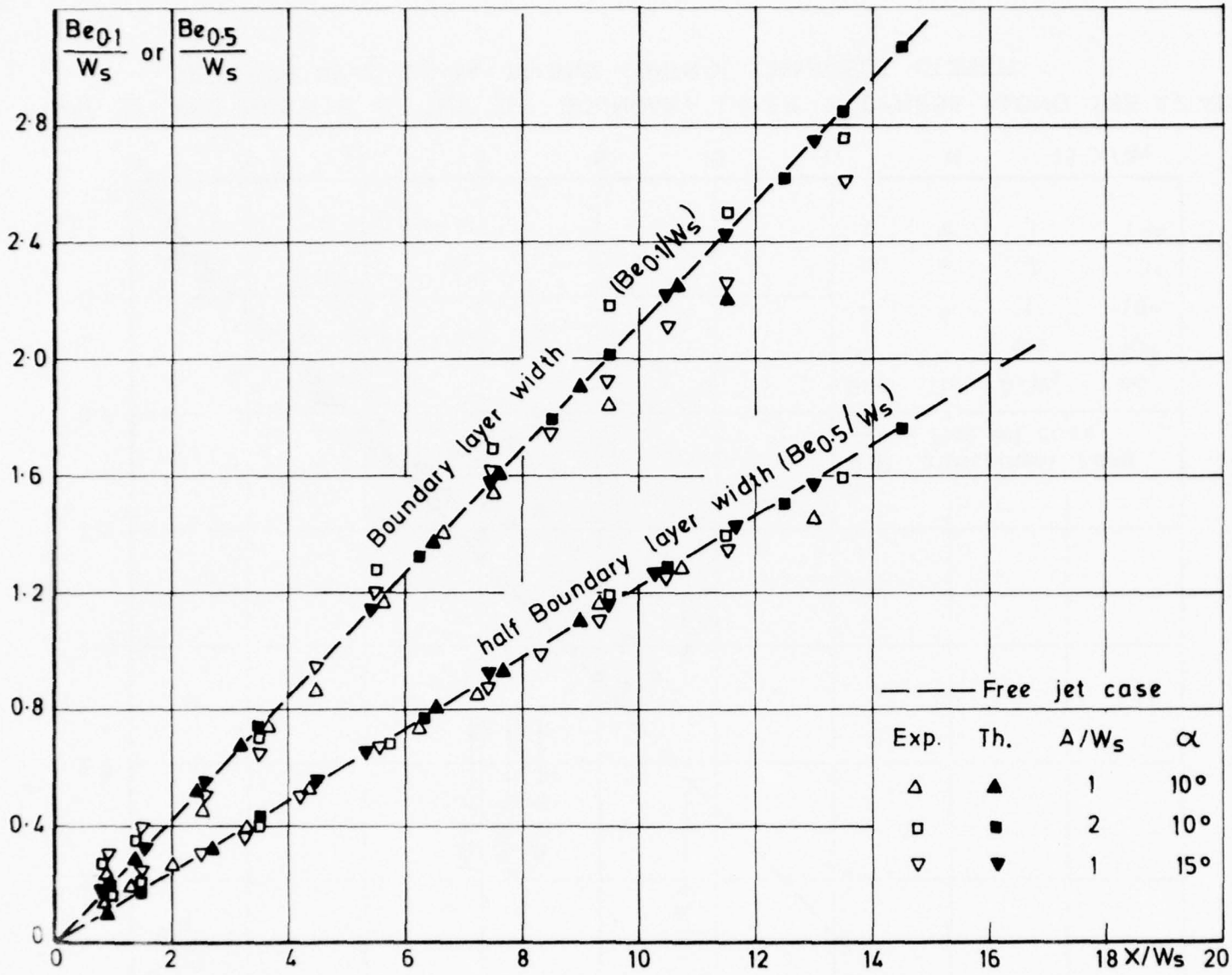


FIG. 14 THE GROWTH OF THE BOUNDARY LAYER ALONG THE UNATTACHED SIDE FOR AR=8 LW/Ws =17 AND CONTROL CHANNELS OPEN

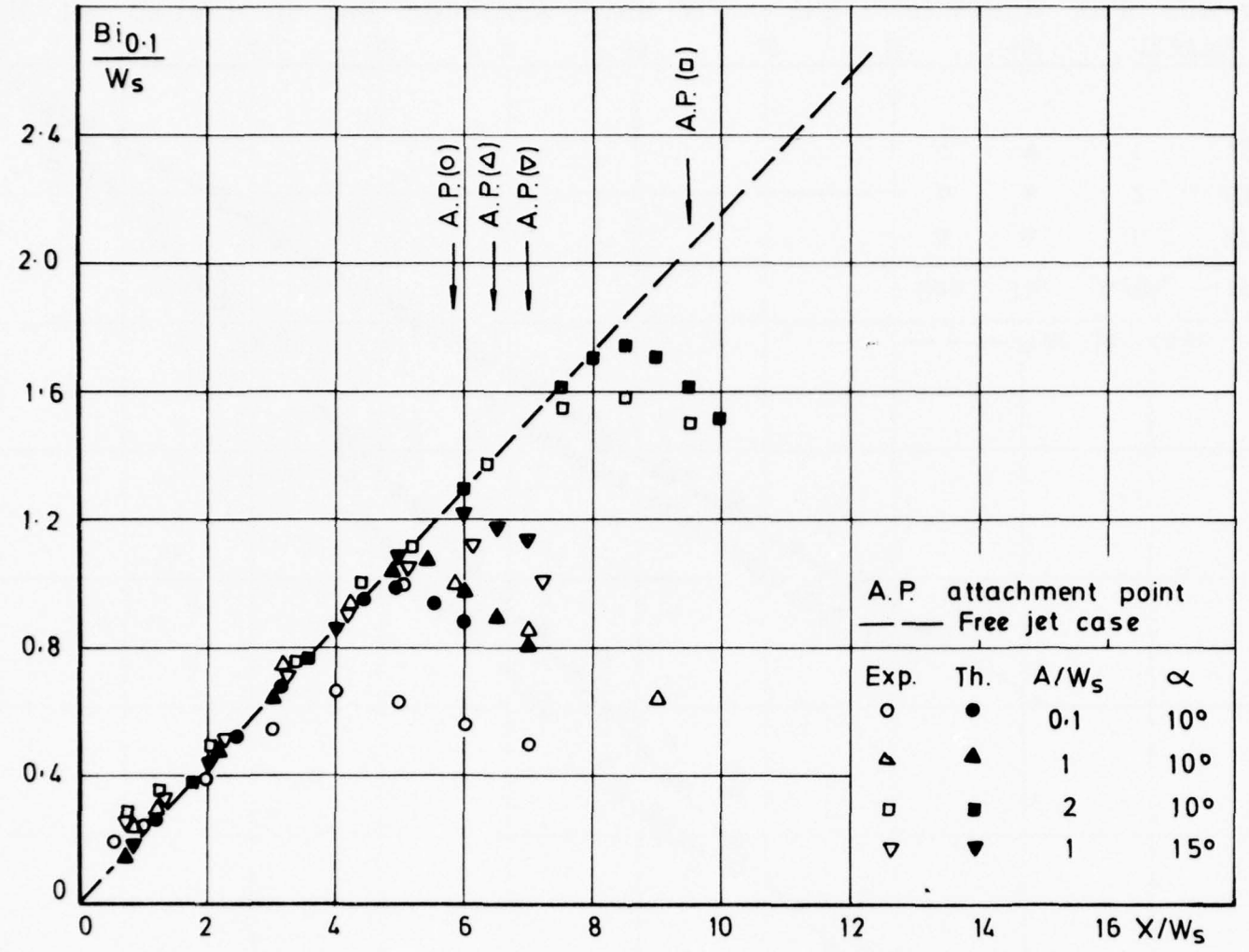


FIG. 15 THE GROWTH OF THE JET BOUNDARY LAYER THICKNESS ALONG THE ATTACHED SIDE FOR AR=8, $L_W/W_s = 17$ AND CONTROL CHANNELS CLOSED

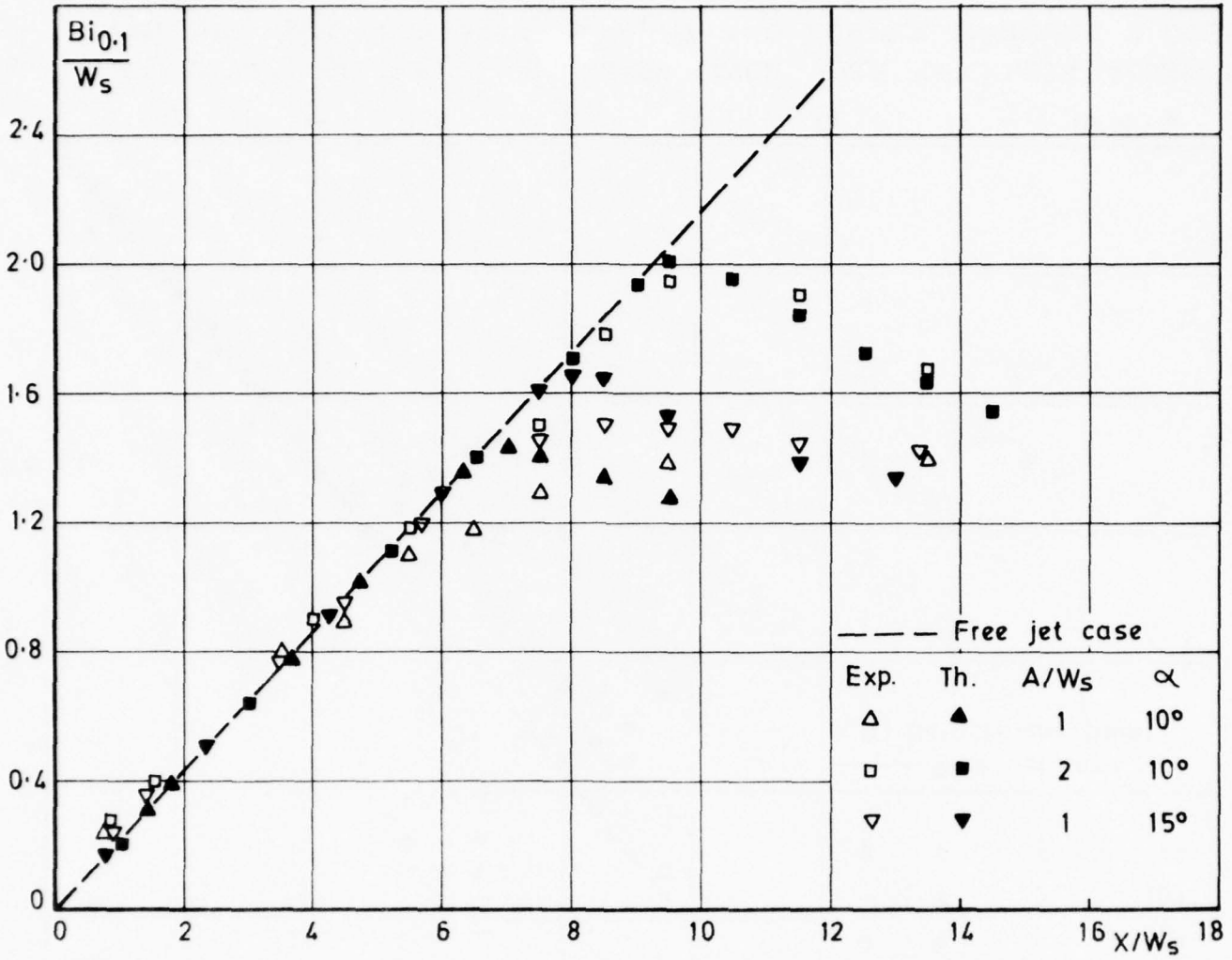


FIG. 16 THE GROWTH OF THE JET BOUNDARY LAYER THICKNESS ALONG THE ATTACHED SIDE FOR AR=8, L_W/W_s = 17 AND CONTROL CHANNELS OPEN

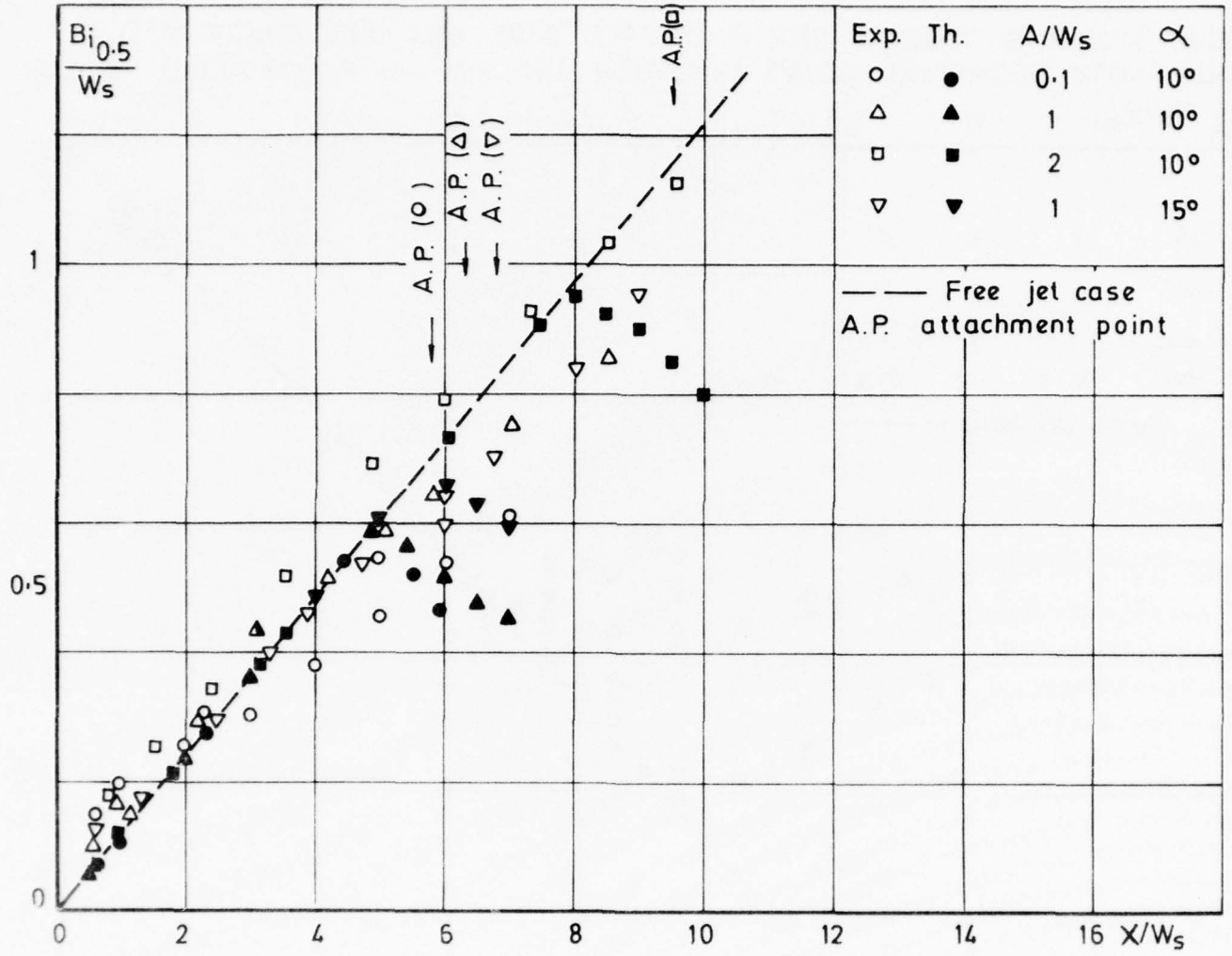


FIG. 17 THE GROWTH OF THE JET BOUNDARY LAYER HALF THICKNESS ALONG THE ATTACHED SIDE FOR AR= 8, LW/Ws =17 AND CONTROL CHANNELS CLOSED

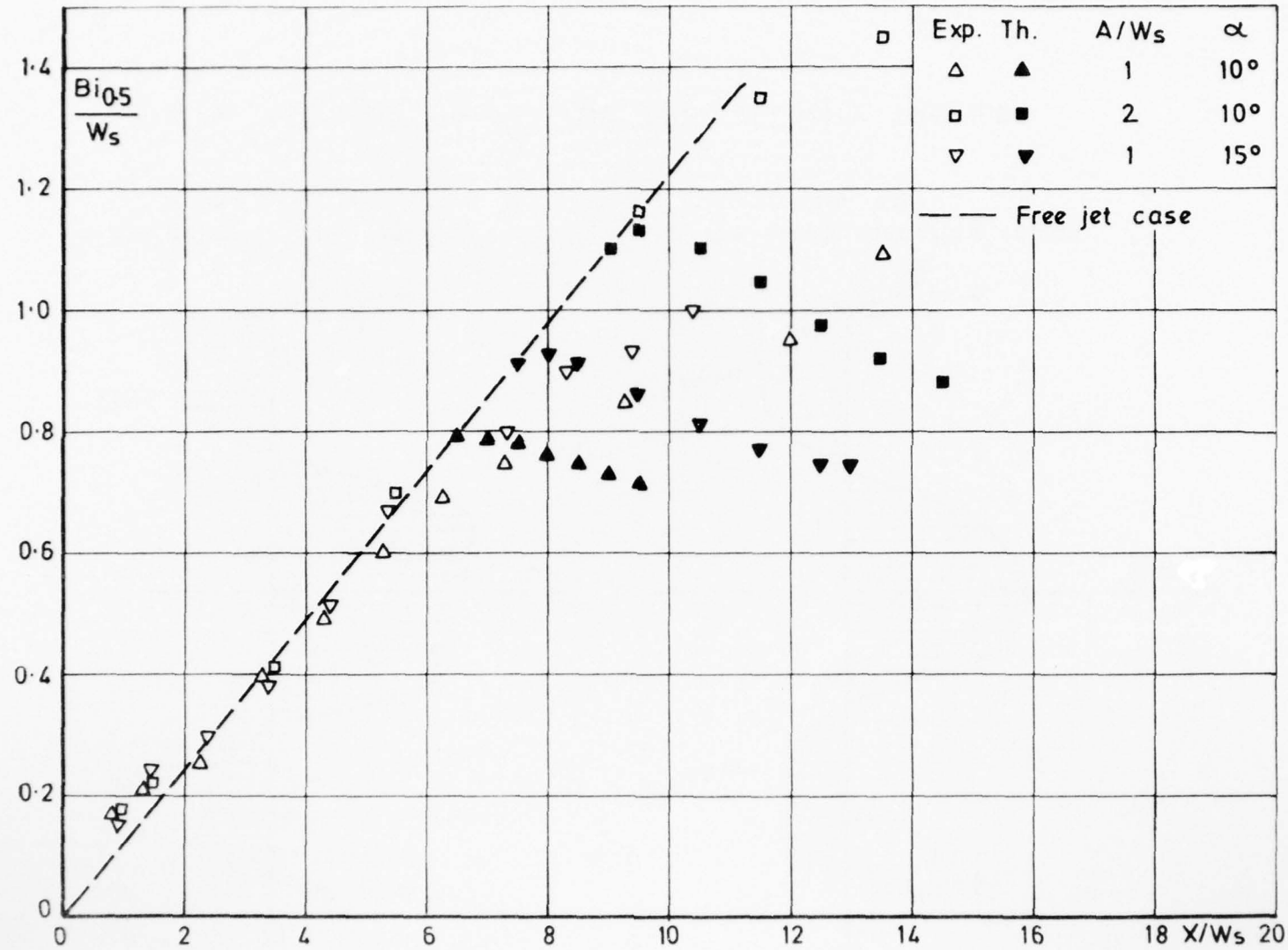
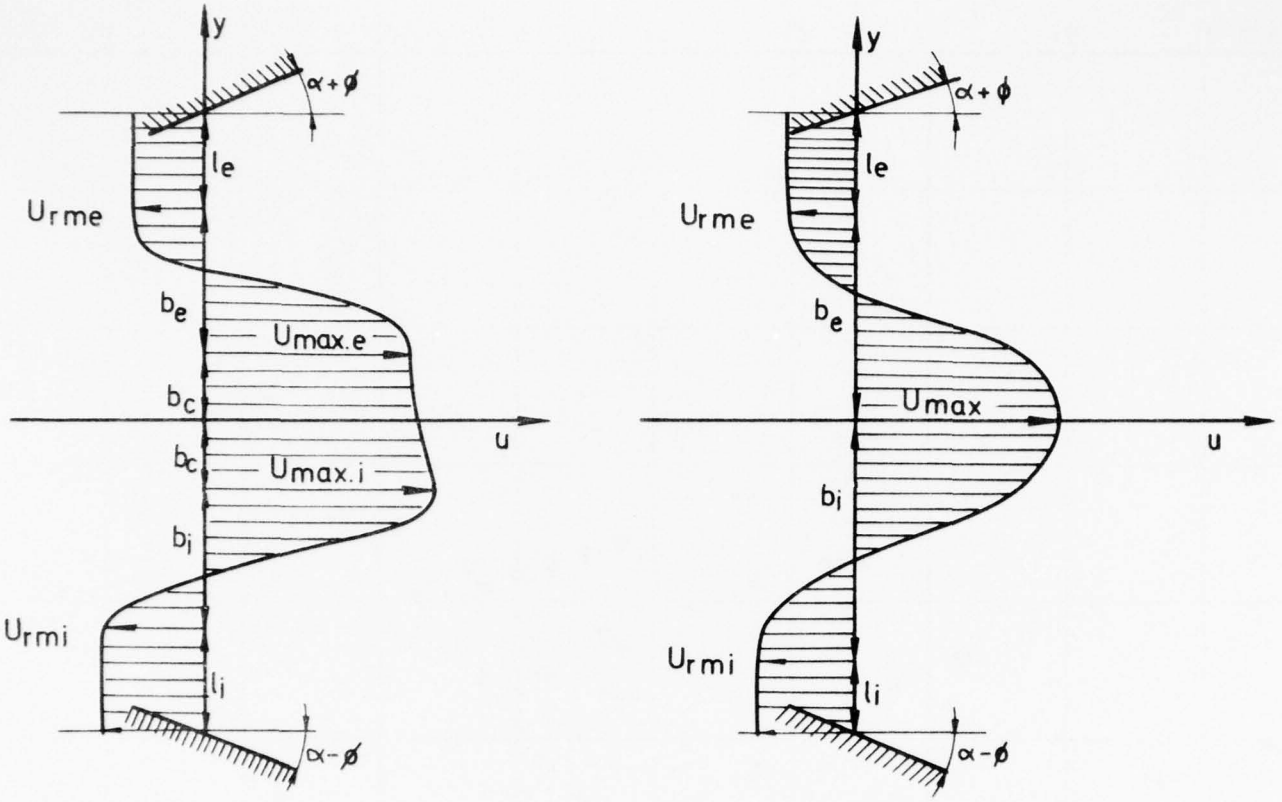


FIG. 18 THE GROWTH OF THE JET BOUNDARY LAYER HALF THICKNESS ALONG THE ATTACHED SIDE FOR AR=8, L_W/W_S =17 AND CONTROL CHANNELS OPEN



in the potential core region
($b_c > 0$)

in the esteblished flow region
($b_c = 0$)

FIG. 19 ASSUMED SHAPE FOR THE VELOCITY PROFILES

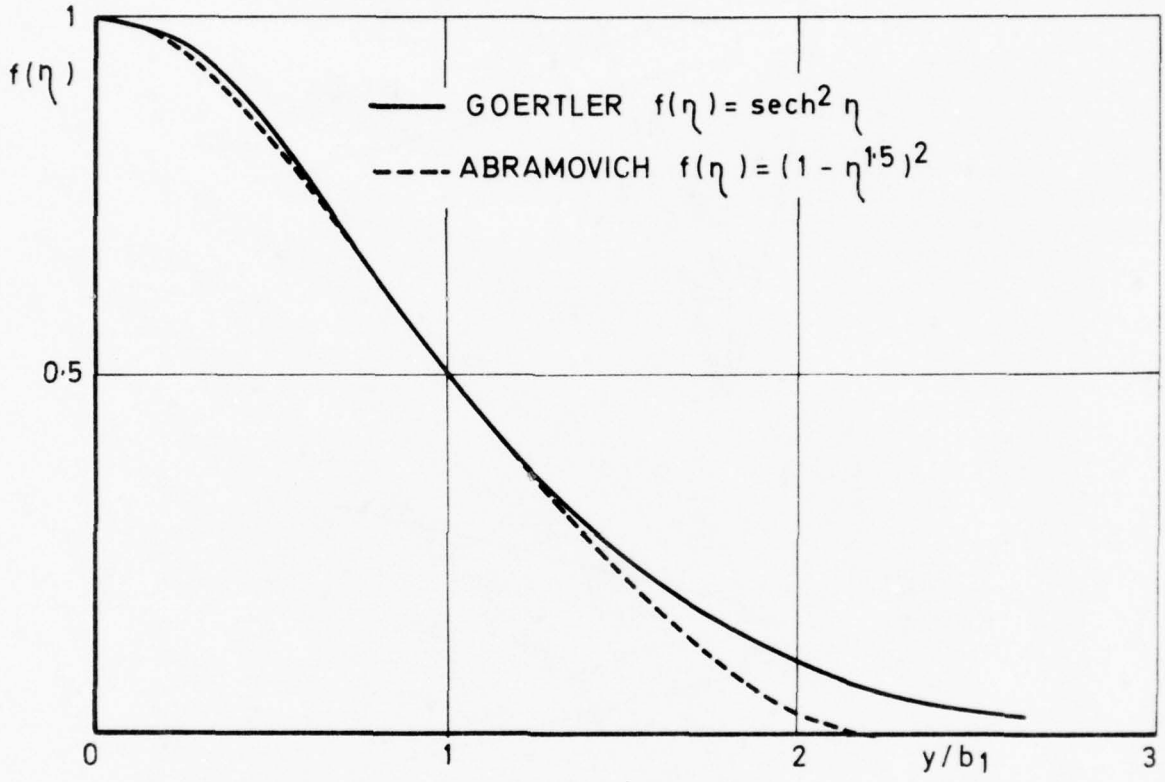


FIG. 20 EXACT AND APPROXIMATE NON DIMENSIONAL JET VELOCITY PROFILES

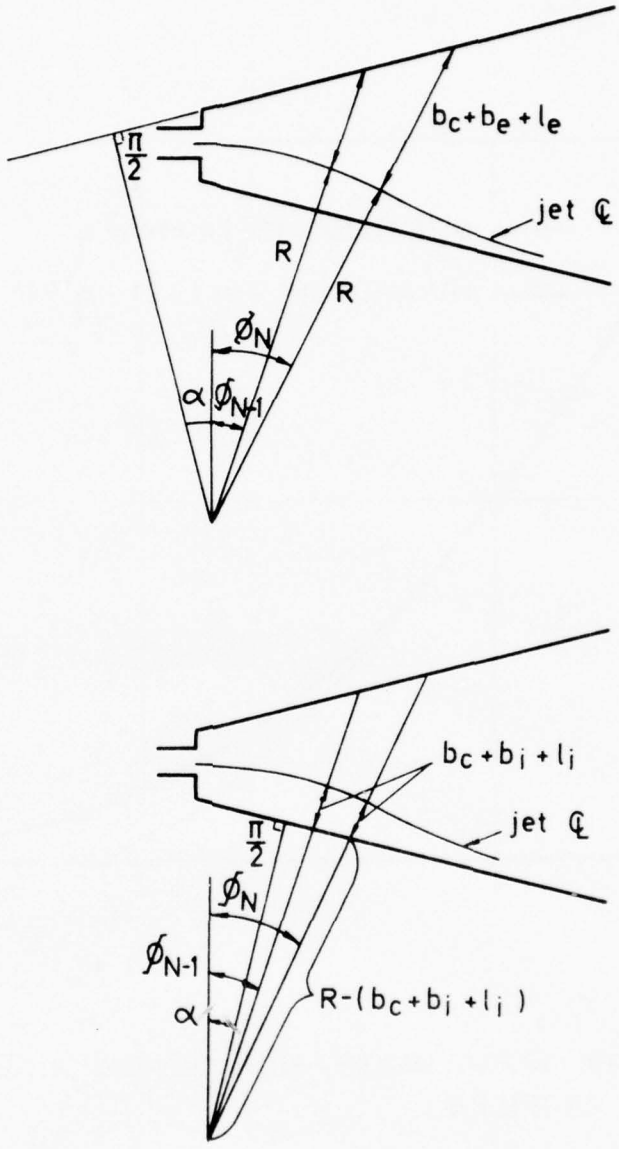


FIG. 21 GEOMETRICAL RELATIONS FOR THE VELOCITY PROFILE WIDTHS

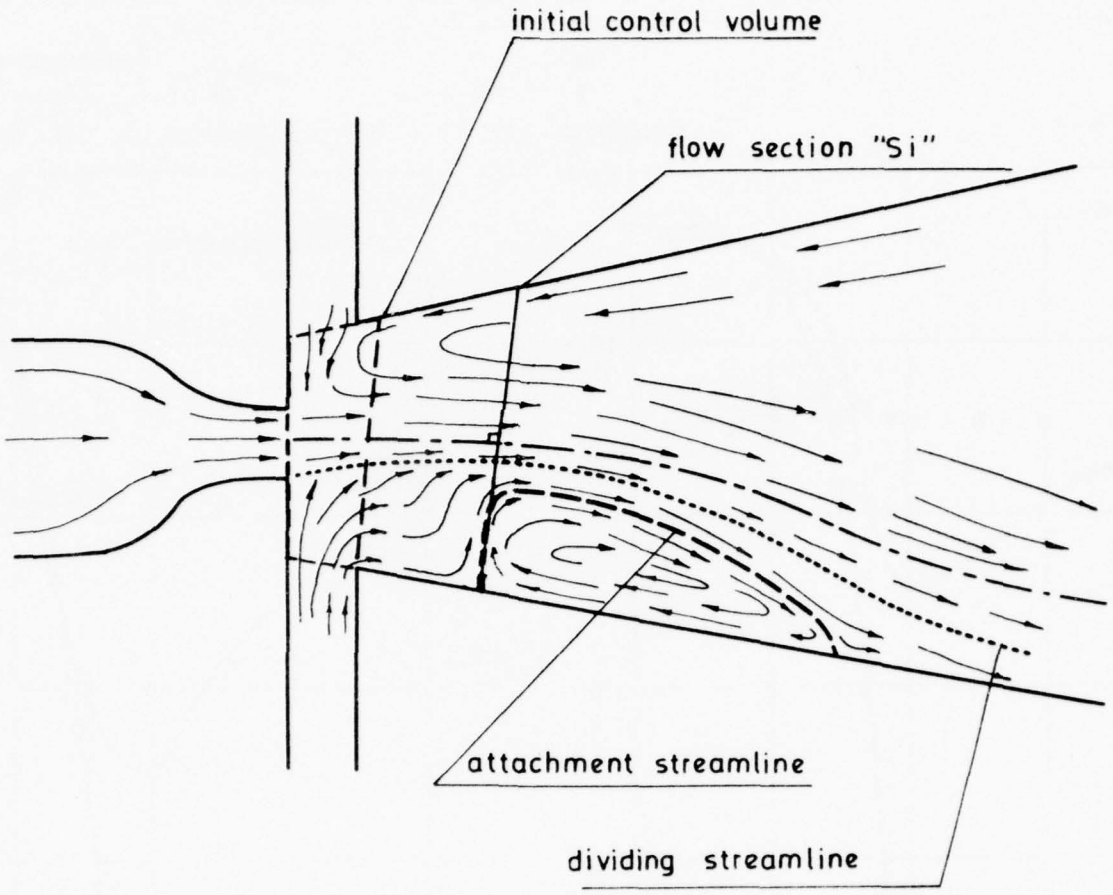


FIG. 22 SKETCH OF THE FLOW FIELD USED IN THE THEORETICAL MODEL FOR OPEN CONTROL CHANNELS OPERATION

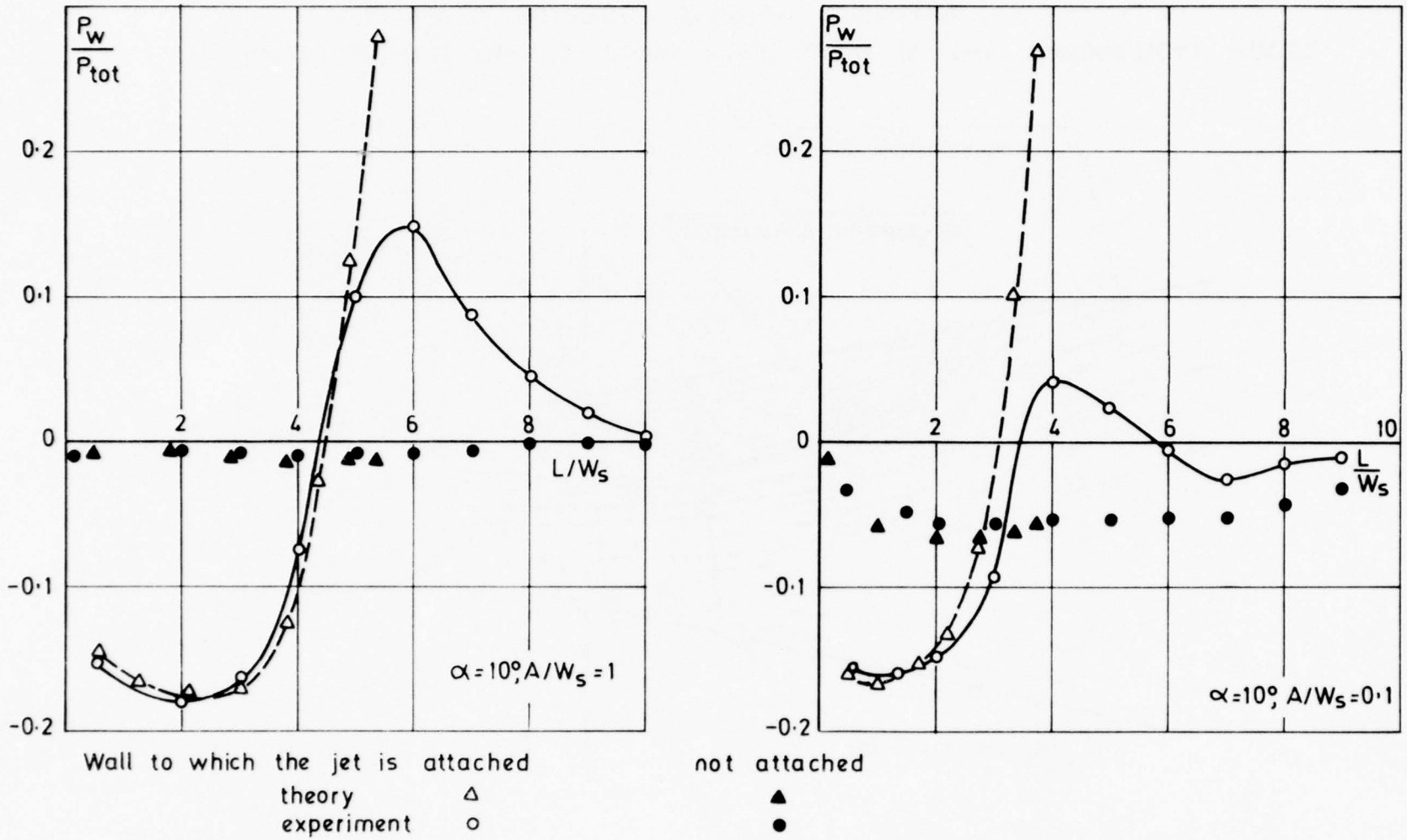


FIG. 23 THE WALL PRESSURE DISTRIBUTIONS FOR AR = 8, L_W/W_s = 17 AND CLOSED CONTROL CHANNELS OPERATION

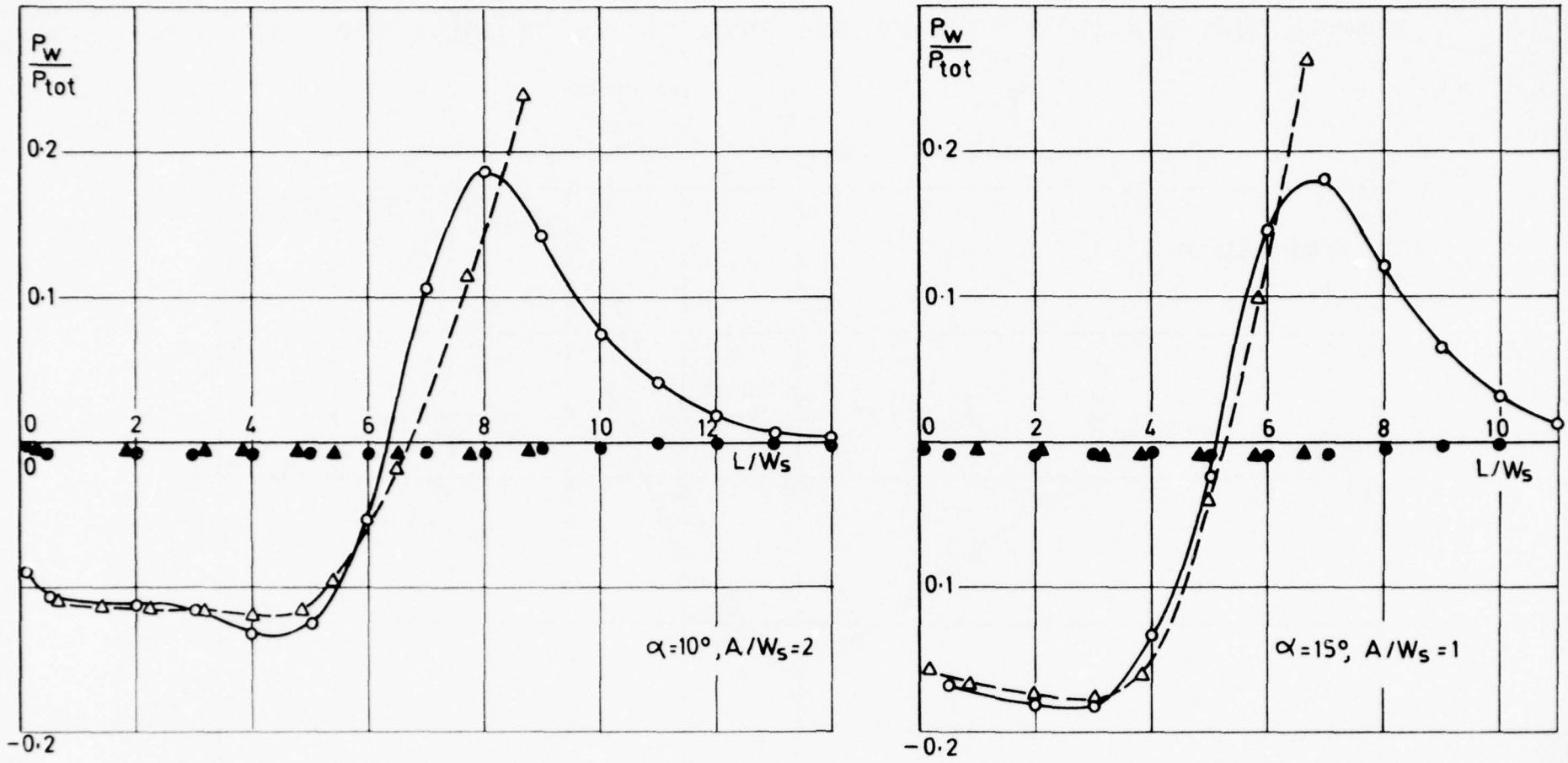


FIG. 24 THE WALL PRESSURE DISTRIBUTIONS FOR AR=8, $L_W/W_s = 17$ AND CLOSED CONTROL CHANNELS OPERATION

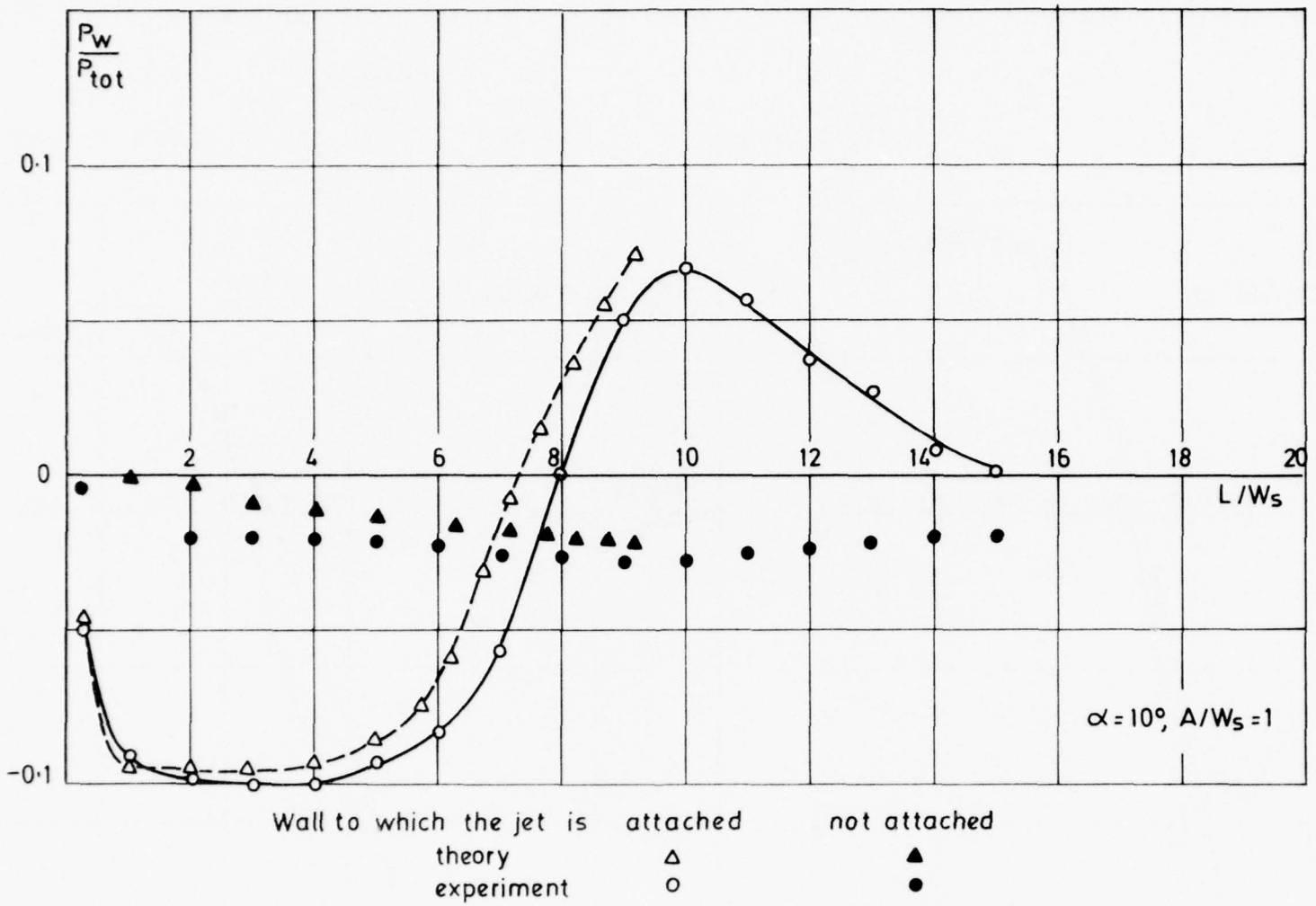


FIG. 25 THE WALL PRESSURE DISTRIBUTIONS FOR AR = 8, L_W/W_S = 17 AND OPEN CONTROL CHANNELS OPERATION

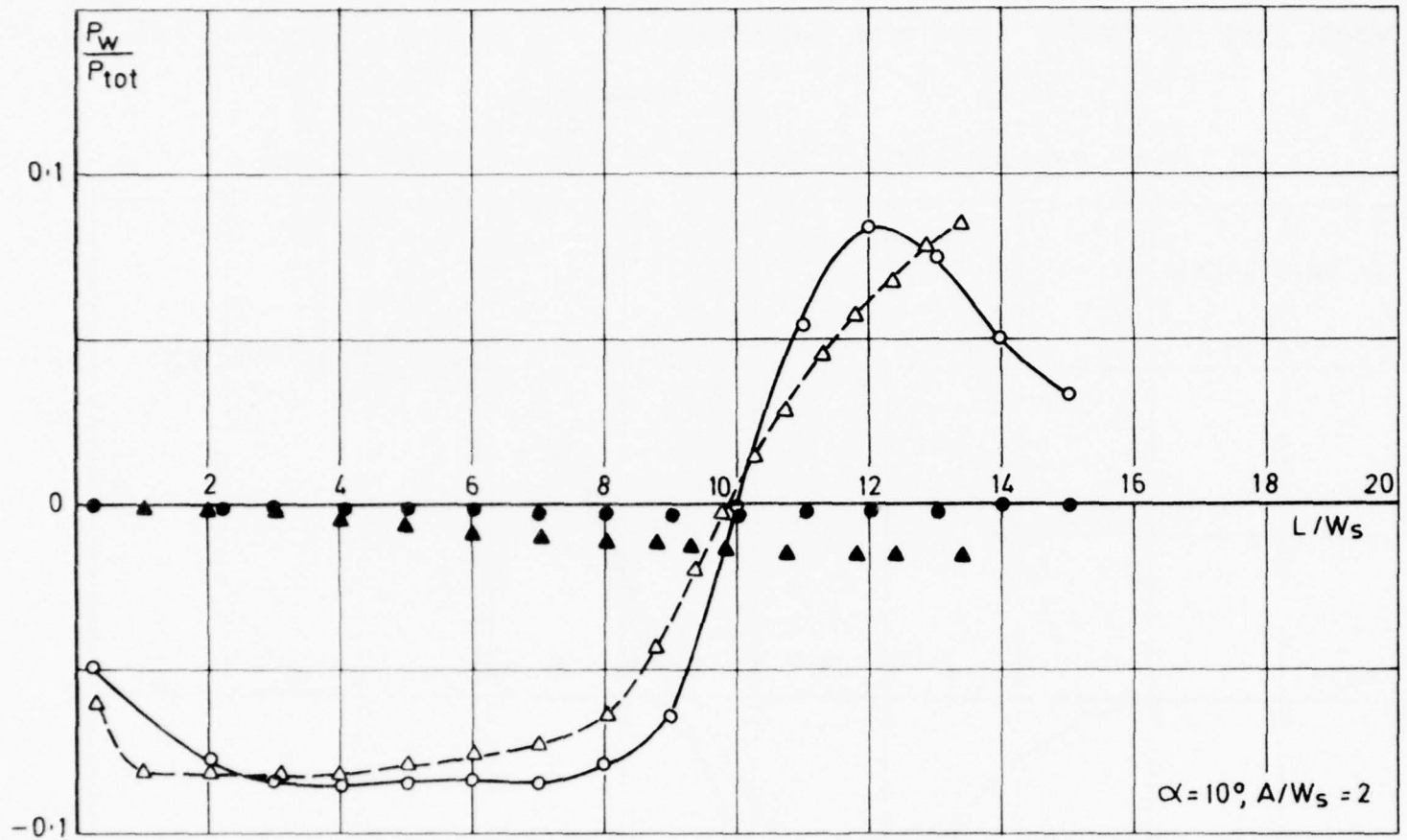


FIG 26 THE WALL PRESSURE DISTRIBUTIONS FOR AR=8, L_W/W_S = 17 AND OPEN CONTROL CHANNELS OPERATION

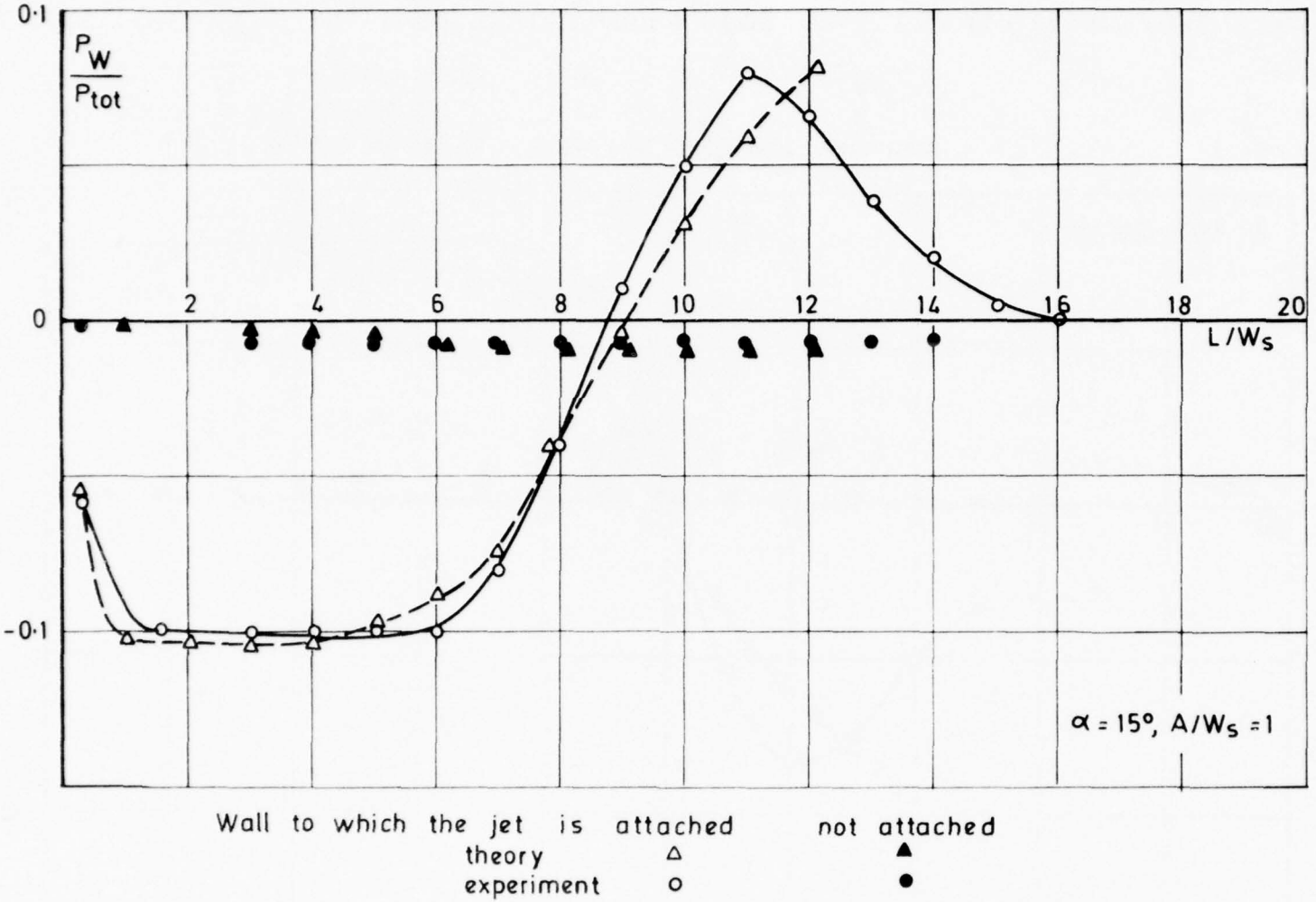
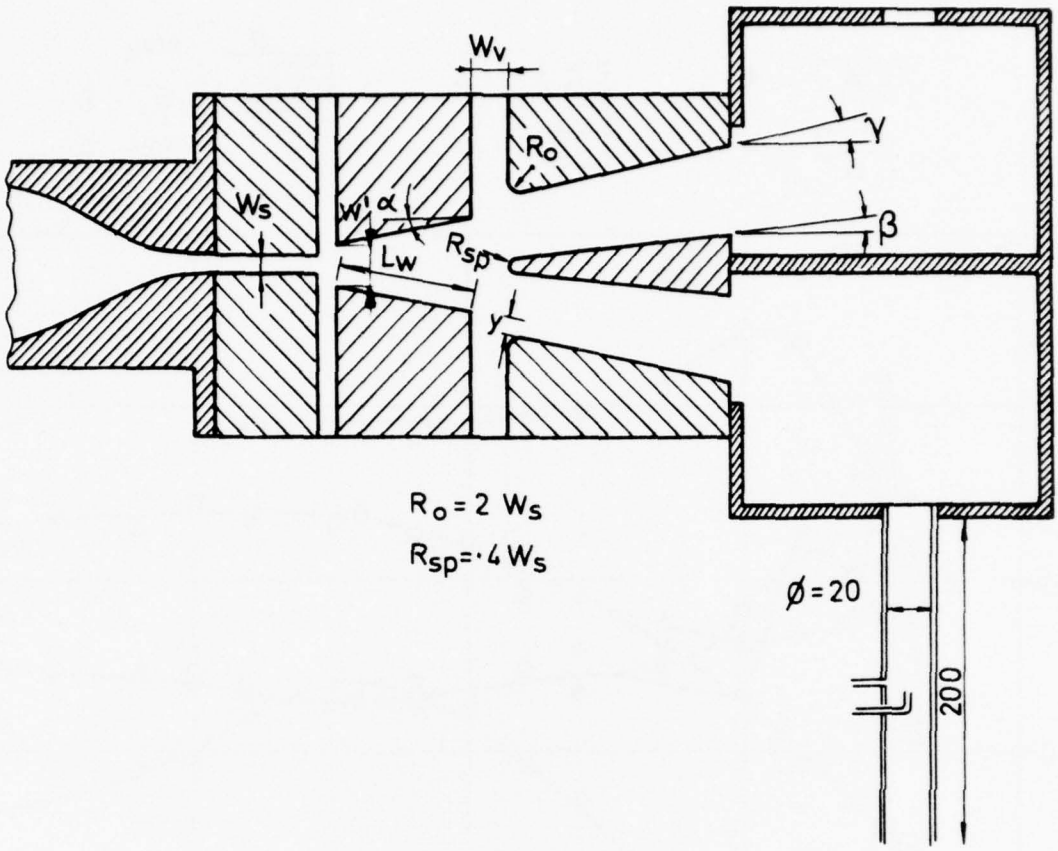


FIG. 27 THE WALL PRESSURE DISTRIBUTIONS FOR AR=8, L_W/W_S=17 AND OPEN CONTROL CHANNELS OPERATION



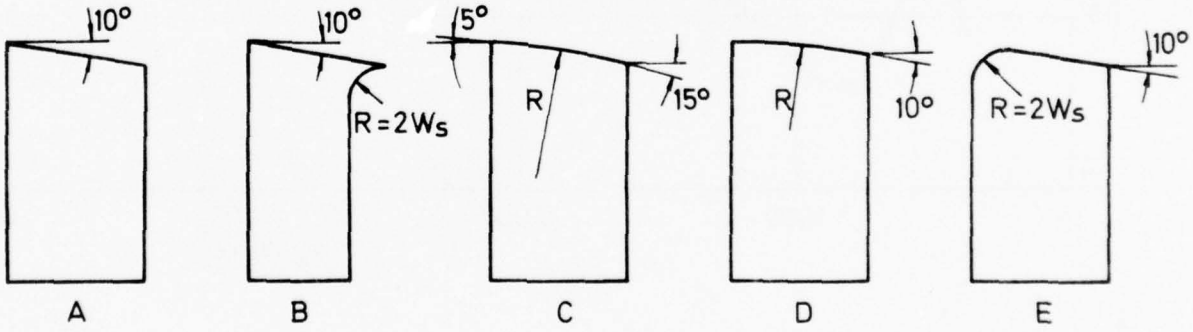


FIG. 28 SKETCH OF THE TURBULENT BISTABLE MODEL AND ITS INTERCHANGEABLE ATTACHMENT WALLS

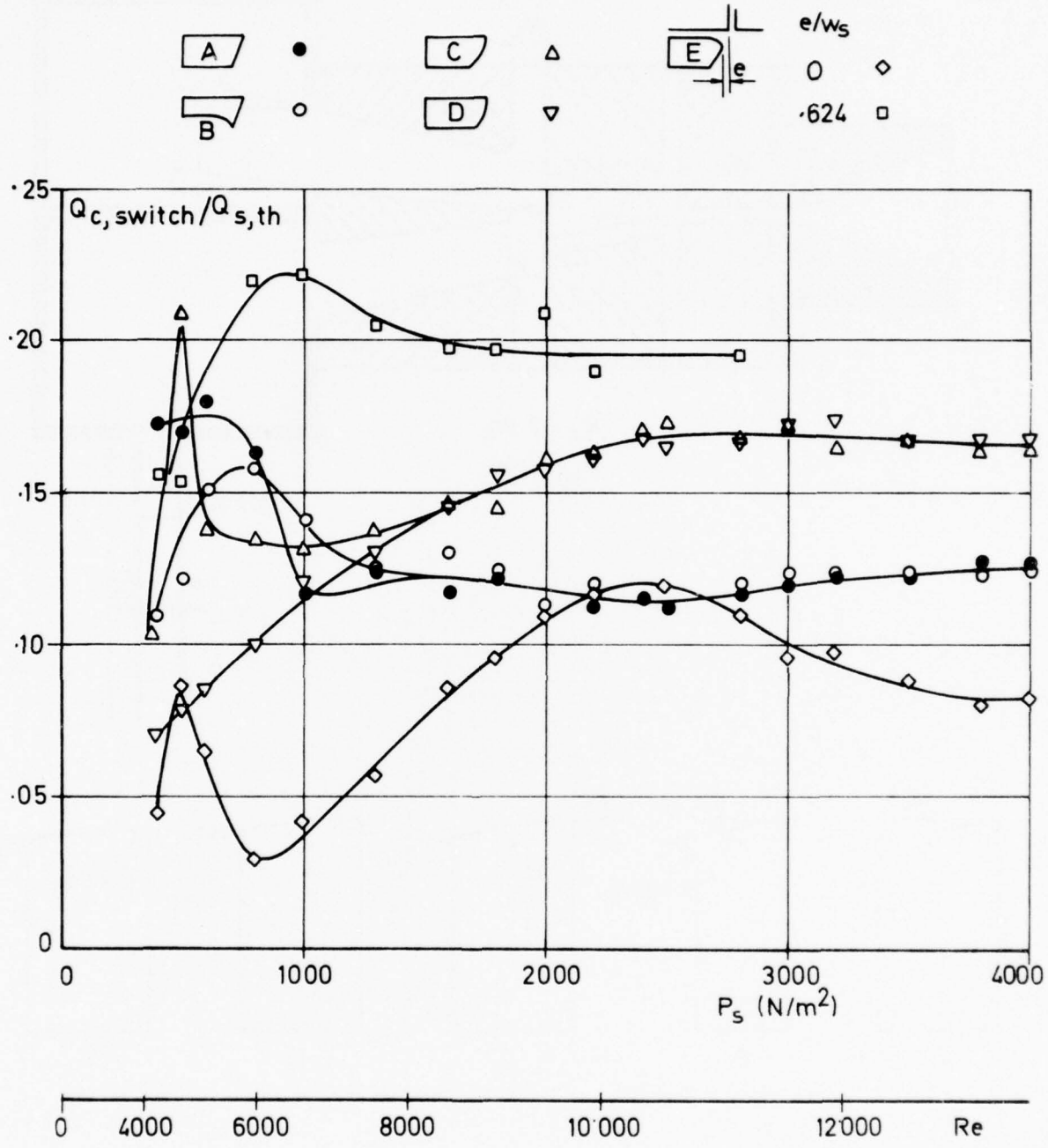


FIG. 29 SWITCHING CHARACTERISTICS OF STRAIGHT AND CURVED WALL BISTABLES WITHOUT OUTPUT DUCTS AND WITHOUT SPLITTER

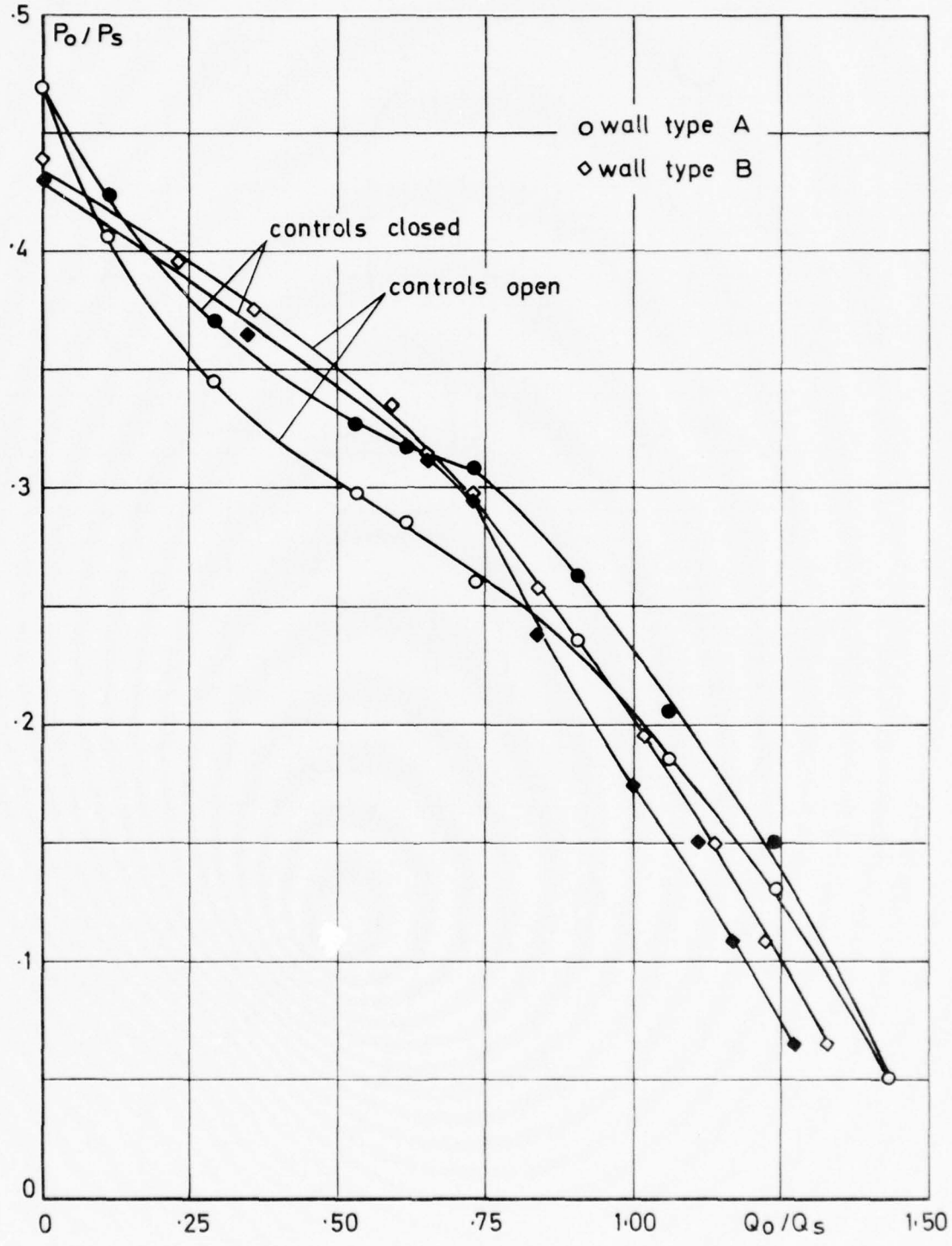


FIG. 30 OUTPUT CHARACTERISTIC OF THE SELECTED DESIGN FOR A TURBULENT BISTABLE AMPLIFIER

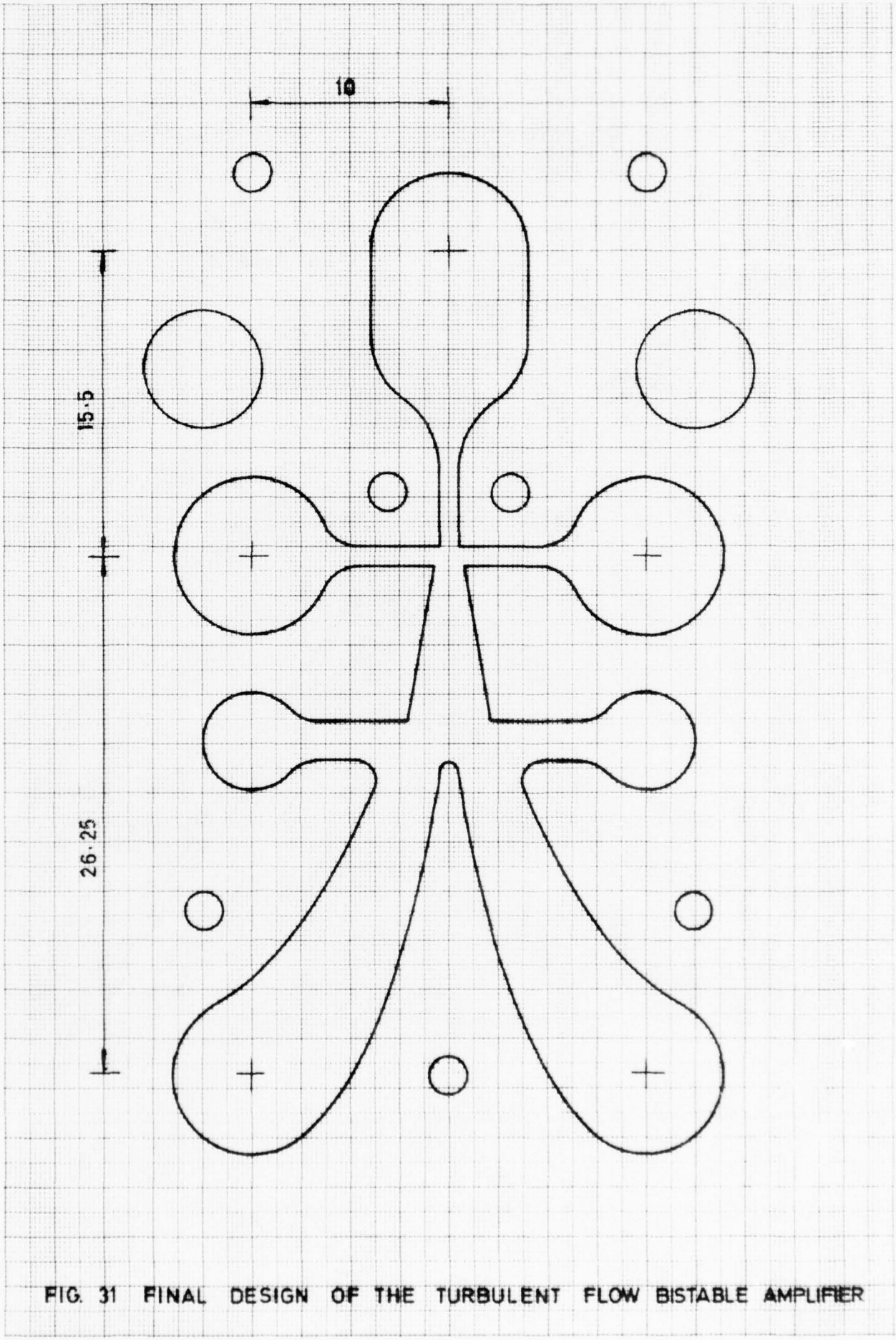


FIG. 31 FINAL DESIGN OF THE TURBULENT FLOW BISTABLE AMPLIFIER

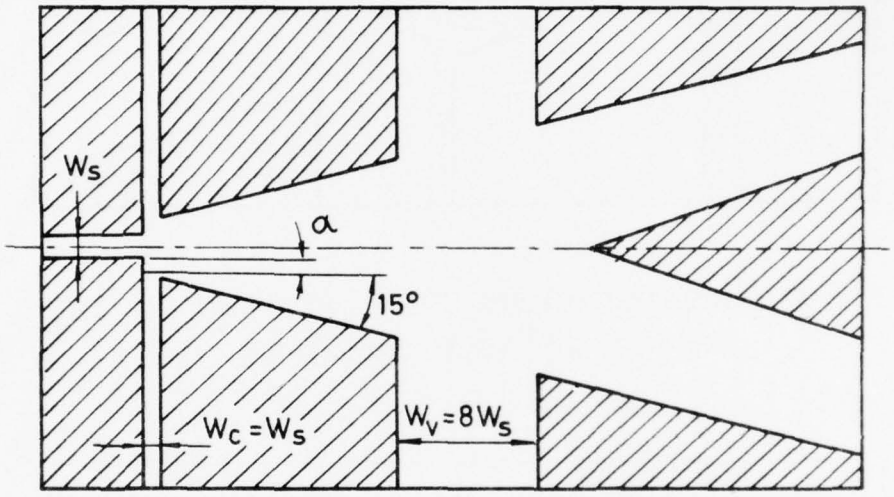


FIG. 32 FIRST CONFIGURATION OF THE LAMINAR BISTABLE AMPLIFIER

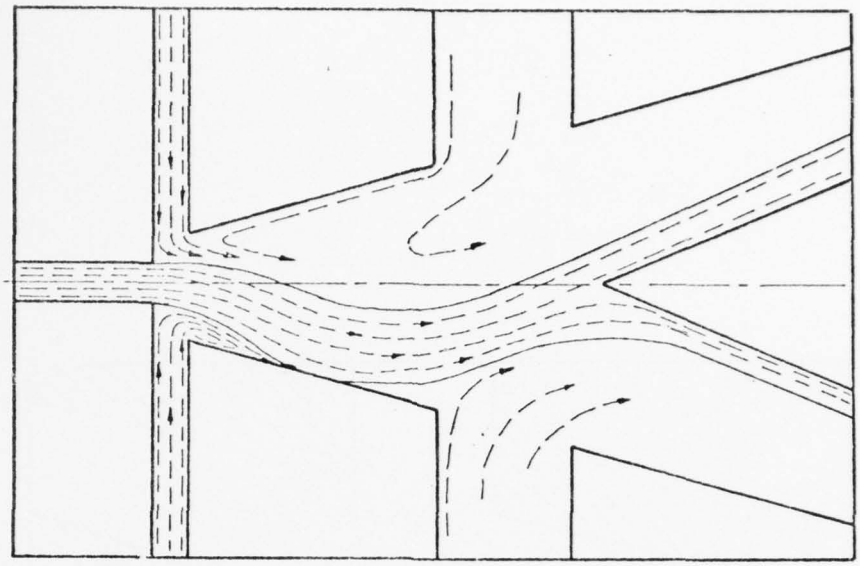


FIG. 33 UNSATISFACTORY FLOW PATTERN IN THE LAMINAR BISTABLE AMPLIFIER

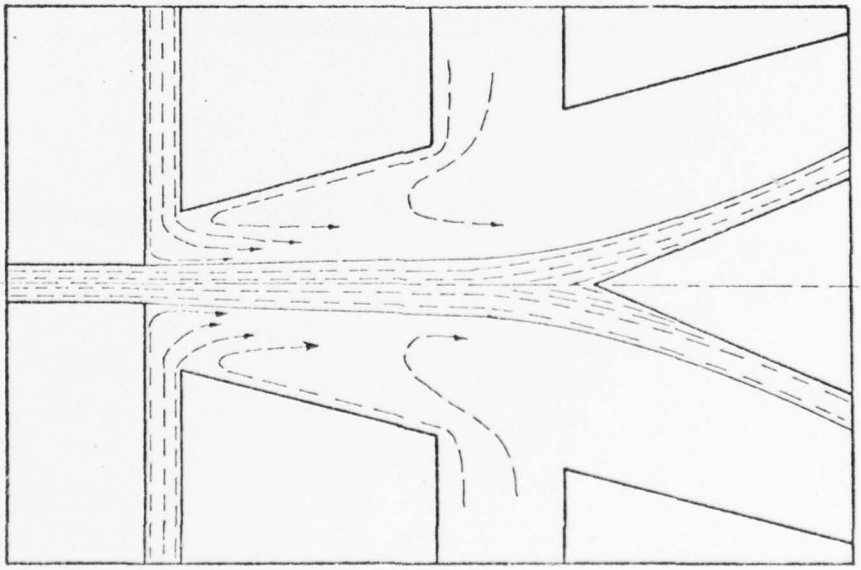


FIG. 34 UNSATISFACTORY FLOW PATTERN IN THE LAMINAR BISTABLE AMPLIFIER

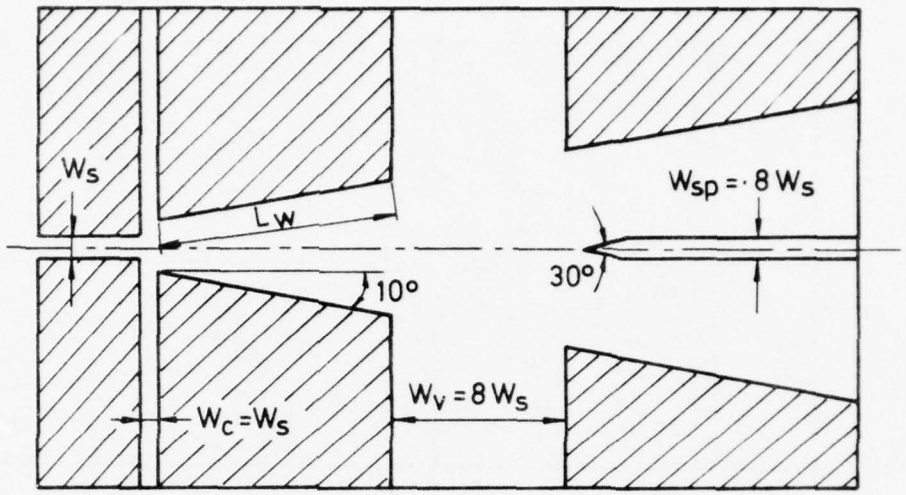


FIG. 35 SECOND CONFIGURATION OF THE LAMINAR BISTABLE AMPLIFIER

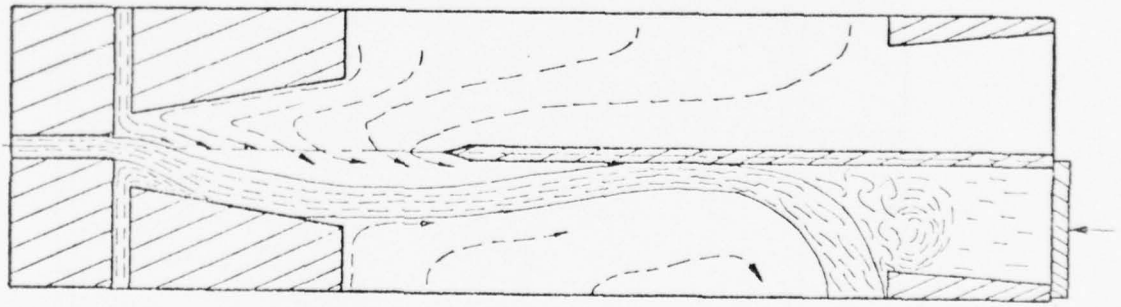


FIG. 36 FLOW PATTERN IN A LAMINAR BISTABLE AMPLIFIER WITH LARGE VENTS

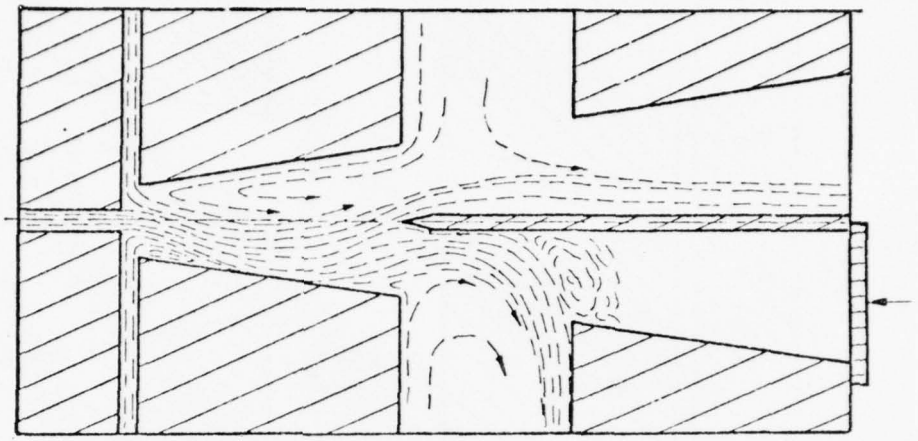


FIG. 37 UNSATISFACTORY FLOW PATTERN IN THE LAMINAR BISTABLE AMPLIFIER

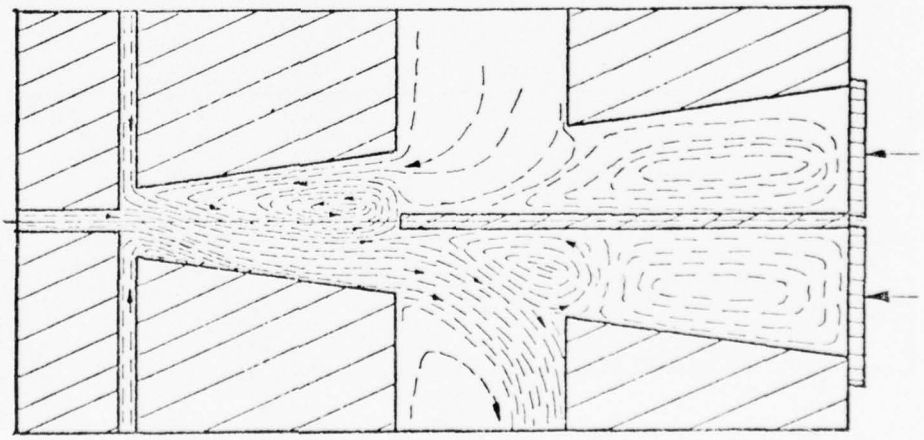


FIG. 38 FLOW PATTERN IN A LAMINAR BISTABLE AMPLIFIER EXHIBITING STABILITY UNDER BLOCKED OUTPUT CONDITION

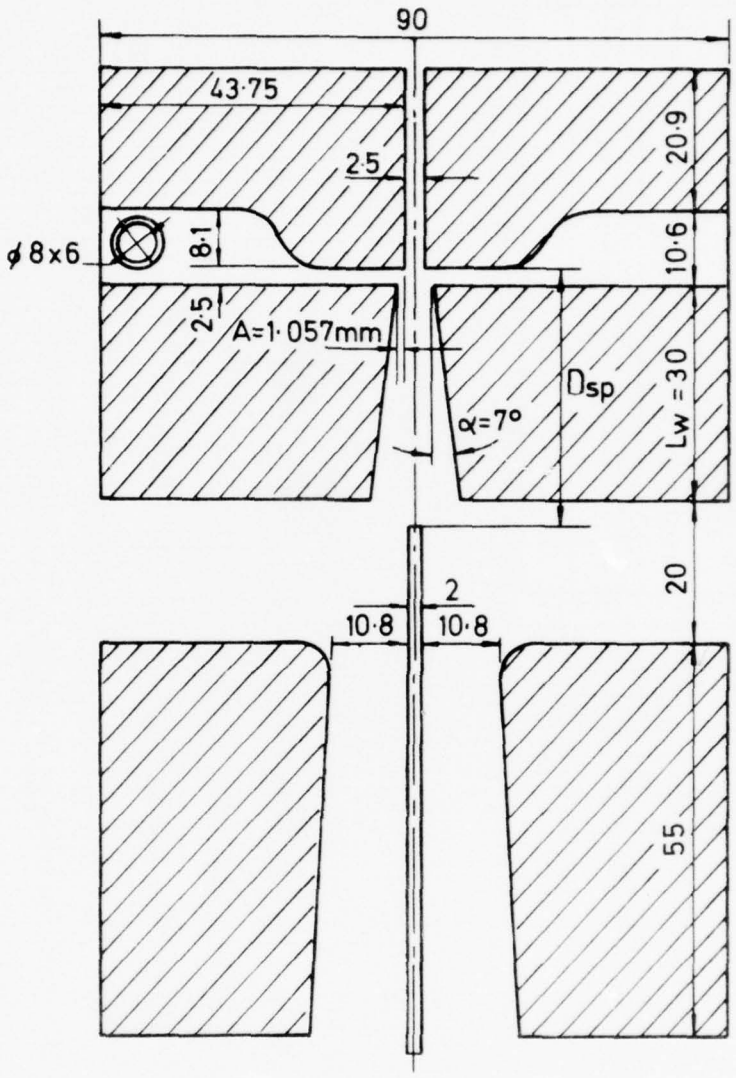


FIG. 39 FINAL CONFIGURATION OF THE LAMINAR BISTABLE AMPLIFIER

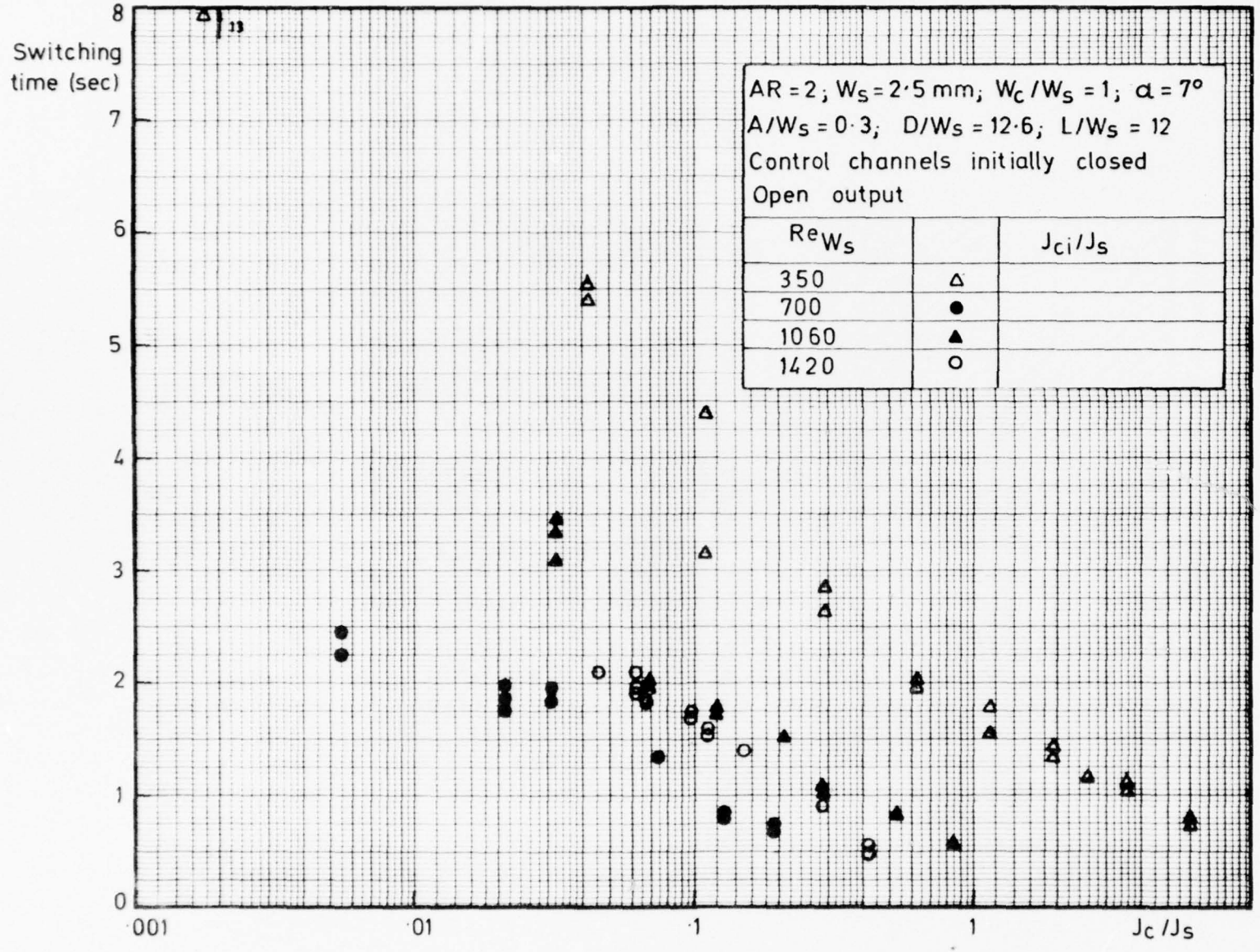

Switching time (sec)
8
7
6
5
4
3
2
1
0
·001
·01
·1
1
Jc /Js
AR = 2; Ws = 2·5 mm; Wc /Ws = 1; α = 7°
A/Ws = 0·3; D/Ws = 12·6; L/Ws = 12
Control channels initially closed
Open output
Re Ws
Jci/Js
350
700
1060
1420

FIG. 40

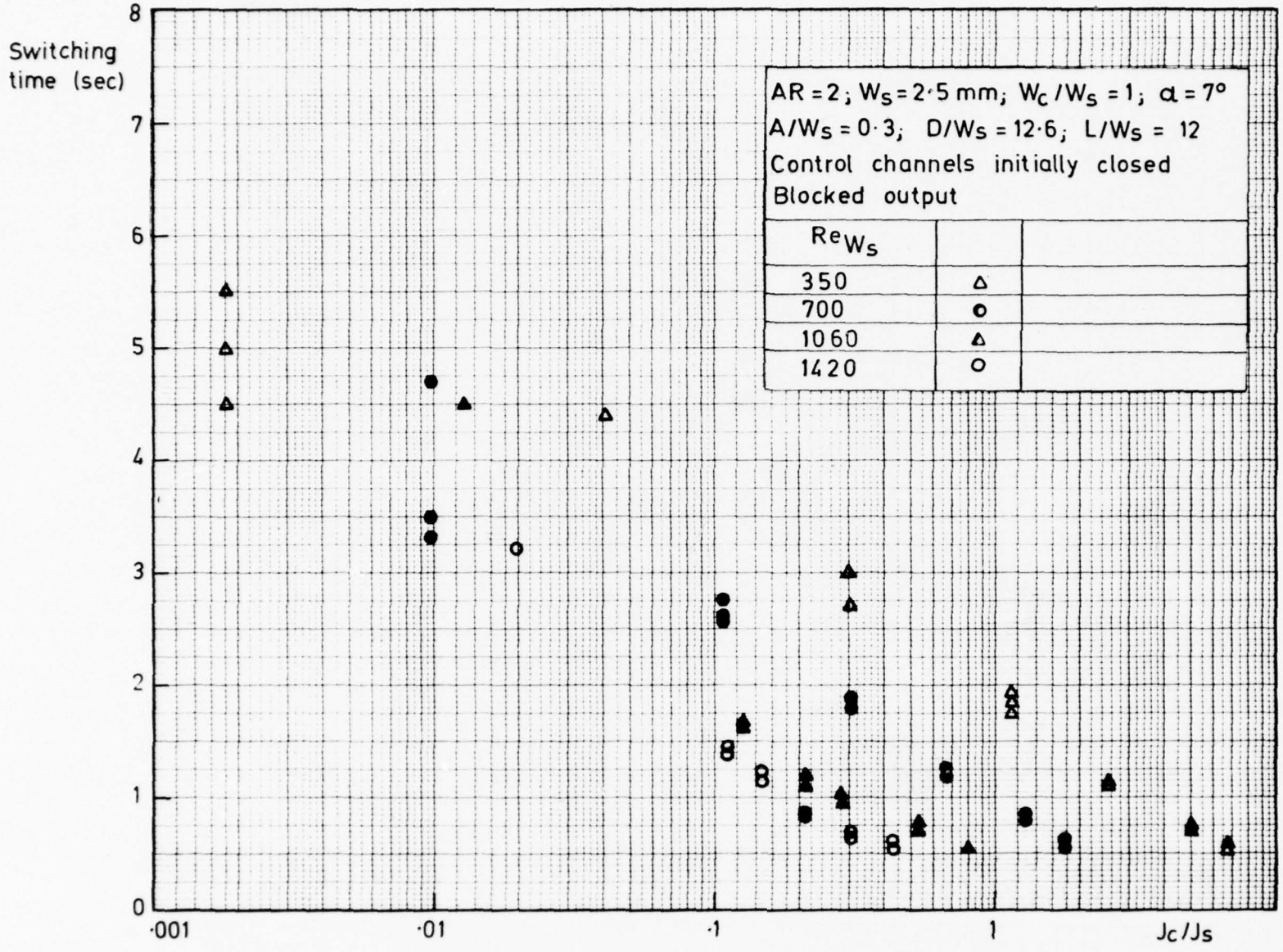

Switching time (sec)
8
7
6
5
4
3
2
1
0
·001
·01
·1
1
Jc/Js
AR = 2; Ws = 2·5 mm; Wc/Ws = 1; α = 7°
A/Ws = 0·3; D/Ws = 12·6; L/Ws = 12
Control channels initially closed
Blocked output
Re Ws
350
700
1060
1420

FIG. 41

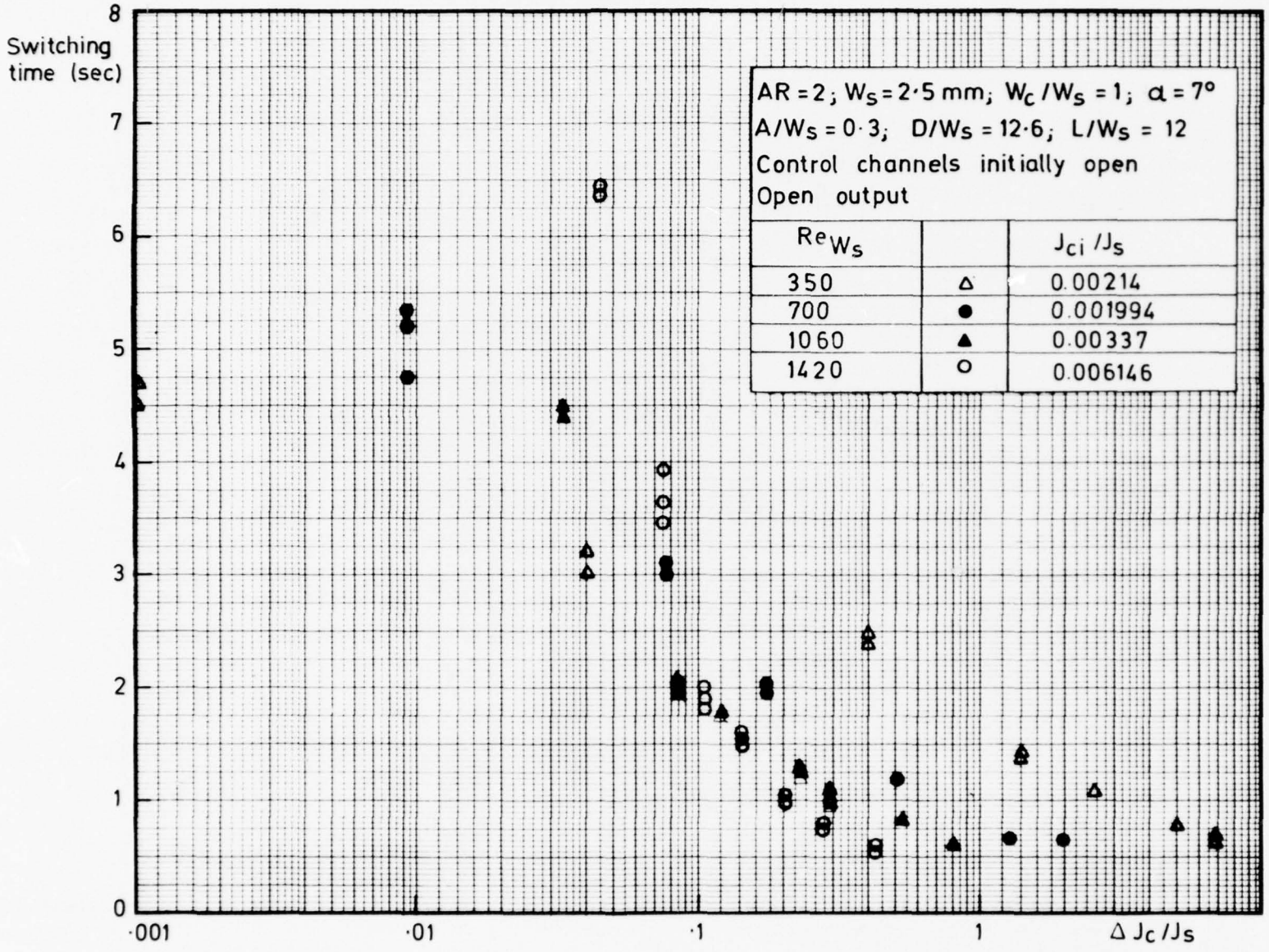

Switching time (sec)
8
7
6
5
4
3
2
1
0
·001
·01
·1
1
Δ Jc/Js
AR = 2; Ws = 2·5 mm; Wc/Ws = 1; α = 7°
A/Ws = 0·3; D/Ws = 12·6; L/Ws = 12
Control channels initially open
Open output
Re Ws
Jci/Js
350
0.00214
700
0.001994
1060
0.00337
1420
0.006146

FIG. 42

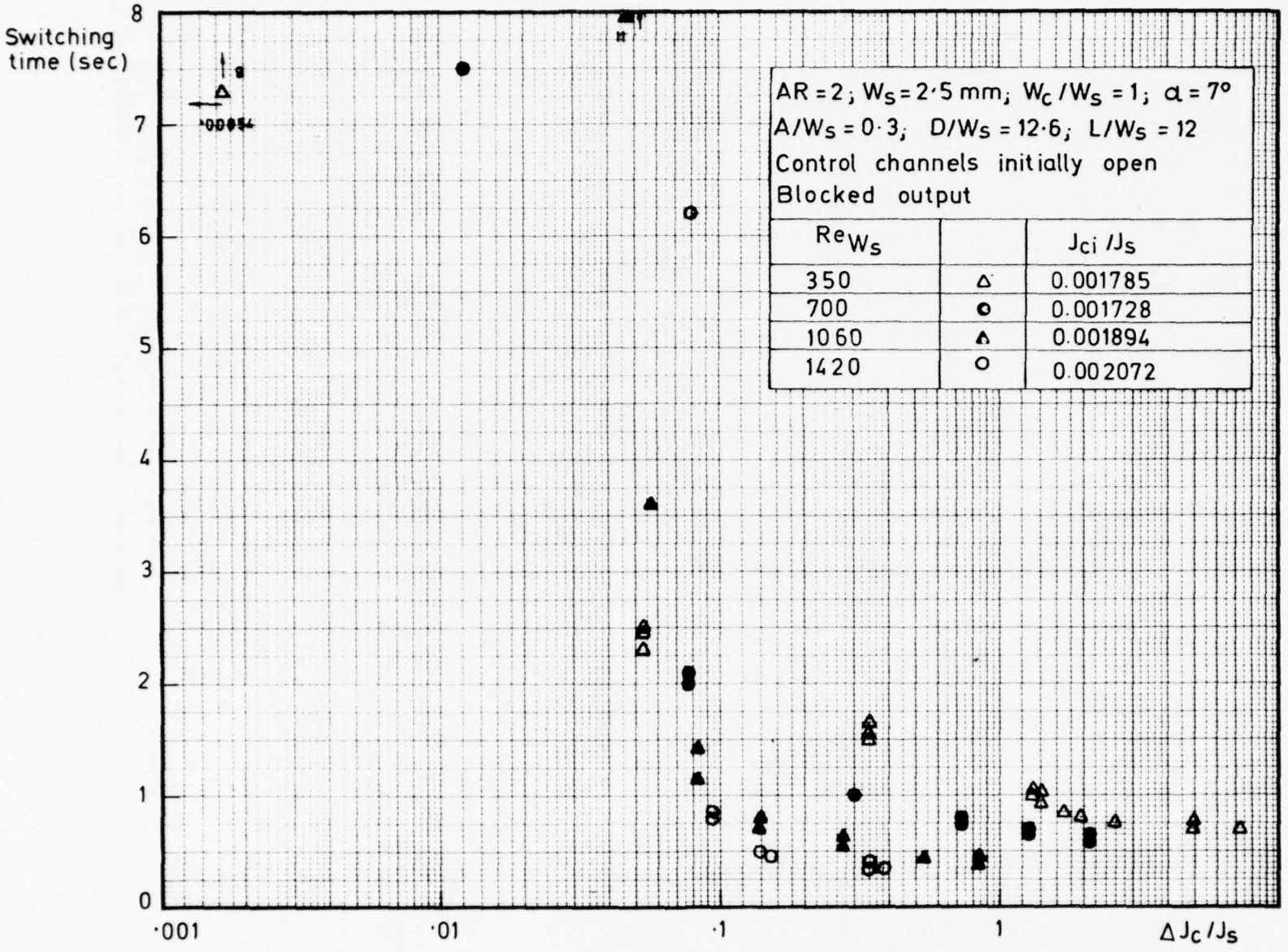

Switching time (sec)
8
7
6
5
4
3
2
1
0
·001
·01
·1
1
ΔJc/Js
AR = 2; Ws = 2·5 mm; Wc/Ws = 1; α = 7°
A/Ws = 0·3; D/Ws = 12·6; L/Ws = 12
Control channels initially open
Blocked output
Re Ws | | Jci/Js
350 | △ | 0.001785
700 | ● | 0.001728
1060 | ▲ | 0.001894
1420 | ○ | 0.002072

FIG. 43

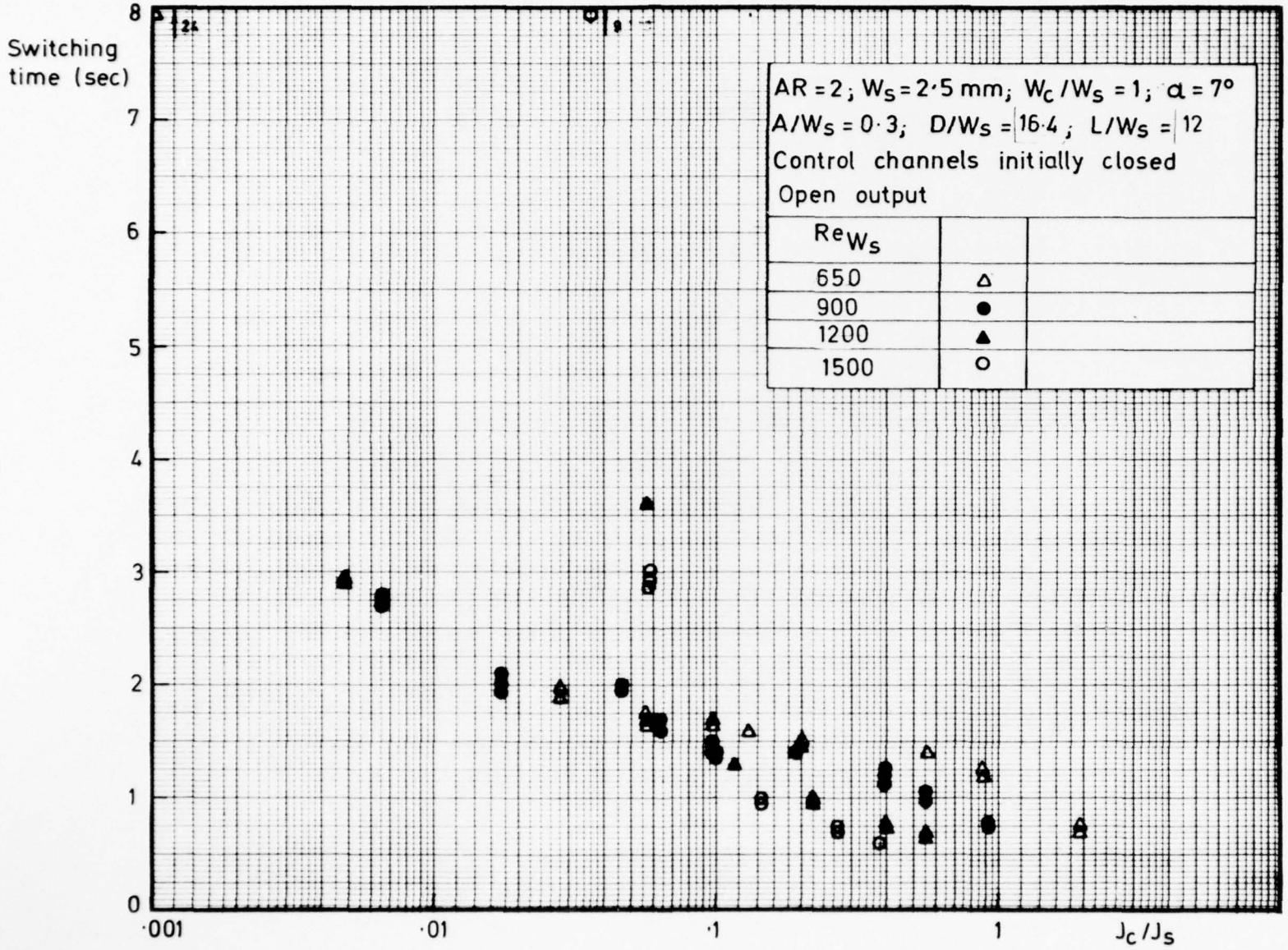

Switching time (sec)
8
7
6
5
4
3
2
1
0
·001
·01
·1
1
J_c/J_s
AR = 2; W_s = 2·5 mm; W_c/W_s = 1; α = 7°
A/W_s = 0·3; D/W_s = 16·4; L/W_s = 12
Control channels initially closed
Open output
Re_{W_s}
650
900
1200
1500

FIG. 44

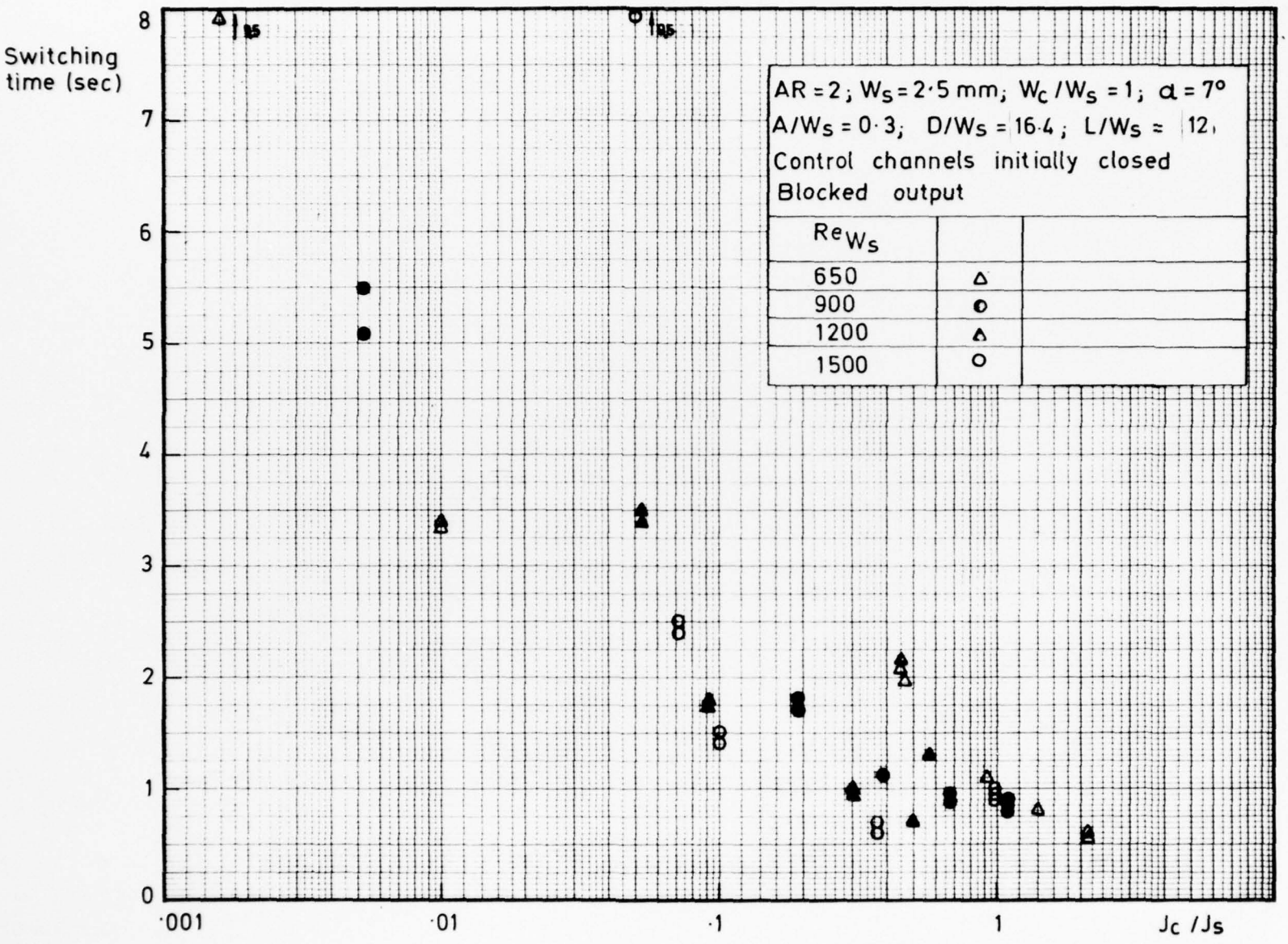

Switching time (sec)
8
7
6
5
4
3
2
1
0
·001
·01
·1
1
Jc /Js
AR = 2 ; Ws = 2·5 mm; Wc /Ws = 1 ; α = 7°
A/Ws = 0·3; D/Ws = 16·4 ; L/Ws = 12
Control channels initially closed
Blocked output
Re Ws
650
900
1200
1500

FIG. 45

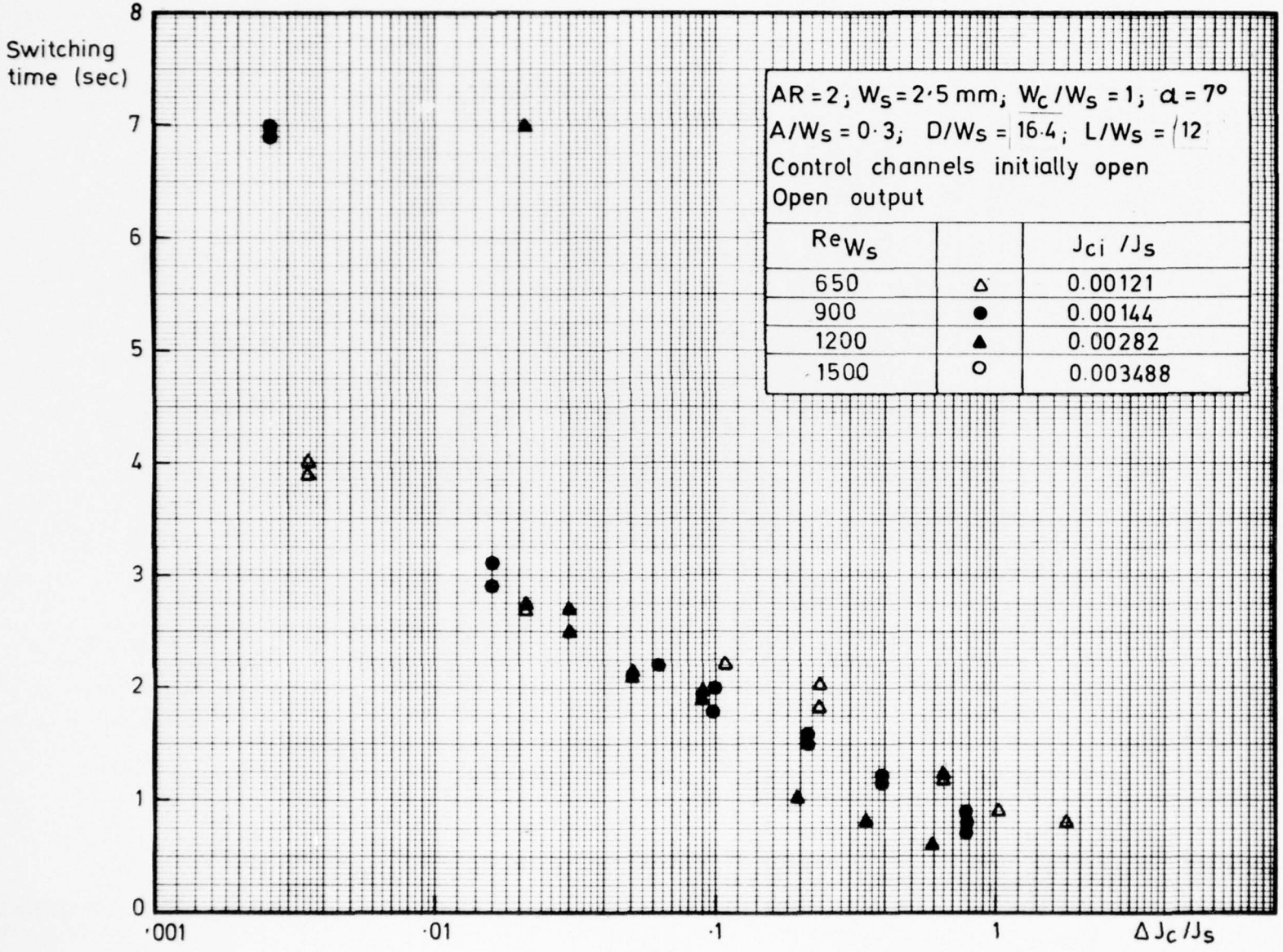

Switching time (sec)
8
7
6
5
4
3
2
1
0
·001
·01
·1
1
ΔJc/Js
AR = 2; Ws = 2·5 mm; Wc/Ws = 1; α = 7°
A/Ws = 0·3; D/Ws = 16·4; L/Ws = 12
Control channels initially open
Open output
Re Ws | | Jci/Js
650 | △ | 0.00121
900 | ● | 0.00144
1200 | ▲ | 0.00282
1500 | ○ | 0.003488

FIG. 46

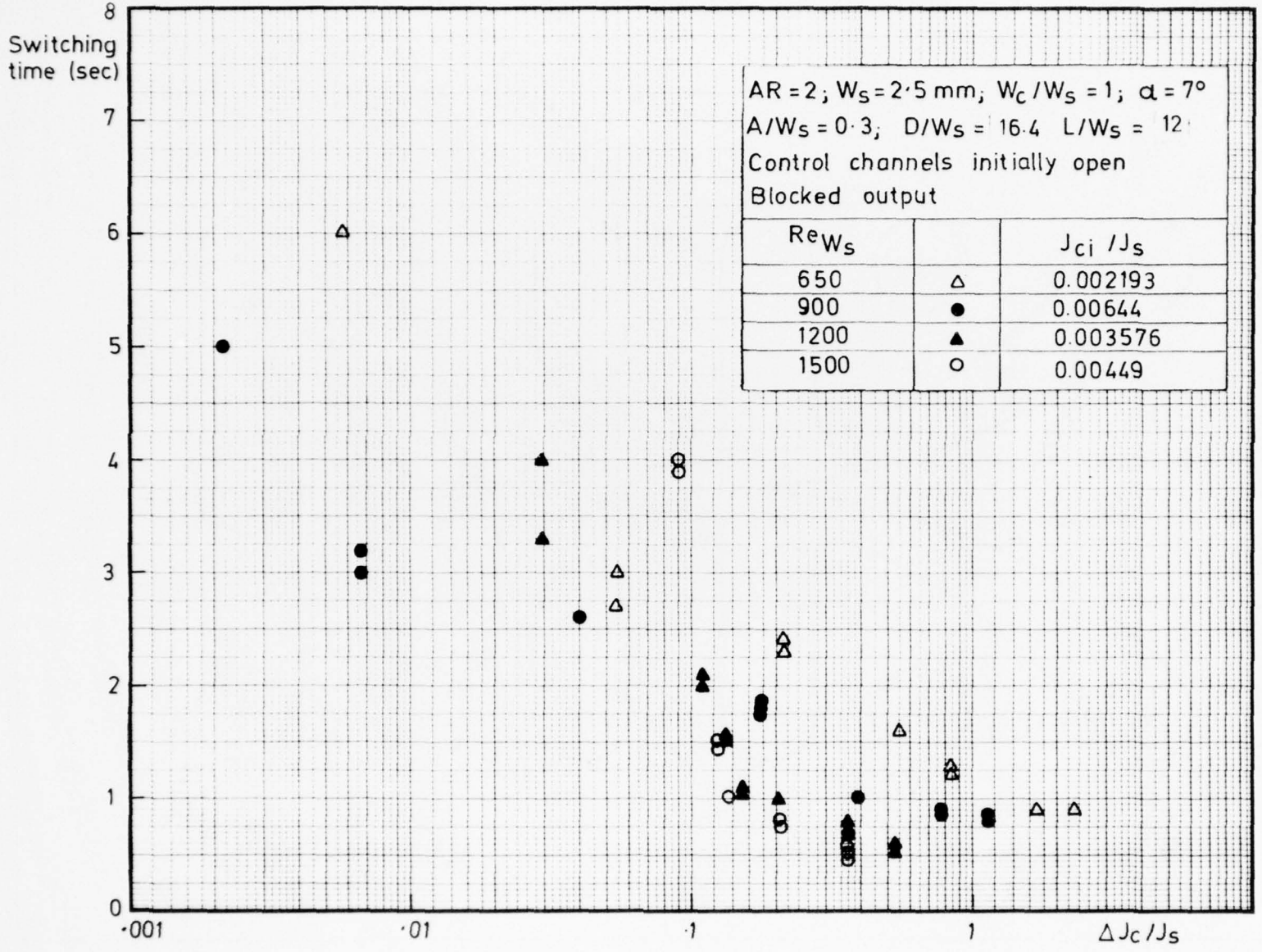

Switching time (sec)
8
7
6
5
4
3
2
1
0
·001
·01
·1
1
ΔJc/Js
AR = 2; Ws = 2·5 mm; Wc/Ws = 1; α = 7°
A/Ws = 0·3; D/Ws = 16·4 L/Ws = 12
Control channels initially open
Blocked output
Re Ws | | Jci/Js
650 | △ | 0.002193
900 | ● | 0.00644
1200 | ▲ | 0.003576
1500 | ○ | 0.00449

FIG. 47

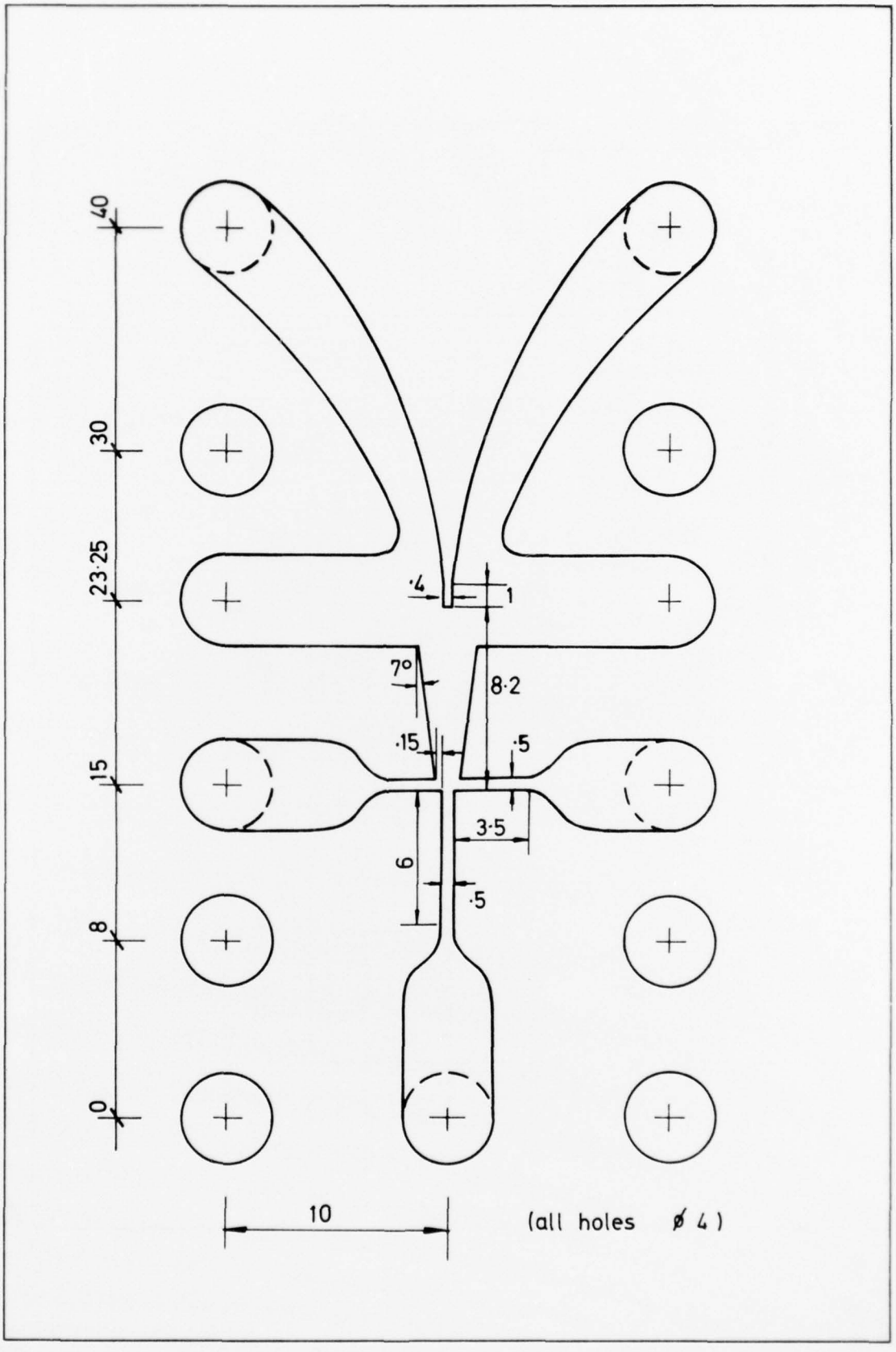


FIG. 48 FINAL DESIGN OF THE LAMINAR BISTABLE AMPLIFIER

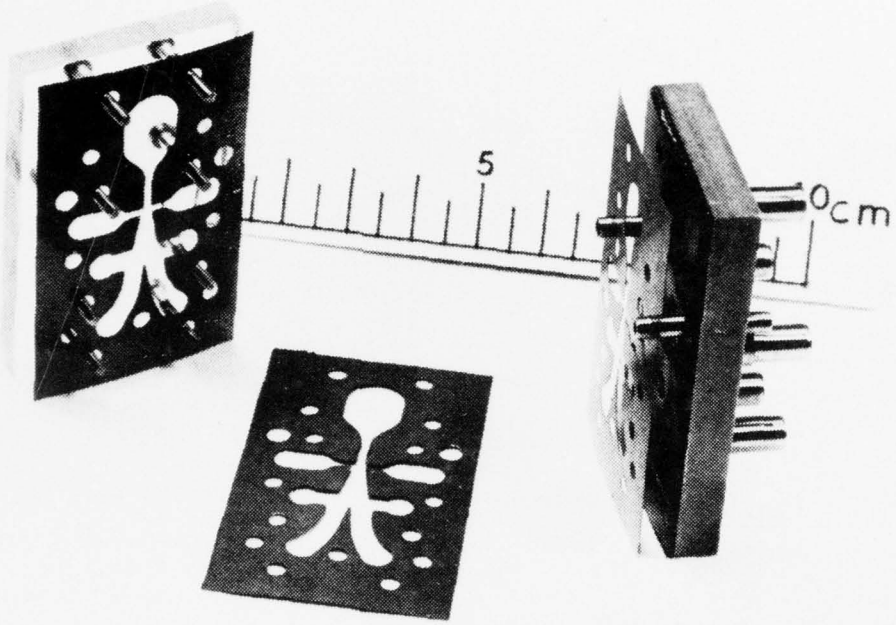


Fig. 49 Exploded view of a fluidic amplifier constructed by a chemical etching technique.

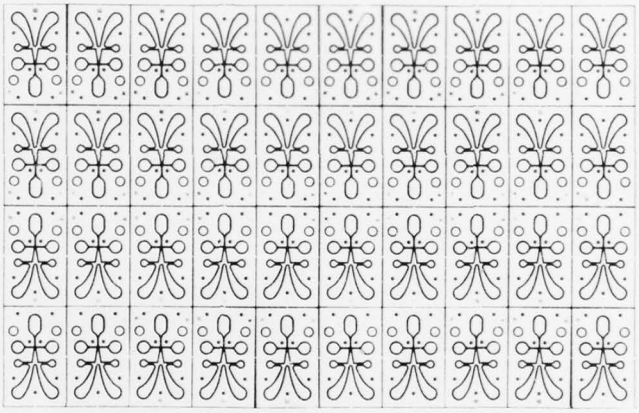


Fig. 50 Typical mask used for the fabrication of turbulent flow bistable amplifiers (scale I:I)

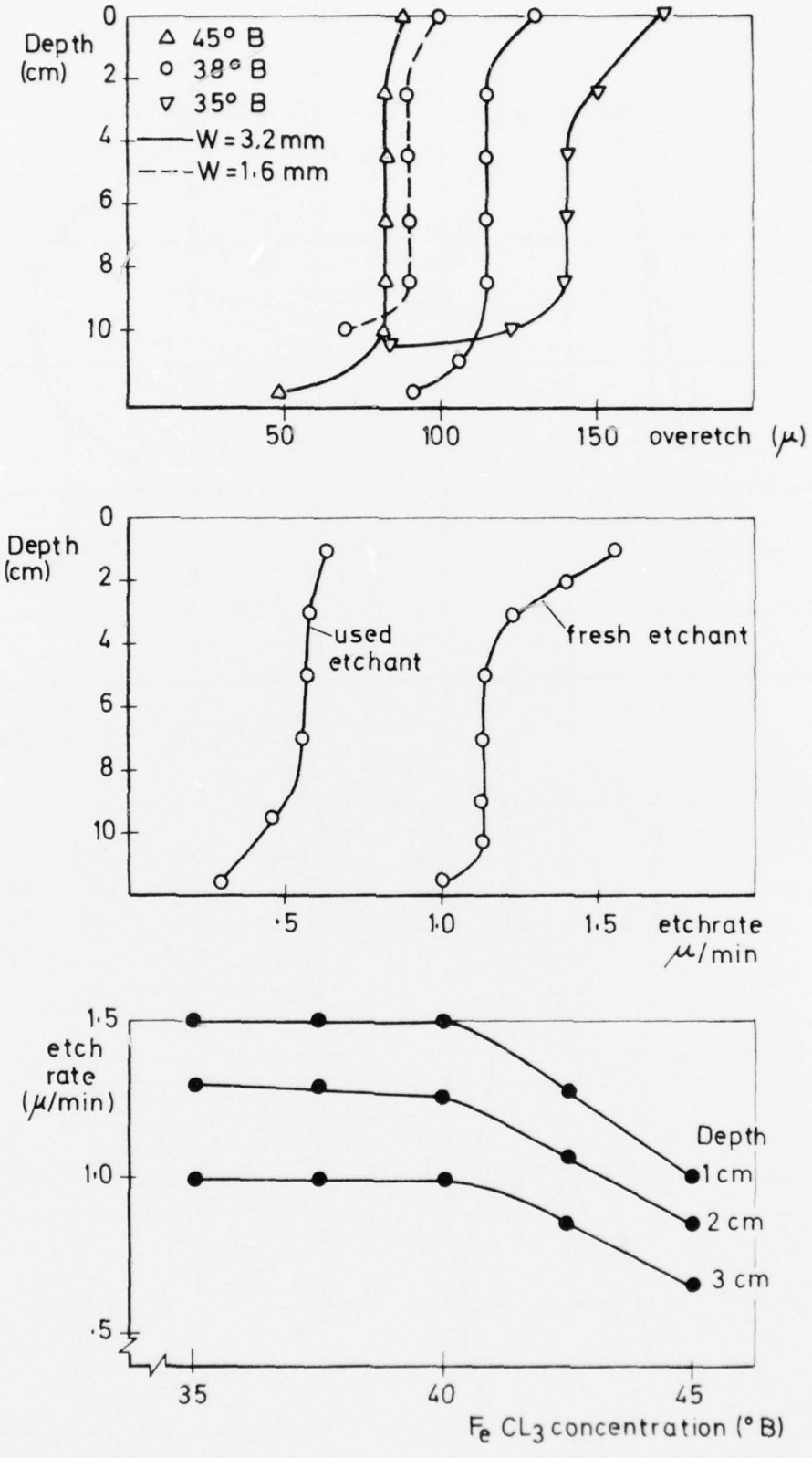
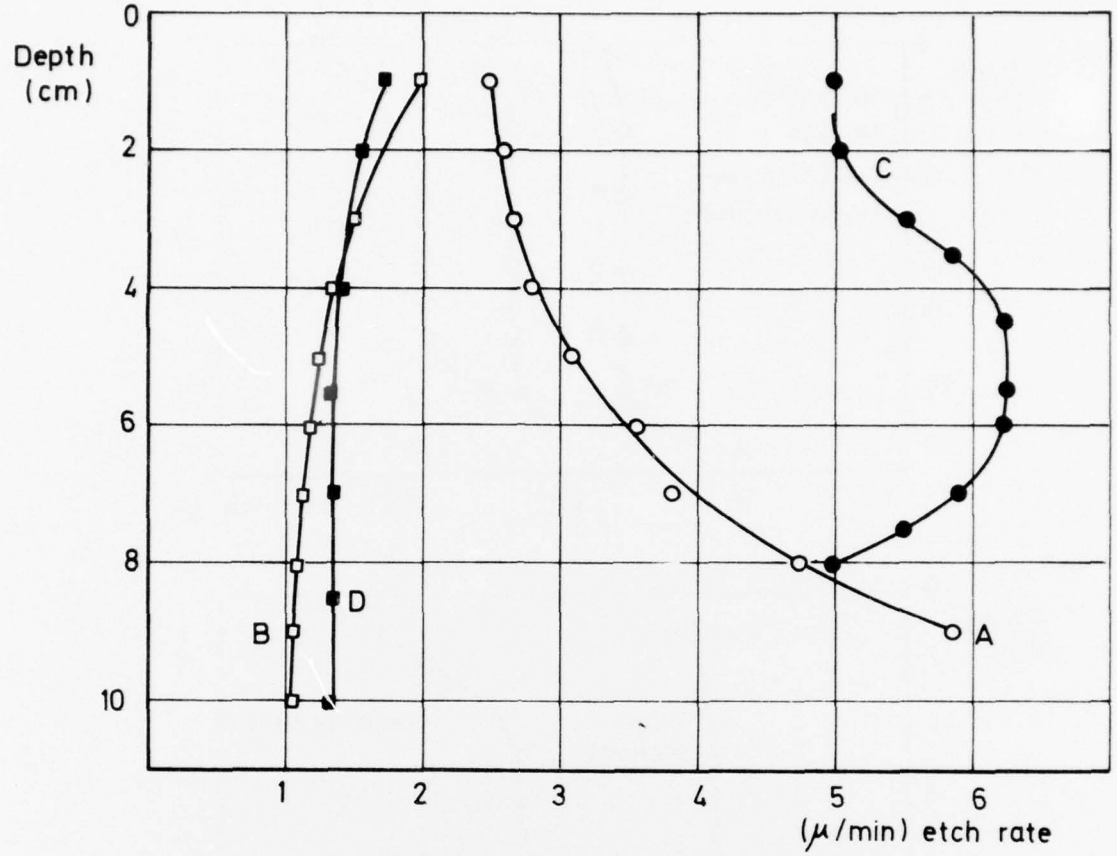


FIG. 51 RESULTS OF ETCHING TESTS WITH A STILL BATH



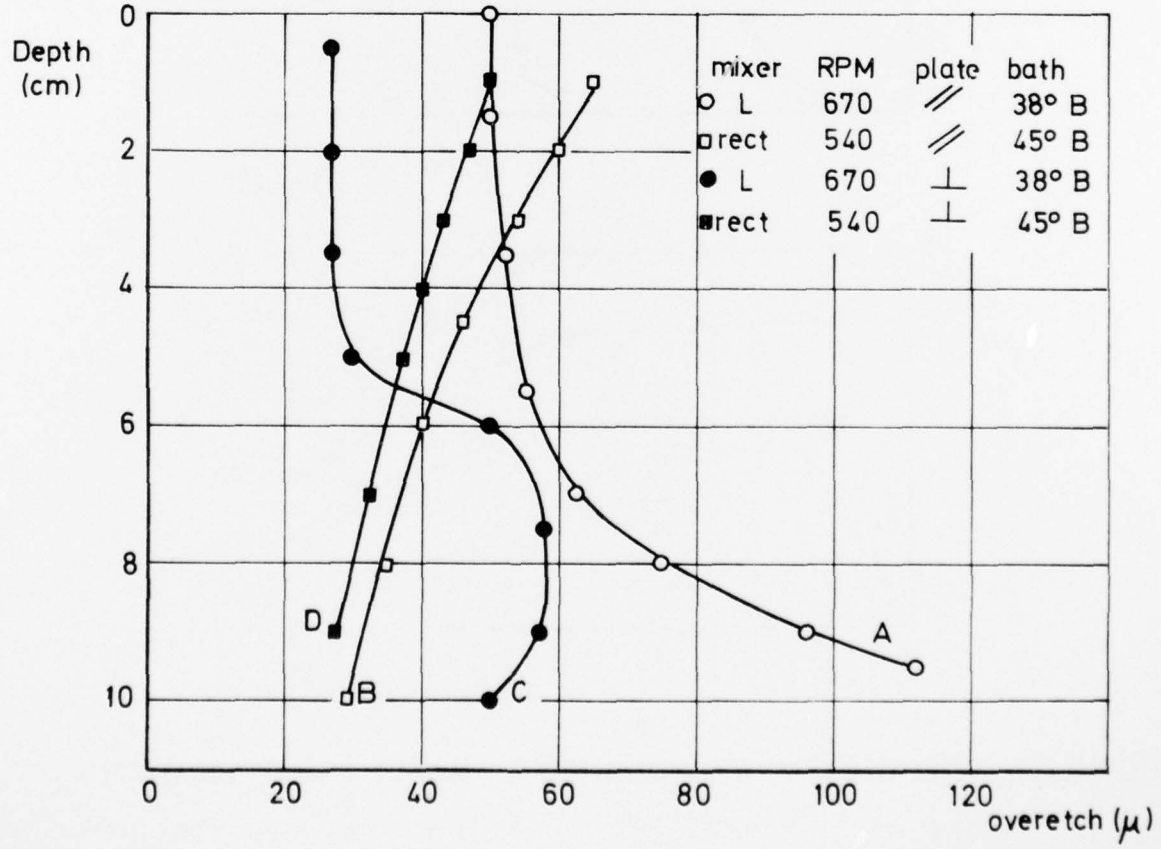


FIG. 52 RESULTS OF ETCHING TESTS WITH AN AGITATED BATH

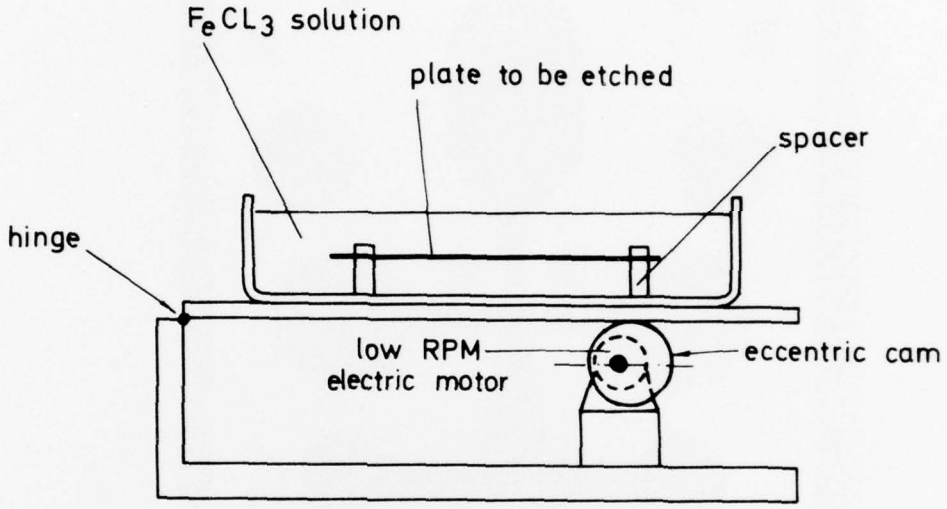


FIG. 53 SKETCH OF THE APPARATUS USED FOR CHEMICAL ETCHING

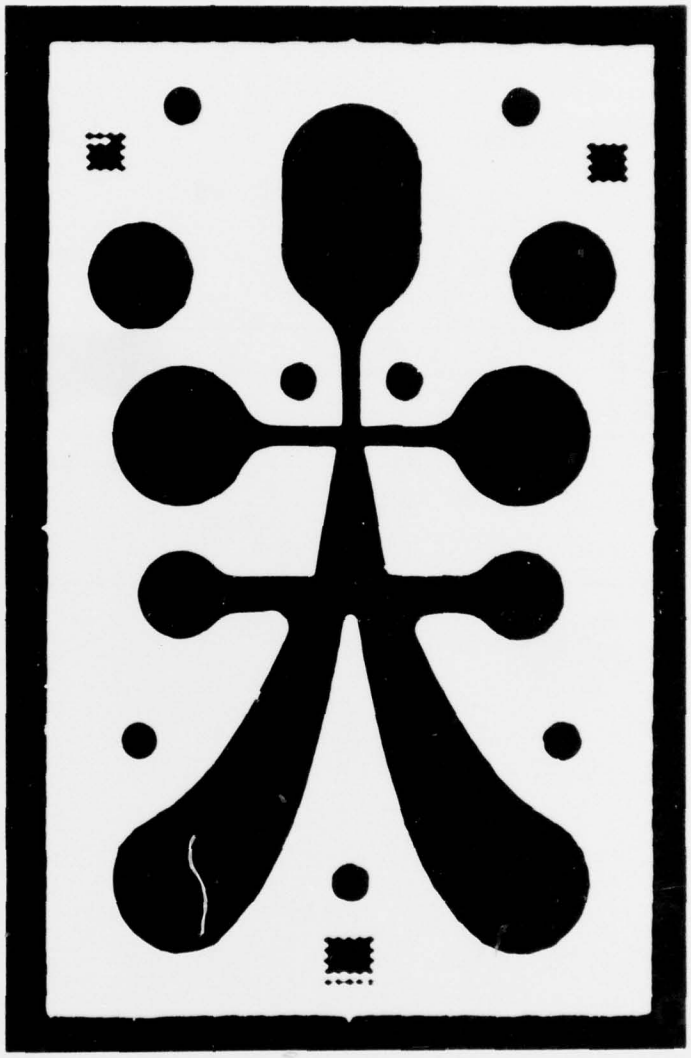


Fig. 54 Enlargement (9,89 X) of an etching made in a 0,Imm thick copper plate

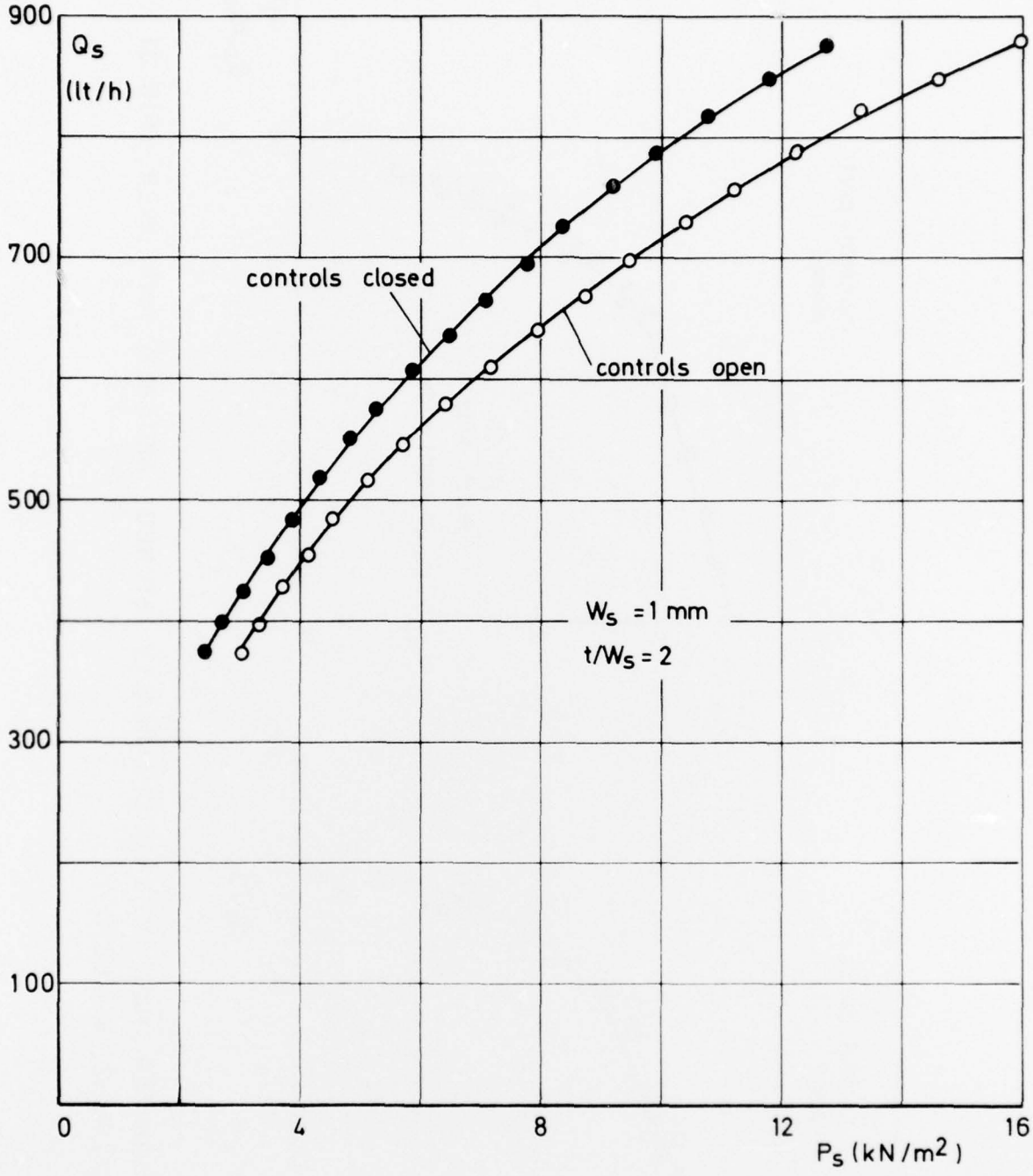


FIG. 55 SUPPLY CHARACTERISTIC OF THE CHEMICALLY ETCHED BISTABLE AMPLIFIER (FIG. 31)

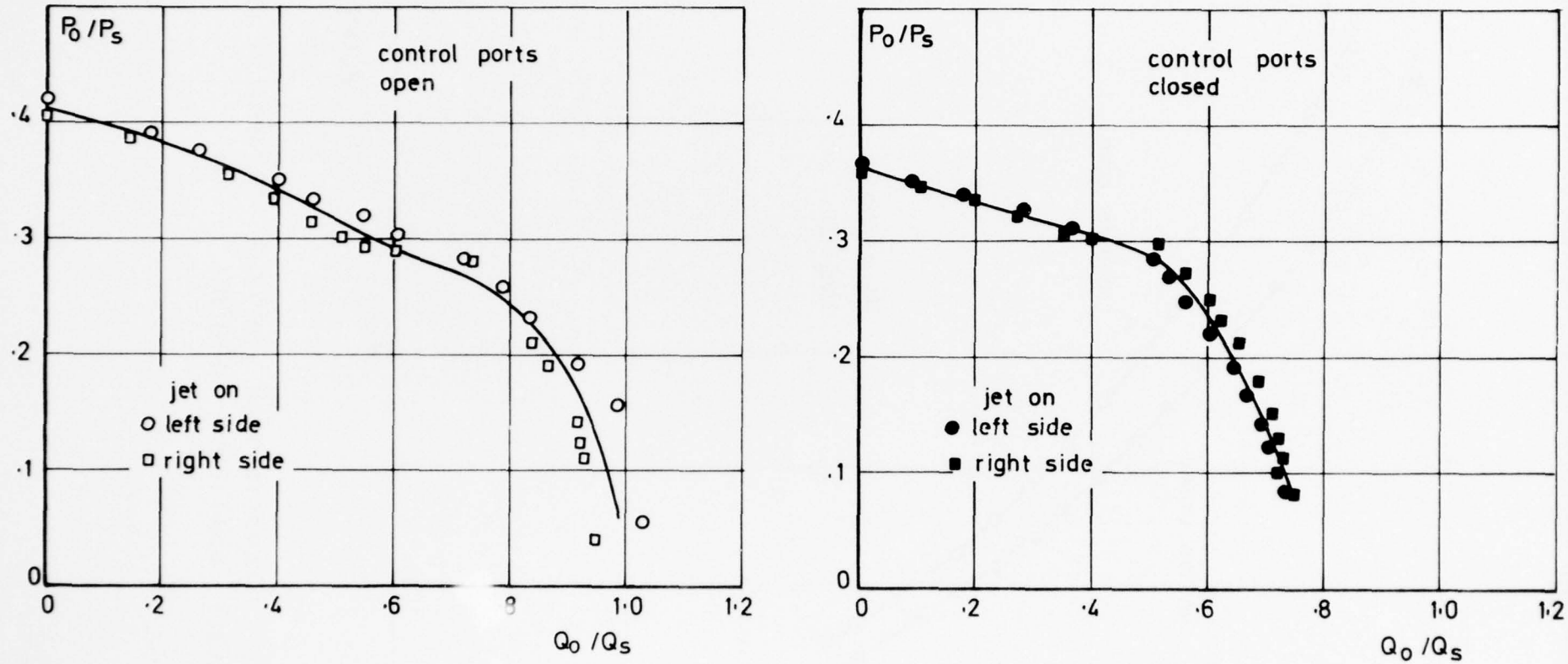


FIG. 56 OUTPUT CHARACTERISTICS OF THE CHEMICALLY ETCHED BISTABLE AMPLIFIER (FIG. 31)
$W_s = 1$ mm, $t/W_s = 2$, $Re = 6670$

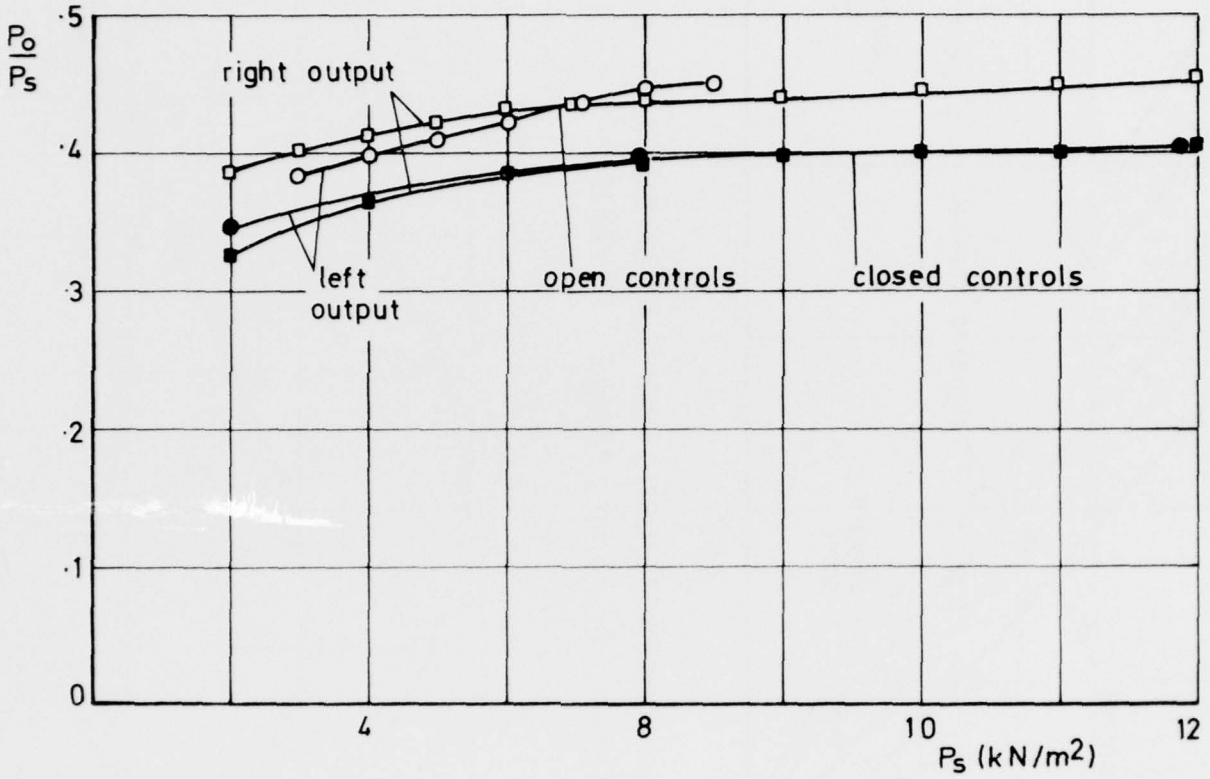


FIG. 57 VARIATION OF MAXIMUM PRESSURE RECOVERY WITH SUPPLY PRESSURE

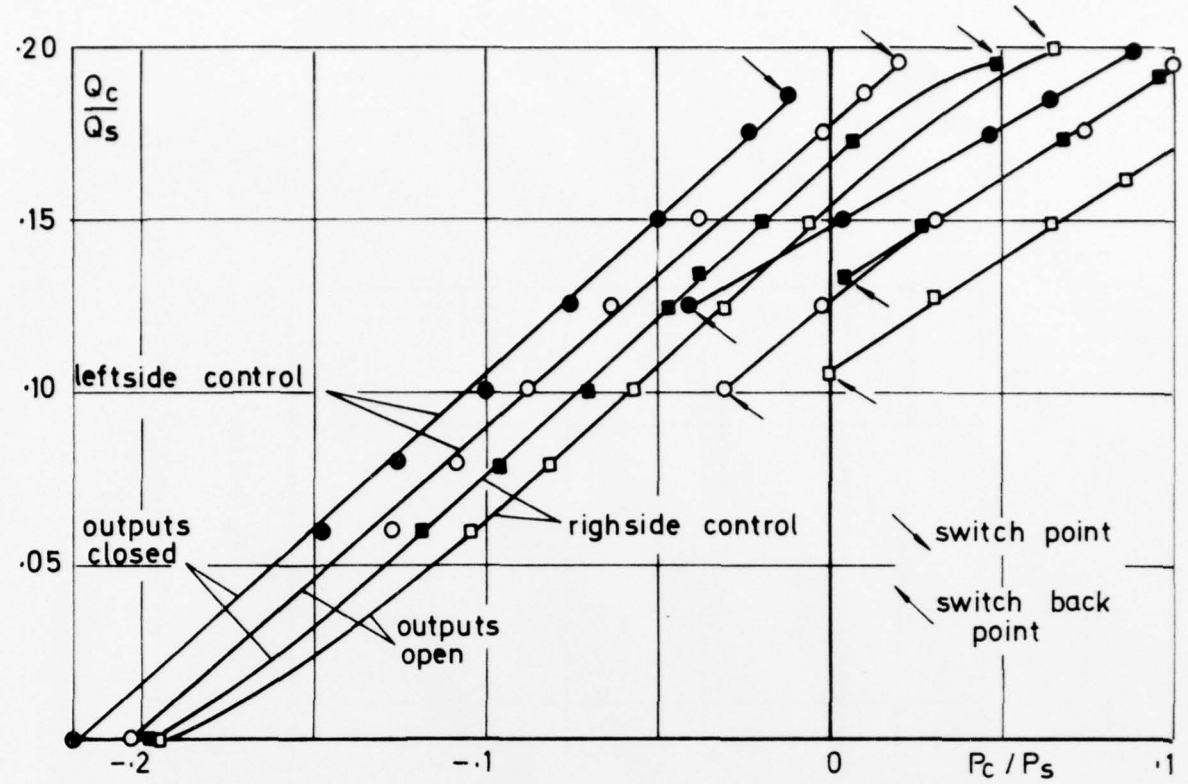


FIG. 58 INPUT CHARACTERISTIC OF THE CHEMICALLY ETCHED BISTABLE (W_s = 1mm, t/W_s = 2, Re = 6670)

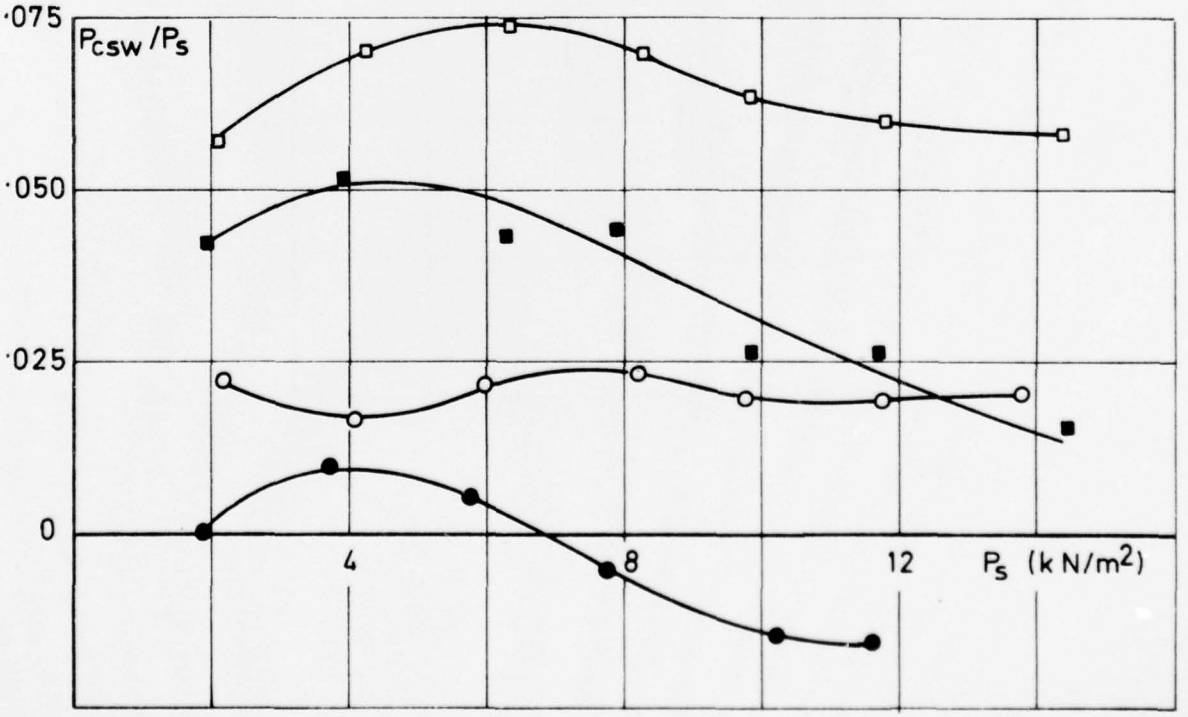


FIG. 59 VARIATION OF SWITCH POINTS WITH SUPPLY PRESSURE